UNIVERSIDAD AUTONOMA DE MADRID

Departamento de Biología Molecular

MECHANISM OF PRIMARY CILIOGENESIS BY POLARIZED EPITHELIAL CELLS

MECANISMO DE FORMACIÓN DEL CILIO PRIMARIO EN CÉLULAS EPITELIALES POLARIZADAS

Miguel Bernabé Rubio

Madrid, 2017

FACULTAD DE CIENCIAS
UNIVERSIDAD AUTÓNOMA DE MADRID

Departamento de Biología Molecular

MECHANISM OF PRIMARY CILIOGENESIS BY POLARIZED EPITHELIAL CELLS

MECANISMO DE FORMACIÓN DEL CILIO PRIMARIO EN CÉLULAS EPITELIALES POLARIZADAS

D. Miguel Bernabé Rubio

Licenciado en Bioquímica

Presenta esta memoria para optar al grado de Doctor en Bioquímica, Biología Molecular, Biomedicina y Biotecnología

DIRECTOR

Dr. Miguel Ángel Alonso Lebrero

Tesis Doctoral realizada en el CENTRO DE BIOLOGÍA MOLECULAR SEVERO OCHOA

MADRID, 2017

Esta tesis ha sido realizada en el Centro de Biología Molecular Severo Ochoa (CSIC-UAM) bajo la dirección del Dr. Miguel Ángel Alonso Lebrero, Profesor de Investigación del CSIC.

La realización de tesis ha sido posible gracias a una ayuda para contratos predoctorales para la formación de doctores concedida a D. Miguel Bernabé Rubio por el Ministerio de Economía y Competitividad.

RESUMEN/SUMMARY

RESUMEN

El cilio primario es una extensión de membrana altamente conservada que protruye de la superficie apical de la mayoría de las células eucariotas. Su estructura consiste en una membrana ciliar que rodea un armazón de microtúbulos, el axonema, que deriva del centriolo más maduro. Aunque su función ha permanecido desconocida durante mucho tiempo, actualmente se sabe que el cilio primario actúa como un biosensor regulando múltiples rutas de señalización y la homeostasis de los tejidos. Durante los últimos años la relevancia clínica y fisiológica del cilio primario se ha hecho evidente debido a que los defectos en su estructura o su disfunción tienen como consecuencia el desarrollo de un grupo de enfermedades genéticas que se agrupan colectivamente con el nombre de ciliopatías. Entre estas enfermedades destacan la poliquistosis renal, la ceguera, la sordera, la obesidad, y los defectos en el desarrollo embrionario. A pesar de que el riñón es el órgano más frecuentemente afectado por las ciliopatías, la biogénesis del cilio primario se ha estudiado mayoritariamente en tipos celulares no polarizados. Hace casi 50 años se propuso que en los epitelios polarizados, como los de los túbulos renales, el proceso de ciliogénesis tiene lugar exclusivamente en la membrana plasmática, mientras que por el contrario, los fibroblastos ensamblan el cilio de manera intracelular. Utilizado el modelo de células epiteliales polarizadas MDCK, he investigado el desconocido proceso de biogénesis del cilio primario en células epiteliales polarizadas. He observado que el cuerpo medio, una estructura basada en microtúbulos localizada en la parte central del puente intercelular formado entre las dos células hijas durante las etapas finales de la división celular, es heredado por una de las dos células en forma de remanente, el cual se posiciona en la periferia de la membrana apical acumulando maquinaria relevante para la ciliogénesis. Posteriormente, este remanente se mueve sobre la membrana apical reuniéndose con el centrosoma. Una vez que se han juntado estos dos orgánulos, el remanente posibilita la formación del cilio primario. Estos hallazgos revelan un mecanismo biológico que conecta funcionalmente el cuerpo medio con el centrosoma y el cilio primario, los otros dos orgánulos celulares basados en microtúbulos. Además, he investigado el papel de la proteína MAL, un componente de la maquinaria general de transporte apical, en el proceso de ciliogénesis. Los resultados obtenidos indican que MAL es necesaria para la correcta condensación de las membranas en la base del cilio, lo que a su vez, es crucial para la elongación eficiente del citado orgánulo. En resumen, este trabajo establece una nueva ruta de ciliogénesis primaria en células epiteliales renales y confiere importancia a las membranas situadas en la base del cilio primario.

SUMMARY

The primary cilium is a highly conserved membrane extension protruding from the cell surface of most mammalian cells. It consists of a ciliary membrane that surrounds a microtubule-based structure termed the axoneme, which is nucleated from the older of the two centrioles. Although its function has been an enigma for a long time, nowadays it is known to act as a biosensor regulating multiple signaling pathways during development and tissue homeostasis. The physiological and clinical relevance of cilia is evident, since defects in primary cilium function cause a wide spectrum of genetic diseases collectively grouped under the term of ciliopathies. Among the disorders produced by primary cilium dysfunction are cystic kidney disease, blindness, deafness, obesity, and developmental and skeletal abnormalities. The kidney is the organ most frequently affected in ciliopathies. However, despite its importance in the kidney, primary cilium biogenesis has mainly been studied in non-polarized cells. Almost 50 years ago, it was proposed that the process of primary ciliogenesis in polarized epithelia, such as that in kidney tubules, takes place entirely at the plasma membrane, in contrast to fibroblasts that assemble the cilium intracellularly. Using the renal epithelial MDCK cell line, I have investigated the unexplored process of primary cilium biogenesis in polarized epithelial cells. I observed that the midbody, which is a microtubule-based structure that occupies the central part of the intercellular bridge connecting the two sister cells during the final stages of cell division, is inherited by one of the cells as a remnant that localizes at the periphery of the apical membrane, and that accumulates important machinery for cilium biogenesis. The remnant then moves along the apical plasma membrane to a central position to encounter the centrosome. Once the two organelles have met, the remnant enables the centrosome for primary cilium formation. These findings reveal a biological mechanism that functionally links the midbody with the centrosome and the primary cilium, which are the other two main microtubule-based organelles. I have also investigated the role of MAL, a component of the machinery of apical transport, in primary cilium assembly. The results indicate that MAL is required for correct membrane condensation at the ciliary base, which, in turn, is essential for efficient primary cilium elongation. In summary, the work presented establishes a novel pathway of primary ciliogenesis in renal polarized epithelial cells and establishes the importance of the condensation of the membranes at the ciliary base.

INDEX

INDEX

INDEX

GLOSSARY

aPKC: atypical Protein Kinase C

BBSome: Bardet–Biedl Syndrome

Cdc42: Cell division control 42 protein

Crb (Crb3a): Crumbs protein

EHD: Eps15 Homology Domain proteins

EM: Electron Microscopy

ESCRT: Endosomal Sorting Complexes Required for Transport

FAPP2: Phosphatidylinositol-4-phosphate adaptor protein-2

GAP: GTPase Activating Protein

GEF: Guanine nucleotide Exchange Factor

GFP: Green Fluorescent Protein

GP: Generalized Polarization

GPCR: G Protein-Coupled Receptor

GPI: Glycophosphatidylinositol

GTP: Guanine nucleotide triphosphate

GTPases: Guanine nucleotide triphosphatase

HA: Hemagglutinin protein from influenza virus

Hh: Hedgehog

IFT: Intraflagellar Transport complex

IMCD3: Inner Medullary Collecting Duct 3 cells

Inpp5e: Inositol polyphosphate-5-phosphatase E

JBTS: Joubert syndromes

KD: Knock-Down

MAL: Myeloid and Lymphocyte protein

Mark4: Microtubule affinity regulating kinase 4

MDCK: Madin-Darby Canine Kidney cells

MEF: Mouse Embryonic Fibroblast

MKS: Meckel syndrome

MKLP1: Mitotic Kinesin-like Protein 1

NPHP: nephronophthisis

Odf2: Outer dense fiber protein 2

PDGF: Platelet-derived growth factor

PDZ: post synaptic density protein (PSD95), *Drosophila* disc large tumor suppressor (Dlg1), and zonula occludens-1 protein (zo-1)

PIPKIγ: Iγ Phosphatidylinositol 4-phosphate 5-kinase

PIPs: phosphoinositides

PLP: Myelin proteolipid protein

PRC1: Protein Required for Cytokinesis 1

PtdIns: Phosphatidylinositol

RPE1: Retinal Pigment Epithelial cells

Smo: Smoothend

SNARE: Soluble N-ethylmaleimide sensitive factor attachment protein receptor

Ttbk2: Tau tubulin kinase-2

TUSP: Take-Up by Suction Pressure

ZO-1: Zonula Occludens-1

INTRODUCTION

1. Types and general functions of cilia

Cilia are highly conserved microtubule-based membrane extensions that protrude from the cell surface of most eukaryotic cells (Goetz and Anderson, 2010; Ishikawa and Marshall, 2011; Satir and Christensen, 2007). They are organized around a central microtubular scaffold, termed the axoneme, which derives from the centrosome and is surrounded by the ciliary membrane. Cilia are classified as 9+2 and 9+0, according to the number of microtubules associated with the axoneme. The numbers indicate the number of peripheral doublets (nine) and the presence (two) or absence (zero) of central microtubule singlets. In the case of 9+2 cilia, protein complexes known as radial spokes connect the central pair and the outer doublets. Mammalian cilia have also customarily been divided into two categories: motile and non-motile cilia. Motile cilia contain outer and inner arms formed by the motor protein dynein in each microtubule doublet. 9+2 cilia are usually called flagella when they are motile and long (<10 μm). Nonmotile cilia lack dynein arms and can adopt the 9+2 or 9+0 configuration (Fig. 1a).

Cilia whose function is to move mucus or other fluids (Fig. 1b), such as multiciliated cells of conducting airways, ependymal cells and the fallopian tubes (Brooks and Wallingford, 2014), and those involved in cell motility, such as the single flagellum of spermatozoa and trypanosomes (Lindemann and Lesich, 2016; Oberholzer et al., 2007) or the two flagella of the green algae *Chlamydomonas*, contain motile 9+2 cilia with dynein arms (Rosenbaum and Witman, 2002). Nonmotile 9+2 cilia without dynein arms are found in some sensory cells (Fig. 1b), such as mammalian olfactory neurons, which have 10-30 cilia, and the hair cells of the inner ear whose cilia, known as kinocilia, are involved in mechanotransduction (Falk et al., 2015; Jenkins et al., 2009). 9+2 cilia vary in length ranging from 3 to 10 μm in multiciliated cells, from 50 to 150 μm for sperm flagella and to 200 μm in the case of olfactory cilia.

Cells in the ventral node, which is an embryonic cavity at the midline filled with extra-embryonic fluid, contain a single motile cilium, referred to as the nodal cilium, which has a 9+0 pattern and contains dynein arms (Fig. 1a, b). Nodal cilia rotate to generate unidirectional leftward fluid flow, which is essential for breaking the left-right symmetry of internal organs in vertebrates during embryogenesis (Shinohara et al., 2015; Yoshiba and Hamada, 2014).

Cells of almost all mammalian tissues have a single copy of a non-motile cilium, referred to as the primary cilium, which has a 9+0 structure and no dynein arms (Fig. 1a, b). The

primary cilium typically attains a length of 3-10 μm and is found in quiescent and differentiated cells (Wheatley et al., 1996).

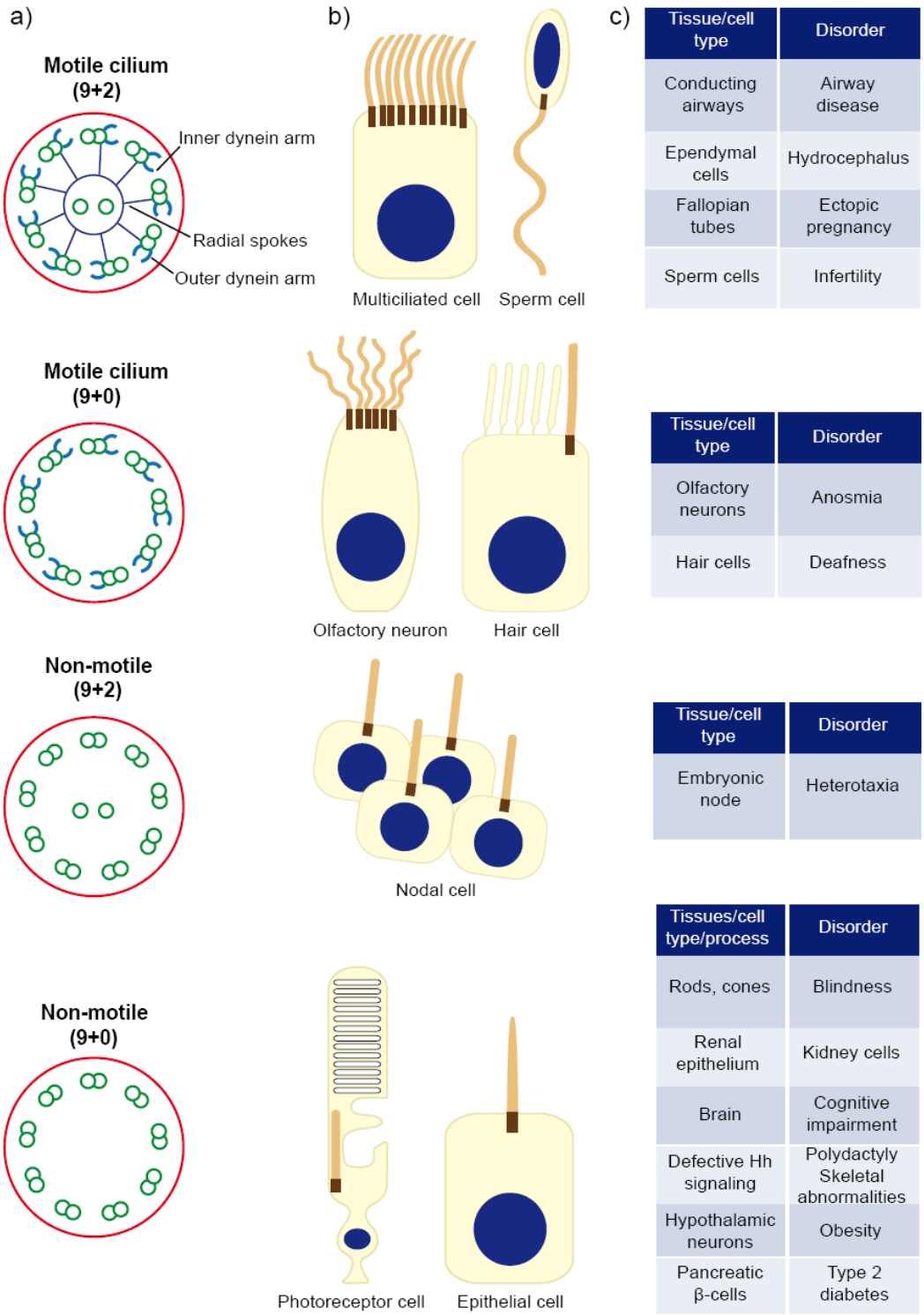

Tissue/cell type	Disorder
Conducting airways	Airway disease
Ependymal cells	Hydrocephalus
Fallopian tubes	Ectopic pregnancy
Sperm cells	Infertility

Tissue/cell type	Disorder
Olfactory neurons	Anosmia
Hair cells	Deafness

Tissue/cell type	Disorder
Embryonic node	Heterotaxia

Tissues/cell type/process	Disorder
Rods, cones	Blindness
Renal epithelium	Kidney cells
Brain	Cognitive impairment
Defective Hh signaling	Polydactyly Skeletal abnormalities
Hypothalamic neurons	Obesity
Pancreatic β-cells	Type 2 diabetes

Figure 1. **Types of cilium**. **a**) Schematic of distinct types of cilium as seen in cross-section. **b**) Examples of cell types harboring each type of cilium. **c**) Examples of disorders associated with the dysfunction of the distinct types of cilium.

2. Primary cilium function

The role of the primary cilium is well known in photoreceptor cells, in which the cilium adopts a specialized structure that concentrates visual pigments for photon absorption (Pearring et al., 2013). Although the primary cilium was first described more than a century ago (Zimmerman, 1898), its function in all other cells has been an enigma for a long time. Nowadays, in addition to photosensors, a fundamental role has been established for primary cilia as mechanosensors and biochemical sensors (Ishikawa and Marshall, 2011; Malicki and Johnson, 2017; Zimmerman and Yoder, 2015).

Mechanosensation refers to the physical sensation of flow, pressure, touch or vibration. Much of our understanding of the mechanosensory functions associated with cilia derives from studies of renal epithelial cells, in which the force of luminal fluid flow is sensed by primary cilia (Ishikawa and Marshall, 2014). The primary cilia of renal epithelial Madin-Darby canine kidney (MDCK) cells become deflected through a combination of bending and pivoting (Battle et al., 2015). Primary cilia perform cell-directed active centrosome and cilia movements that seem to be mediated by internal activity in the cell and involve fluctuations in the actin–myosin network that act above the pivot point. Ciliary bending and pivoting can both trigger membrane channels, and are able to induce Ca^{2+} influx through the action of polycystin-2 (Battle et al., 2015). Polycystin-2 is a transient receptor potential family Ca^{2+} channel that associates with polycystin-1 at the ciliary membrane. Mutations of polycystin-1 and polycystin-2 both cause autosomal dominant polycystic kidney disease (Zhou, 2009). It has been reported that, upon shear stress, cilia import extracellular Ca^{2+}, raising their ciliary concentration (DeCaen et al., 2013; Delling et al., 2013; Praetorius et al., 2003; Praetorius and Spring, 2001). Increased Ca^{2+} ciliary levels have been proposed to act as a second messenger to regulate multiple downstream processes in primary cilia (Delling et al., 2013; Doerner et al., 2015; Praetorius, 2015; Takao et al., 2013; Zimmerman and Yoder, 2015). However, although the role of Ca^{2+} in mechanotransduction had been generally accepted, it has recently been challenged on the grounds that cilia-specific Ca^{2+} influxes have not been observed in physiological or even highly supraphysiological levels of fluid flow in primary cilia of cultured kidney epithelial cells, the thick limb of the ascending kidney tubule, crown cells of the embryonic node, hair cells, and several cell lines (Delling et al., 2016). Therefore, the induction of Ca^{2+} flow as the mechanism of primary cilia in transducing mechanosensation is being reexamined (Hofherr and Kottgen, 2016).

Primary cilia act as biochemical sensors when they respond to hormones or other soluble factors capable of triggering a number of signaling cascades. Primary cilia transduce environmental stimuli through surface receptors specifically localized on the ciliary membrane, and regulate signaling pathways important for development, cell proliferation, differentiation, survival and migration (Ishikawa and Marshall, 2011; Malicki and Johnson, 2017; Zimmerman and Yoder, 2015). Hedgehog (Hh) proteins regulate the development of a wide range of metazoan embryonic and adult structures, and disruption of Hh signaling pathways results in human disease (Briscoe and Therond, 2013; Robbins et al., 2012). Platelet-derived growth factor (PDGF)-α signaling, which controls cell migration, proliferation and survival, also occurs in the primary cilia since its receptor localizes to primary cilia in fibroblasts, where PDFG-α activates it and triggers the activation of downstream signaling machinery (Schneider et al., 2005). Besides, the primary cilium plays important roles in regulating other signaling pathways such as canonical and non-canonical Wnt pathways (May-Simera and Kelley, 2012; Wallingford and Mitchell, 2011) and Hippo pathway (Aguilar et al., 2014; Habbig et al., 2011), both being master regulators of developmental and morphogenetic processes (Wilcockson et al., 2016; Zhao et al., 2010). In addition, G protein-coupled receptors (GPCRs) of hormones, peptides, lipids and neurotransmitters, including for instance those of dopamine, serotonin, neuropeptide Y and somatostatin, reside in primary cilia and use cilia for signaling (Hilgendorf et al., 2016; Schou et al., 2015).

2.1 Ciliopathies

Given the importance of cilia, it is not surprising that ciliary dysfunction by mutation in cilia-related genes causes a great variety of disorders in humans (Fig. 1c). If the mutated gene affects motile 9+2 cilia the disorders caused are related to mucociliary clearance (bronchitis, rhinosinusitis), hydrocephalus and infertility; defective functioning of nodal cilia causes heterotaxia (the abnormal arrangement of internal organs in the chest and/or abdomen). Dysfunction of nonmotile cilia produces defects in signaling that result in a large variety of symptoms (renal and liver cysts, blindness, cognitive impairment, deafness, anosmia, polydactyly, skeletal abnormalities, obesity, etc.). Depending on the gene(s) affected, these alterations combine to produce numerous heterogeneous human developmental and degenerative genetic diseases, collectively known as ciliopathies that affect nearly every major body organ (Fliegauf et al., 2007; Hildebrandt et al., 2011; Novarino et al., 2011). Ciliopathies are characterized by overlapping phenotypes that may include multiple symptoms caused by

the dysfunction of motile and/or primary cilia. For instance, primary cilia dyskinesia and Kartagener syndrome are caused by defective motile cilia (Zariwala et al., 2007), whereas in other ciliopathies, such as nephronophthisis (NPHP), Meckel (MKS) and Joubert syndromes (JBTS), only primary cilia function tends to be affected (Tobin and Beales, 2009). Largely due to their medical relevance, there has been an immense increase in research in recent times aimed at better understanding the structure, mechanisms of assembly, maintenance and function of primary cilia.

3. Structure of primary cilia

The general structure of cilia is evolutionarily conserved, despite the obvious difference between the distinct types of axoneme (Mitchell, 2017). In contrast to specialized cilia such as those in photoreceptor cells, the primary cilium of epithelial cells, fibroblasts, muscle cells, neurons, etc., adopts a similar morphology and size (Fig. 2) (Mizuno et al., 2012; Satir and Christensen, 2007).

Primary cilia have a basal body, which consists of the older of the two centrioles, also known as the mother centriole in the centrosome, and the associated accessory structures (Garcia and Reiter, 2016; Vertii et al., 2016a). These accessory structures include transition fibers, basal feet and ciliary rootlets (Garcia and Reiter, 2016; Vertii et al., 2016a; Vertii et al., 2016b). Transition fibers and basal feet are ultrastructurally similar to the distal and subdistal appendages, respectively, of the mother centriole. Transition fibers emerge from the central microtubule of each triplet of the basal body, and are involved in docking the basal body to the plasma membrane (Wei et al., 2015). Basal bodies have up to nine subdistal appendages, but only one or two basal feet. The basal feet further differ from the subdistal appendages in that they are larger and more electron-dense (Bornens, 2002). The outer dense fiber protein 2 (Odf2)/Cenexin, a component of the distal and subdistal appendages, is essential for the formation of transition fibers and basal feet (Tateishi et al., 2013). The rootlet is a thick (80–100 nm) striated bundle of filaments made of the protein rootletin (Yang et al., 2002). Basal feet, which anchor microtubules, and striated rootlets, which project from the proximal end of the basal body and extend close to the nucleus, provide structural support to the cilium.

Beyond the basal body is the transition zone, which is an intermediate region between the basal body and the axoneme (Benzing and Schermer, 2011; Szymanska and Johnson, 2012). The transition zone is distinguished by the shift from triplet microtubules in the basal body to axonemal doublets, and by the presence of characteristic scallop-like structures at

the ciliary surface, and of inner structures, known as Y-links, that appear Y-shaped under electron microscopy (EM) and connect the outer doublet microtubules to the overlying ciliary membrane (Garcia-Gonzalo and Reiter, 2012, 2017; Reiter et al., 2012). The transition zone houses a network of two biochemically distinct protein complexes involved in ciliopathies. One of the modules spans the membrane and contains many of the proteins (Tctn1-3, MKS1, B9d1, B9d2, Cep290, Ahi and the transmembrane proteins Tmem67, Tmem216, Tmem17, Tmem231, Tmem107, etc.) involved in MKS and JBTS. The second module, called the NPHP module, includes three proteins (Nphp1, Nphp4 and Rpgrip1l) encoded by genes mutated in NPHP, and is proximal to the axoneme. The collaboration of the two modules explains the overlapping phenotypes seen in MKS, JBTS and NPHP, in which proteins belonging to these modules are involved (Li et al., 2016; Yee et al., 2015).

Following the transition zone, the axoneme of primary cilia is constructed from the elongation of the nine parallel doublet microtubules formed at the transition zone (Jana et al., 2014; Li et al., 2012). As the axoneme becomes longer it loses microtubules and the doublets transform into singlets. Singlets are also lost gradually in such a way that the tip of the cilium often contains only a few of them. The axoneme is subject to numerous post-translational modifications, including acetylation, detyrosination, glutamylation and glycylation, which are related to microtubule structure, flexibility and function (Portran et al., 2017; Wloga et al., 2016).

Ciliary growth is regulated at the tip by the receipt of tubulin and other axonemal precursors that elongate the axoneme and by their removal during axoneme disassembly. Defined structures at the tip were reported for the 9+2 flagella of *Chlamydomonas* and of other organisms (Dentler, 1980; Dentler and Rosenbaum, 1977; Portman et al., 1987; Satir, 1968). These structures cap the central singlet microtubules at their tip and are involved in cargo loading and unloading, and signal transduction (Sloboda, 2005). However, such well-defined structures have not been detected in primary cilia of mammalian cells. Not only is the tip of primary cilia the place where ciliary growth is regulated, as in 9+2 cilia, but also it is involved in cell signaling. Kif7, a kinesin-4 family protein that is a conserved regulator of the Hh signaling pathway and a human ciliopathy protein, binds to the distal end of axonemal microtubules and organizes a specialized compartment where the activity of the Gli family of Hh transcription factors is regulated (Gorojankina, 2016; He et al., 2014; Pusapati and Rohatgi, 2014). Recent evidence from *Chlamydomonas* flagella and *Caenorhabditis elegans* and mammalian primary cilia showed that ciliary signaling is also regulated at the ciliary tip by shedding receptors and other material in the form of extracellular vesicles (Cao et al., 2015;

Nager et al., 2017; Phua et al., 2017; Wang et al., 2014; Wood et al., 2013; Wood and Rosenbaum, 2015). Cilia typically begin to form during the G_0 phase of the cell cycle and begin to disassemble as cells re-enter the cell cycle to free the centrosome (Kim and Tsiokas, 2011; Kobayashi and Dynlacht, 2011). While cilia disassembly has for some time been considered to occur solely through resorption (Liang et al., 2016), release of extracellular vesicles also helps to regulate ciliary disassembly and size (Nager et al., 2017; Phua et al., 2017; Wood and Rosenbaum, 2015). In conclusion, although the nature of the tip of primary cilia is not well understood, it appears to act as a hub that coordinates many important ciliary functions.

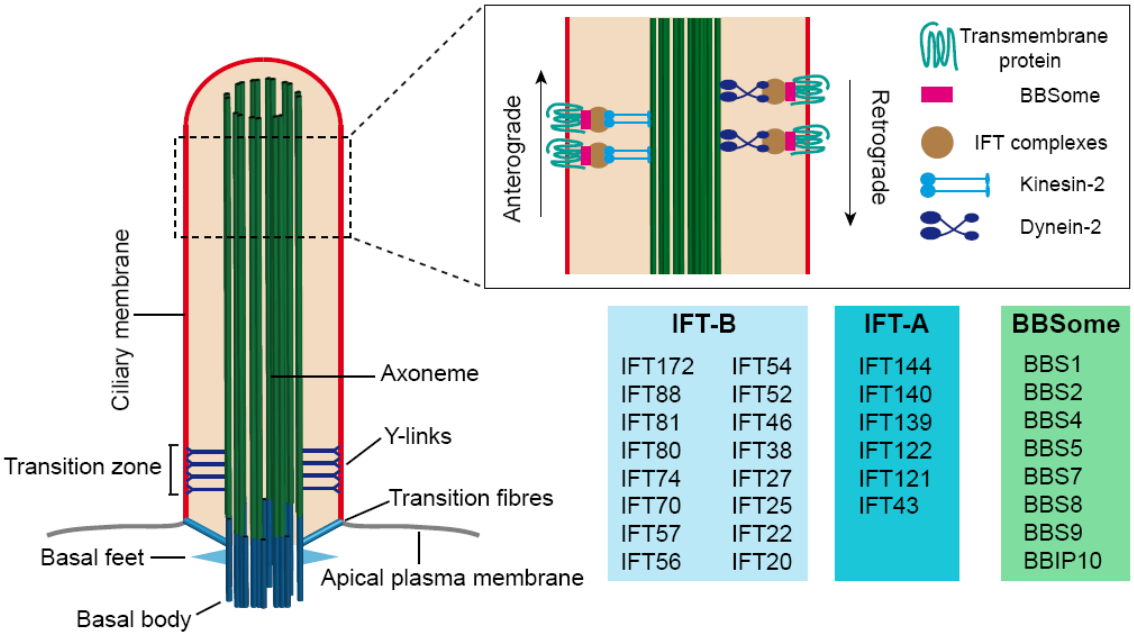

Figure 2. General structure of the primary cilium. The basal body is attached to the ciliary membrane by the transition fibers. The axoneme constitutes the backbone of the cilium and is surrounded by the ciliary membrane, which is continuous with the plasma membrane. IFT is carried out by the IFT-A and -B complexes powered by dynein-2 and kinesin-2 motors, respectively, and with the participation of the BBSome complex.

4. Protein machinery for ciliary growth, targeting and transport

Cilia require general machinery for the processes of licensing the centrosome to initiate cilium formation, and protein transport along the ciliary membrane. These general tasks are performed by the regulators of the centriolar protein Cp110 and by intraflagellar transport (IFT) machinery, respectively. The BBsome complex is also responsible for the traffic of certain receptors at the primary cilium. Rab-family proteins control membrane trafficking during primary cilium initiation and the targeting of cargo to the ciliary base once the cilium has formed.

4.1 The protein CP110 and its regulators

Well known negative regulators of ciliogenesis, such as centriolar protein Cp110 and its network of interacting partners, have been studied in the human bone osteosarcoma U2OS cell line, as well as in NIH-3T3 fibroblasts and retinal pigment epithelial (RPE)-1 cells (Spektor et al., 2007; Tsang et al., 2008; Tsang and Dynlacht, 2013). Cp110 localizes at the mother and the daughter centrioles, blocking primary cilium formation. It interacts with Cep97 and Cep290, and these interactions are essential for suppressing primary cilium formation (Spektor et al., 2007; Tsang et al., 2008). Cp110 removal requires the activity of positive ciliary regulators, such as Tau tubulin kinase-2 (Ttbk2), whose knockout inhibits Cp110 removal from the basal bodies in mouse embryonic fibroblasts (MEFs) (Goetz et al., 2012). Cep164, which is present in transition fibers, is essential for ciliogenesis and for recruiting Ttbk2 to the basal body (Cajanek and Nigg, 2014). Microtubule affinity regulating kinase 4 (Mark4) is also required for Cp110 removal and accumulates at the basal body as Cp110 is displaced (Kuhns et al., 2013). These findings indicate that disappearance of Cp110 from the mother centriole is crucial for initiating primary cilium biogenesis. Cp110 removal seems universally required for initiating the ciliation process since cells that normally do not form a primary cilium, such as T lymphocytes, assemble one when Cp110 expression is knocked down (Prosser and Morrison, 2015).

4.2 Intraflagellar transport (IFT) machinery.

Soluble and membrane proteins are transported along the primary cilium by the IFT machinery (Bhogaraju et al., 2013; Rosenbaum and Witman, 2002; Taschner and Lorentzen, 2016). IFT is highly conserved and is required for the assembly of cilia. It is formed of two multisubunit complexes: IFT-A and IFT-B, comprising 6 and 16 subunits, respectively (Fig. 2). Mutations in IFT proteins can cause several ciliopathies (Braun and Hildebrandt, 2017). Whereas IFT-B mediates anterograde movement (from the cell body to the cilium) of ciliary proteins, IFT-A directs retrograde transport (from the cilium to the cell body) and anterograde transport of certain proteins such as Arl13b and Smo. The IFT-B complex transports cargo to the ciliary tip with the participation of kinesin-2 motors, whereas turnover products or signaling components destined for internalization are returned to the cell body via the IFT-A complex propelled by cytoplasmic dynein-2 (Taschner and Lorentzen, 2016). The switch of the machinery for anterograde and retrograde IFT and their respective motors takes place at the ciliary tip. In *Chlamydomonas*, it has been demonstrated that each microtubule doublet is used as a bidirectional double-track railway in such a way that

anterograde IFT trains move along B-microtubules, and retrograde trains move along A-microtubules (Stepanek and Pigino, 2016). Thus, the microtubule doublet geometry provides direction-specific rails to coordinate the bidirectional transport of ciliary components.

4.3 The BBSome

Bardet–Biedl syndrome (BBS) is a compound phenotype disorder exhibiting cystic kidneys, obesity, mental retardation, hypogonadism, heterotaxia, polydactyly and retinal degeneration (Hernandez-Hernandez and Henkins, 2015; Sheffield, 2010). The BBSome is a multimeric protein complex composed of seven highly conserved BBS proteins (BBS1, BBS2, BBS4, BBS5, BBS7, BBS8 and BBS9) and BBIP10, each of which is present in stoichiometric amounts (Jin and Nachury, 2009). In humans, defects in the BBSome result in BBS (Sheffield, 2010). Live analysis of cargo transport in olfactory sensory neurons revealed that the BBSome complex moves in association with IFT trains and cargo through cilia, suggesting that the BBsome acts as a cargo adaptor between membrane cargoes and the IFT machinery (Nachury et al., 2007).

The BBSome was initially implicated in GPCR delivery to cilia (Berbari et al., 2008; Jin et al., 2010; Loktev and Jackson, 2013). However, it is now known to be important in retrograde trafficking. The BBsome regulates the removal of GPCRs (Domire et al., 2011; Eguether et al., 2014; Liew et al., 2014), polycystin-2 (Xu et al., 2015), and membrane-associated proteins from cilia (Lechtreck et al., 2009; Lechtreck et al., 2013). The conflict resulting from the role of the BBsome in anterograde transport is explained by the observation that when membrane receptors fail to undergo BBSome-mediated retrieval from the cilium back into the cell, they are removed by ectocytosis giving the impression that their sorting to the cilium is defective (Nager et al., 2017).

4.4 Small Rab GTPases

In a screening of 39 human GTPase-activating proteins, GAPs for Rab8a, Rab17 and Rab23 were identified as necessary for primary cilium formation in RPE-1 cells (Yoshimura et al., 2007). Rab8a was the only one of the three GTPases in that study found to localize to the cilium. Rab8a is recruited to the centrosome by a direct interaction with Odf2/Cenexin and is required for primary ciliogenesis (Westlake et al., 2011; Yoshimura et al., 2007). Although they were not identified in the original screening, Rab11 and Rab10 have also been implicated in this process (Babbey et al., 2010; Knodler et al., 2010; Westlake et al., 2011). Two centrosome appendage proteins, centriolin and Odf2/Cenexin, regulate the association of Rab11 vesicles with the distal part of the mother centriole (Hehnly et al., 2012). The GTP-

bound form of Rab11 interacts directly with its downstream effector Rabin8 to target it to the centriole and stimulates its guanine nucleotide exchange factor (GEF) activity toward Rab8 in RPE-1 cells (Knodler et al., 2010). Rabin8, in turn, interacts with the membrane-tethering transport protein particle II complex, which is a GEF for Rab11 (Thomas and Fromme, 2016). It has been proposed that, similar to the Rab5-Rab7 switch (Rink et al., 2005), Rab11 vesicles are converted into a Rab8 preciliary vesicle with the participation of Rabin8 and transport protein particle II complex (Westlake et al., 2011). Knockdown (KD) of Rab11, Rabin8 or Rab8 inhibits ciliogenesis, highlighting the importance of this signaling cascade (Knodler et al., 2010; Westlake et al., 2011). Despite evidence supporting a crucial role for Rab8 in primary cilium formation in cultured cells, the absence of its two isoforms, Rab8a and Rab8b, in Rab8a and Rab8b double-knockout mice does not disturb ciliogenesis of olfactory epithelium, photoreceptors and MEFs (Sato et al., 2014). However, the additional KD of Rab10, but not of Rab13, in MEFs from these mice greatly reduces the percentage of ciliated cells (Sato et al., 2014). This finding suggests that the Rab8a, Rab8b and Rab10 proteins are simultaneously, rather than individually, involved in ciliogenesis.

5. Polarity proteins for cilium formation

In polarized epithelial cells, tight junctions allow the generation of well-defined apical and basal membrane domains. Cilium elongation is the final event of the polarization process in these cells. Thus, many components of the polarity machinery, such as those involved in apical membrane biogenesis, establishment of cell junctions, and lumen formation, are directly linked to cilium formation. The exocyst, which is a protein complex previously implicated in polarized transport in epithelial cells, and the Par complex, which is involved in acquisition of cell polarity, are important for ciliogenesis in polarized epithelial MDCK cells and kidney tubulogenesis.

5.1 The exocyst complex

Tethering complexes are large protein complexes that establish long-range interactions between donor and acceptor membranes to capture transport vesicles and enable their fusion with acceptor organelles before contacts between v- and t-soluble N-ethylmaleimide sensitive factor attachment protein receptors (SNAREs) occur (Yu and Hughson, 2010). In addition to capturing vesicles, tethering complexes appear to regulate the spatial and temporal assembly of the SNARE complex.

The exocyst is an eight-subunit (Sec3, Sec5, Sec6, Sec8, Sec10, Sec15, Exo70, and Exo84) complex (Hertzog and Chavrier, 2011; Munson and Novick, 2006) that delineates its function

as a tethering complex in the trafficking of vesicles from a post-Golgi compartment, the recycling endosome, to the basolateral plasma membrane in polarized epithelial cells (Heider and Munson, 2012).

The exocyst has been shown to be a downstream effector of exocytic Rab GTPases (Heider and Munson, 2012). The exocyst subunit Sec15 directly interacts with Rab11 and Rabin8 and allows activation of Rab8 (Wu et al., 2005; Zhang et al., 2004). The exocyst subunit Sec10 localizes to the primary cilium (Polgar et al., 2015; Zuo et al., 2009). Consistent with the role of the exocyst in primary ciliogenesis, KD of the exocyst component Sec10 leads to shorter cilia, whereas its overexpression leads to elongated cilia in MDCK cells. In addition, confirming the importance of Sec10, Sec10-knockout mice have defects in primary cilium assembly.

5.2 The Par complex and Crumbs

The Par complex consists of Par3, Par6, atypical protein kinase C (aPKC), and the small Rho-family GTPase cell division control 42 protein (Cdc42). In epithelial cells, the Par complex has been shown to play a role in regulating tight junction formation (Joberty et al., 2000). Par3, Par6 and aPKC localize to the cilia of MDCK and inner medullary collecting duct 3 (IMCD3) cells, and Par3 and aPKC activity have been shown to be essential for efficient primary cilium formation in MDCK cells (Fan et al., 2004; Sfakianos et al., 2007). In addition, the coiled-coil domain of Par3 interacts with Kif3a, and was demonstrated to be essential for ciliogenesis (Sfakianos et al., 2007).

Cdc42, a component of the Par complex, interacts with exocyst subunit Sec10 and colocalizes with Sec10 at the primary cilium (Zuo et al., 2011). Cdc42 KD inhibits ciliogenesis and ciliary targeting of polycystin-2. Moreover, depletion of Cdc42 affects the ciliary localization of Sec8, indicating that Cdc42 function is necessary for targeting the exocyst to the primary cilium. Moreover, Sec10 directly interacts with the Par complex protein Par6, which itself associates with Cdc42. This observation led to the proposal that the exocyst complex is targeted to the primary cilium by Cdc42 and is then stabilized by binding to the Par complex via the Sec10-Par6 interaction (Fig. 3). Once it has become stabilized at the primary cilium, the exocyst targets and docks vesicles carrying ciliary proteins, such as polycystin-2, by interacting with Rab8 (Zuo et al., 2011).

Crumbs (Crb3a), which is a transmembrane protein that plays an important role in the biogenesis of apical membrane and that is a key component in cell polarization (Hurd et al., 2003), localizes to the primary cilium of MDCK and IMCD3 cells and is critical for primary

cilium assembly (Fan et al., 2004). Crb3a directly interacts with the post synaptic density protein (PSD95), *Drosophila* disc large tumor suppressor (Dlg1), and zonula occludens-1 protein (zo-1) (PDZ) domain of Par6 (Lemmers et al., 2004; Sfakianos et al., 2007). This interaction is necessary for targeting Crb3a to the primary cilium, indicating that Par complex might act as an adaptor for targeting membrane proteins to the ciliary membrane via Kif3a (Sfakianos et al., 2007). Therefore, the Par complex is required for targeting both Crb3a and the exocyst complex to the primary cilium via Par6 and Cdc42, respectively (Fig. 3).

As the ciliary membrane is a subdomain of the apical membrane, ciliary and apical trafficking are tightly connected. Several proteins involved in apical transport, including annexin-13, caveolin-1, galectin-3, syntaxin-3, syntaxin-2 and the myeloid and lymphocyte (MAL) protein, are shown to be involved in ciliogenesis (Reales et al., 2015; Takiar et al., 2012; Torkko et al., 2008). This finding is further evidence of the participation of the machinery for apical membrane morphogenesis in primary cilium biogenesis and strengthens the relationship between the two processes.

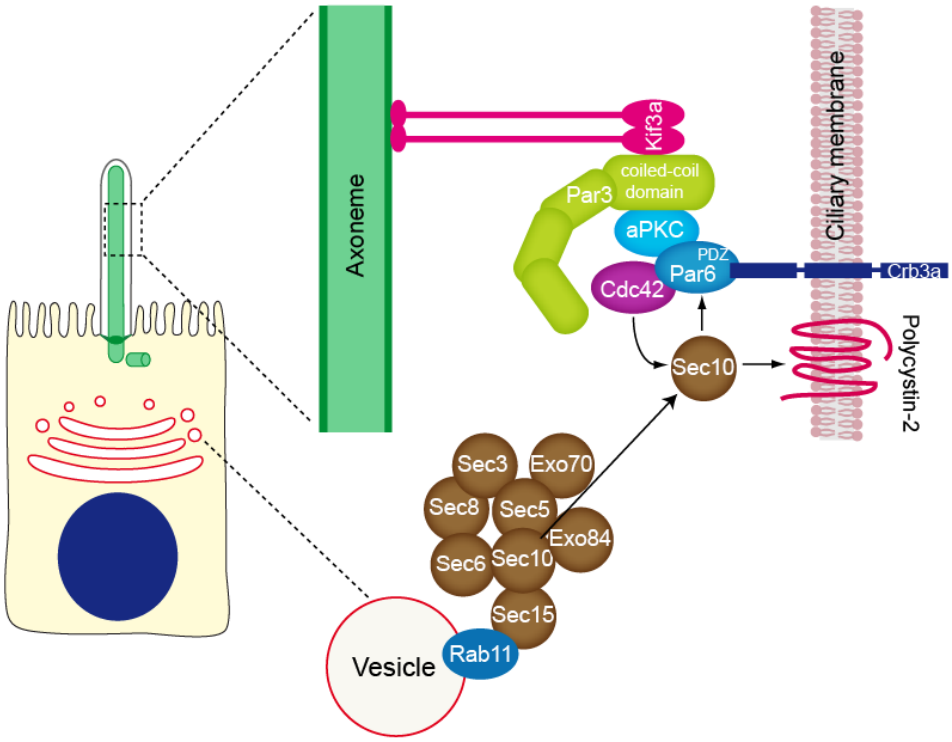

Figure 3. Multi-protein complexes involved in polarized trafficking and cell polarity implicated in primary cilium formation by polarized epithelial cells. In addition to their role in polarization process, the exocyst and the Par complexes participate in primary cilium assembly. Par complex consists of Par3, Par6, aPKC and Cdc42. The motor Kif3a targets the Par complex to the ciliary axoneme through interaction with the coiled-coil domain of Par3. The Par complex has been proposed to be an adaptor for targeting the transmembrane protein Crb3a to the ciliary membrane through association with the Par6 PDZ domain. Cdc42 is responsible for recruitment of exocyst complex, which targets important cargo, such as polycystin-2, to the cilium.

6. Pathways of primary ciliogenesis

Despite the evolutionary conservation of the ciliary structure and ciliogenic machinery, cilia in different cell types and tissues are not created equal. The pioneering work of Sorokin (Sorokin, 1968) established that primary ciliogenesis proceeds by two distinct pathways, depending whether the position of the centrosome in the cell is near the nucleus or close to its apex.

In cells of connective tissues, such as fibroblasts and chondrocytes, the primary cilium is present within an invagination of the plasma membrane, known as the ciliary pocket, whereas in other cell types such as lung or renal cells, it directly protrudes from the plasma membrane and no pocket forms (Benmerah, 2013; Ghossoub et al., 2011; Rohatgi and Snell, 2010). The ciliary pocket is characterized by containing budding clathrin-coated pits, and is thought to mediate ciliary endocytic activity and vesicular trafficking (Molla-Herman et al., 2010; Rattner et al., 2010). It has also been proposed as a compartment of signal transduction including transforming growth factor-β signaling, which plays critical roles in cell-cycle control, migration and differentiation (Clement et al., 2013). In some cell types with ciliary pocket, the pocket is deep and the cilium is almost completely submerged, whereas in other cell types the pocket is shallow and the cilium is mostly exposed to the extracellular environment (Mazo et al., 2016; Satir and Christensen, 2007; Sorokin, 1962). Cells without a ciliary pocket or with a shallow one are free to sense motion, a process crucial for mechanosensation (Galati et al., 2016).

The presence or absence of the ciliary pocket appears to be a consequence of the route of primary cilium assembly used and, therefore, of the position of the centrosome (Benmerah, 2013; Rohatgi and Snell, 2010). When the centrosome is near the nucleus ciliogenesis starts intracellularly and finishes at the plasma membrane, generating a pocket, whereas when the centrosome is close to the plasma membrane the process takes place entirely at the plasma membrane and no pocket appears. The first route is referred to as the intracellular or "classic" pathway, whereas the second route is known as the alternative pathway (Fig. 4).

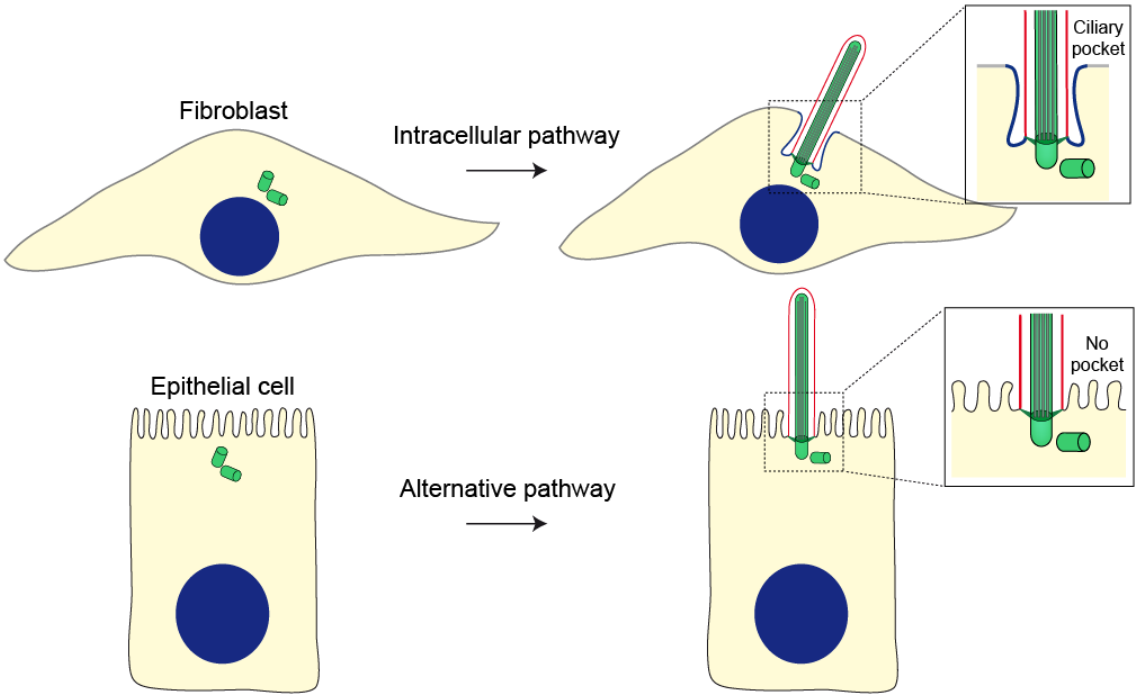

Figure 4. Routes of primary ciliogenesis. The position of the centrosome, near the nucleus or close to the plasma membrane, and the presence or absence of a ciliary pocket predicts the type of pathway used for primary ciliogenesis. Fibroblasts and polarized epithelial cells are shown as examples of cells that use the intracellular and alternative routes, respectively.

The process of primary ciliogenesis by the intracellular route was investigated in great detail in the seminal EM work of Sorokin (Sorokin, 1962), who analyzed the process in fibroblasts and smooth muscle cells. Primary cilium biogenesis has been recapitulated entirely by EM analysis of cultured cells such as RPE-1 cells and NIH-3T3 fibroblasts (Baron Gaillard et al., 2011; Cajanek and Nigg, 2014; Kuhns et al., 2013; Lu et al., 2015; Tucker et al., 1979). Primary cilium formation in these cells starts intracellularly with the docking of small cytoplasmic vesicles to the mother centriole (Fig. 5). The distal appendage protein Cep164 and the distal centriolar protein Talpid3 are indispensable for the docking of these vesicles (Schmidt et al., 2012). The origin of those vesicles is unclear, although they are presumably generated in the Golgi and recycling endosomes (Pedersen et al., 2008; Sánchez and Dynlacht, 2016), and in embryonic neocortical stem cells they appear to derive from a previous ciliary membrane (Paridaen et al., 2013). The vesicles associated with the mother centriole then fuse, generating a large ciliary vesicle that encapsulates the nascent axoneme. The membrane-shaping proteins Eps15 homology domain 1 (EHD1) and EHD3 have been identified as being crucial for the fusion of the small cytoplasmic vesicles in RPE-1 cells and zebrafish (Lu et al., 2015; Yee and Reiter, 2015). SNAP-29, a SNARE membrane fusion regulator and EHD1-binding protein, also intervenes in the fusion process. EHD1 is

required for Cp110 loss from the mother centriole, and in its absence the mother centriole fails to recruit the transition zone protein Cep290 and IFT20, suggesting an important role for EHD1 in the early steps of primary cilium biogenesis. It is of note that Rabin8 colocalizes with EHD1 on preciliary vesicles but does not require EHD1 for accumulation at the mother centriole. Rabin8 activates Rab8 for ciliary extension only after ciliary vesicle assembly (Lu et al., 2015). Hook2, a member of the Hook family of adaptor proteins, is also necessary for the formation of the large ciliary vesicle at the mother centriole (Baron Gaillard et al., 2011). During its conversion to a basal body, at the time that the centriole migrates towards the cell surface for docking, the two internal microtubules of each of the nine triplets at the distal tip of the mother centriole elongate, and the centriolar appendages mature into transition fibers. Ttbk2 or Mark4 KD blocks axoneme extension at this stage by impeding removal of Cp110 (Cajanek and Nigg, 2014; Kuhns et al., 2013). The axoneme then elongates and deforms the ciliary vesicle in such a way that an outer membrane (sheath) and an inner membrane (shaft) surround the incipient axoneme and the distal part of the mother centriole. After transitional fiber-mediated docking of the mother centriole to the plasma membrane, the ciliary vesicle is exocytosed and fuses with the plasma membrane, exposing the nascent cilium to the extracellular milieu. Upon fusion, the sheath gives rise to the ciliary pocket, while the shaft forms the ciliary membrane. Finally, the axoneme continues elongating from its tip to reach its final size and the part proximal to the basal body remains structurally distinct from the rest of the cilium, forming the transition zone (Rohatgi and Snell, 2010) (Fig. 5).

In polarized epithelial cells, however, the centrosome lacks a large ciliary vesicle and it moves to the apical surface before it begins to assemble the axoneme (Fig. 5). Despite its fundamental relevance in polarized epithelia, research on primary ciliogenesis and underlying mechanisms in cells that rely on the alternative route, has remained largely unexplored.

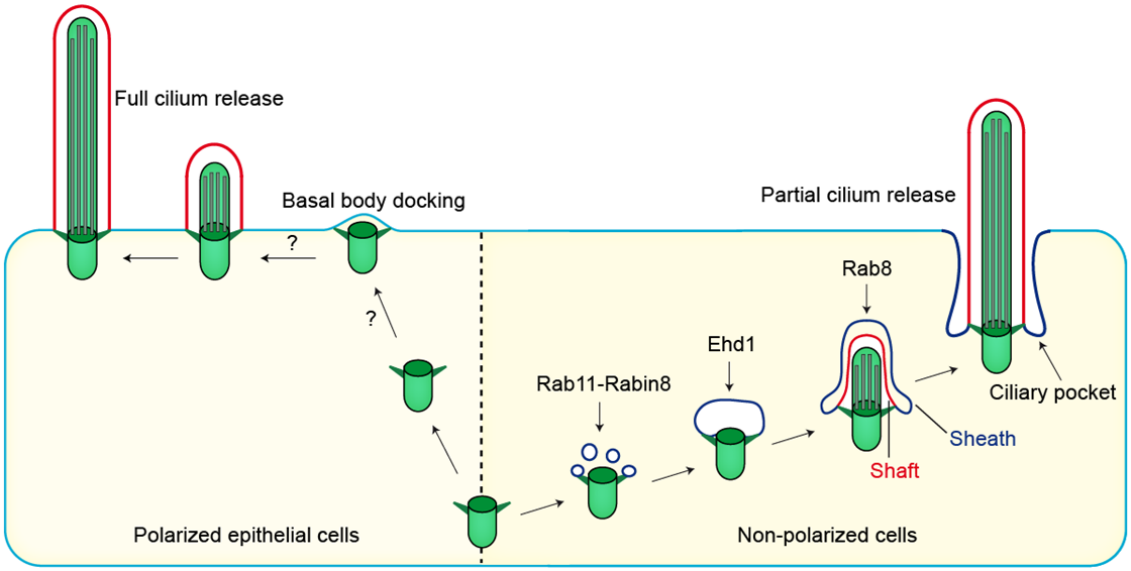

Figure 5. Primary cilium biogenesis. In polarized epithelial cells, such as renal cells, initiation of axoneme assembly takes place entirely at the apical cell surface once the basal body has docked to the plasma membrane. In fibroblasts or smooth muscle cells, ciliogenesis initiates intracellularly with the formation of a large ciliary vesicle at the distal end of the appendages of the mother centriole by fusion of smaller vesicles. The axoneme starts forming intracellularly and, as it grows, deforms the ciliary vesicle and establishes an inner membrane (shaft) and an outer membrane (sheath). The incipient cilium is finally exocytosed and the cilium becomes exposed in the plasma membrane. The sheath gives rise to the ciliary pocket, and the shaft forms the ciliary membrane.

7. The ciliary gate

Cilia have no machinery for protein synthesis, so all ciliary proteins must be synthesized elsewhere in the cell and imported selectively into the cilium. Although the ciliary compartment lacks a limiting membrane that separates it from the cytosol, the base of the primary cilium selectively regulates the entry of proteins (Takao and Verhey, 2016; Verhey and Yang, 2016). Protein segregation is made possible by a functional gate at the ciliary base that is responsible for selective entry of proteins into the primary cilium (Hu and Nelson, 2011; Nachury et al., 2010). The injection of fluorescent dextrans or soluble proteins of different sizes enables a size threshold of 40-60 kD to be defined, above which they cannot gain access into the cilium by simple diffusion. The most proximal line of defense against indiscriminate entry of material into the ciliary compartment is provided by the transition fibers (Reiter et al., 2012; Wei et al., 2015). Selective import of soluble proteins to the cilium appears to involve a ciliary pore complex, analogous to the nuclear pore complex, involving importins and the small GTPase Ran (Kee et al., 2012). Experimental evidence also points to a role for the transition zone, whereby Y-shaped structures and a protein network including proteins encoded by genes related to ciliopathies validate soluble cargo to allow its access into the cilium (Chih et al., 2011; Garcia-Gonzalo et al., 2011).

The ciliary membrane presents continuity with the plasma membrane, but the two membranes have a very different composition (Rohatgi and Snell, 2010). In epithelial IMCD3 cells, Septin2 localizes at the base of the axoneme and its depletion increases the diffusion mobility of ciliary membrane proteins (Hu et al., 2010). This observation led to the proposal that Septin2, probably in collaboration with other septins, forms polymers at the ciliary base that can restrict the access of membrane proteins.

The interfiber space between the transition fibers is too small (<60 nm) for vesicles to pass through and, instead, vesicles transporting membrane proteins dock and fuse with the ciliary base to deliver their cargo. Similar to the sorting signals for transport to other compartments, selective targeting of transmembrane proteins to the cilium requires specific ciliary targeting sequences (Mukhopadhyay et al., 2017; Pazour and Bloodgood, 2008; Sung and Leroux, 2013).

Diffusion between plasma and ciliary membranes is also prevented by interactions between plasma membrane proteins and actin cytoskeleton. It has been reported that some apical membrane proteins such as podocalyxin, are excluded from the base of the cilium and from the ciliary compartment (Francis et al., 2011). In MDCK cells, podocalyxin is prevented to enter the ciliary base and the cilium by interaction of its PDZ-binding domain with Na^+/H^+ exchanger 3 regulatory factor 1, and thus with the apical actin network via ezrin, radixin, and moesin proteins, suggesting the existence of a selective mechanism of retention for certain proteins that participates in the specificity of the ciliary membrane (Francis et al., 2011).

A zone of specialized condensed membranes also exists at the ciliary base of epithelial MDCK cells, as revealed by using the Laurdan probe (Annex I; Fig.6; Vieira et al., 2006). This region has been proposed to serve as a barrier to lipid movement between the ciliary and the apical plasma membranes, although the precise mechanisms by which this phenomenon occurs are unknown. Possible functions postulated for this specialized membrane region also include that it acts to facilitate the docking of the basal body to the plasma membrane, that it regulates the elongation of the ciliary membrane, or that it has a structural role (Reiter and Mostov, 2006; Vieira et al., 2006). It has been revealed that KD of phosphatidylinositol-4-phosphate adaptor protein-2 (FAPP2, also known as PLEKHA8), a protein involved in apical transport, alters the condensation of the apical membrane and reduces primary cilium formation suggesting that there is a link between apical membrane condensation and primary ciliogenesis (Vieira et al., 2006). However, despite their potential importance, the questions of how membrane condensation is regulated at the ciliary base and

what role these specialized membranes play in primary cilium assembly have not yet been addressed.

8. The MAL protein

The MAL protein is a highly hydrophobic protein containing 153 amino acids organized in four transmembrane domains separated by three short hydrophilic segments (Alonso and Weissman, 1987). Its N- and C- terminus ends are oriented towards the cytosol. One of the striking characteristics of the MAL protein is that, like other characterized members of the MAL family, it can be extracted into organic solvents commonly used to isolate cell lipids. This feature is typical of a heterogeneous group of proteins termed proteolipids, such as myelin proteolipid protein (PLP) that exhibit lipid-like properties (Rancaño et al., 1994).

A second characteristic of the MAL protein family is their abundance in highly condensed membrane fractions enriched in glycolipids and cholesterol. These membranes are resistant to solubilization by non-ionic detergents (e.g. Nonidet P-40, Triton X-100) at low temperature due to their high degree of condensation (Kim et al., 1995; Millán et al., 1997; Zacchetti et al., 1995). It has been postulated that this type of lipid organizes into membrane nanodomains, known as membrane rafts, which allow the selective incorporation of certain membrane proteins while excluding most of them (Simons and Ikonen, 1997). According to the prevailing model of biological membrane organization, this specific segregation of proteins enables rafts to function as platforms for the recruitment of specific proteins for selective transport to specific compartments, and for cell signaling processes (Alonso and Millán, 2001; Simons and Toomre, 2000; Simons and Wandinger-Ness, 1990).

9. The function of MAL

The function of MAL has been investigated in the three cell types in which it is mainly expressed: polarized epithelial cells, human T lymphocytes, and myelin-forming cells. In all of them, MAL has been shown to play a role in polarized trafficking mediated by raft membranes. Since the work presented in this thesis has been done in polarized epithelial cells, I will focus on the function of MAL in this type of cell.

9.1 The raft model of apical transport

Glycosphingolipids are highly insoluble in non-ionic detergents at low temperature. This fact, together with the observations that the apical membrane is enriched in these lipids and that some apical proteins become insoluble in non-ionic detergents during their biosynthetic transport, led to the original proposal of the raft model of organization of biological

membranes. According to this, apical proteins associate during their biosynthetic transport with membrane nanodomains or rafts enriched in glycosphingolipids and cholesterol at the *trans*-Golgi network. These nanodomains then vesiculate to form transport carriers destined for the apical surface. The model was supported by the observation that specific apical proteins, such as the influenza virus hemagglutinin (HA) or proteins anchored to the membrane by a glycosylphosphatidylinositol (GPI) moiety, become insoluble in detergent during biosynthetic transport. The original formulation of the raft hypothesis postulated that, like in other membrane transport processes, although the rafts are the platform for the formation of the transport vesicles, they require specific protein machinery for recruitment of specific cargo coat assembly, fission, correct targeting to the apical membrane, and fusion with the acceptor membrane (Simons and Wandinger-Ness, 1990).

9.2 MAL in apical transport

Given that MAL associates with membrane raft fractions and localizes to the Golgi in MDCK cells and in all other cell types examined, MAL was considered to be an excellent candidate for forming part of the machinery of apical transport. To investigate the requirement for MAL in this process, the apical transport of apical raft-associated protein markers, such as the transmembrane hemagglutinin HA protein, GPI-anchored proteins and specific secretory proteins such as thyroglobulin, was compared in the presence or absence of MAL expression. The apical sorting of all of them was dramatically reduced in MAL-silenced cells indicating that MAL is required for apical targeting of these three types of raft-associated protein (Cheong et al., 1999; Martin-Belmonte et al., 2001; Martin-Belmonte et al., 2000; Puertollano et al., 1999).

To determine whether the involvement of MAL in apical transport was restricted to raft-associated proteins or if, by contrast, MAL plays a more general role in apical transport, the sorting of non-raft-associated proteins such as the transmembrane neutrophin receptor (p75) and dipeptidylpeptidase IV proteins and the secretory protein clusterin (p55) was subsequently assessed. As was the case for raft-associated markers, apical transport of these proteins was abrogated in the absence of MAL expression, highlighting MAL as an essential component of the general machinery of apical transport (Martin-Belmonte et al., 2001; Martin-Belmonte et al., 2000). Two alternative models of biosynthetic apical transport can explain these results (Martin-Belmonte et al., 2001). The first proposes that apical proteins detected in or excluded from membrane rafts travel in the same transport vesicle by a pathway directly involving MAL. The second model proposes the existence of two distinct

transport vesicles, one for raft-associated proteins and the other for those that are not associated with rafts. Given that MAL is exclusively present in membrane rafts and that MAL is necessary for the transport of all types of protein, the second model implies that the vesicular transport of non-raft associated proteins would depend on the correct functioning of the raft-mediated route.

10. Molecular basis of MAL protein function

MAL expression in insect cells, which do not endogenously express MAL, resulted in extensive accumulation of cytoplasmic vesicles (Puertollano et al., 1997). This result is consistent with a possible role for MAL in vesicle formation.

In a different set of experiments, it was observed that MAL is directly involved in the recruitment of cargo —HA, Lck, and neurofascin 55— to membrane rafts in T lymphocytes (Antón et al., 2008; Antón et al., 2011), epithelial cells (Puertollano et al., 1999) and myelin-forming cells (Schaeren-Wiemers et al., 2004), respectively. This observation led to the proposal that the main role of MAL is to organize raft lipids to make membrane rafts competent for selective protein recruitment (Fig. 7). This hypothesis was supported by *in vitro* experiments showing that MAL overexpression in culture cells generates giant domains with sorting properties similar to those predicted for rafts in the plasma membrane (Magal et al., 2009). In summary, the current model of MAL function postulates that MAL compartmentalizes membranes by creating raft nanodomains that selectively recruit specific proteins.

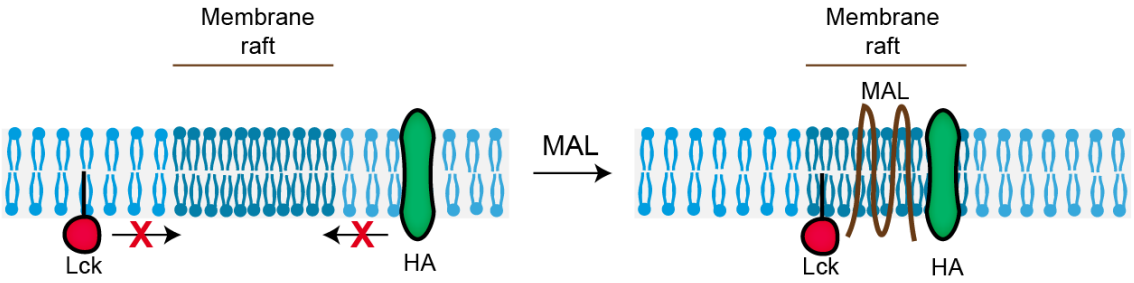

Figure 7. Proposed model for MAL protein function. In the absence of MAL, membrane rafts fail to recruit specific proteins, such as Lck and HA. When MAL is present, it organizes membrane lipids generating competent raft nanodomains that selectively recruit specific proteins, such as Lck or HA.

OBJECTIVES

Considering the physiological relevance of the primary cilium in renal epithelial cells, and taking into account that the process of ciliogenesis remains largely unexplored in this cell type, the **first objective** of this thesis is to investigate the mechanism of primary cilium biogenesis in polarized renal epithelial MDCK cells.

Since the MAL protein has been previously identified as being an element of the machinery of membrane condensation for polarized transport to the apical membrane proteins of epithelial MDCK cells, and because there are condensed membranes at the ciliary base whose origin and function are unknown, the **second objective** of the present work is to investigate whether MAL plays a role in the condensation of the membranes at the ciliary base, and to determine the role of such membranes in primary cilium assembly.

MATERIALS AND METHODS AND RESULTS

Novel role for the midbody in primary ciliogenesis by polarized epithelial cells

Miguel Bernabé-Rubio, Germán Andrés, Javier Casares-Arias, Jaime Fernández-Barrera, Laura Rangel, Natalia Reglero-Real, David C. Gershlick, José J. Fernández, Jaime Millán, Isabel Correas, David G. Miguez, Miguel A. Alonso.

Publicado en julio de 2016 en The Journal of Cell Biology *214 (3)*; págs 259-273.

doi: 10.1083/jcb.201601020

RESUMEN

Hace casi 50 años de que se estableciera que la biogénesis del cilio primario puede ocurrir de dos formas diferentes, dependiendo de si el centrosoma está próximo al núcleo o cerca de la membrana plasmática. Se ha propuesto que en las células mesenquimales, en los fibroblastos y en las células musculares, en las que el centrosoma está cercano al núcleo, el cilio se forma en el interior de la célula. Por el contrario, en células epiteliales polarizadas como las células del riñón, donde el centrosoma se sitúa en cerca de la membrana apical, la biogénesis del cilio tiene lugar enteramente en la superficie apical. La mayoría de los trabajos relacionados con el proceso de ciliogénesis se han realizado utilizando modelos celulares que ensamblan el cilio de manera intracelular. Sin embargo, el mecanismo por el que tiene lugar la biogénesis del cilio primario en la superficie apical es un apartado que ha permanecido prácticamente sin ser examinado. En este trabajo, utilizando el modelo de túbulo distal de riñón de células epiteliales MDCK, hemos investigado el mecanismo de formación del cilio primario por esta ruta tan poco conocida. En este trabajo observamos que el cuerpo medio o el cuerpo de Flemming, una estructura muy electrodensa formada durante las últimas etapas de la división celular, comparte muchas proteínas con el cilio primario. Después de completarse la citocinesis, el remanente del cuerpo medio es heredado por una de las dos células hijas situándose en la membrana apical próximo a las uniones estrechas celulares. También observamos que en un proceso dependiente del área celular, el remanente del cuerpo medio se transloca por la superficie apical desde una posición periférica hasta el centro de la célula. Una vez situado en el centro de la célula, el remanente contacta con el centrosoma facilitando el proceso de ciliogénesis. Para examinar si el contacto entre el remanente del cuerpo medio y el centrosoma es necesario para la formación del cilio, en este trabajo diseñamos un nuevo método para eliminar físicamente el cuerpo medio de la célula, y así poder evaluar los efectos causados por su pérdida. Este

nuevo método consiste en aplicar presión negativa a una pipeta de cristal conectada a un aparato de *patch-clamp*. De esta forma, pudimos evaluar que la pérdida del remanente del cuerpo medio resulta en una reducción significativa del número de cilios en comparación con las células control. Además, desarrollamos un modelo matemático que mediante simulaciones nos permitió averiguar que la conservación del remanente del cuerpo medio y su translocación al centro de la célula son dependientes del área celular. Asimismo este modelo predice que la mayoría de la población celular sigue esta ruta de ciliogénesis. Por tanto, en este trabajo describimos una nueva ruta de ciliogénesis en la que el cuerpo medio es esencial para la formación del cilio primario de las células epiteliales polarizadas renales.

Published July 25, 2016

Novel role for the midbody in primary ciliogenesis by polarized epithelial cells

Miguel Bernabé-Rubio,[1] Germán Andrés,[2] Javier Casares-Arias,[1] Jaime Fernández-Barrera,[1] Laura Rangel,[1] Natalia Reglero-Real,[1] David C. Gershlick,[3] José J. Fernández,[4] Jaime Millán,[1] Isabel Correas,[1] David G. Miguez,[5] and Miguel A. Alonso[1]

[1]Department of Cell Biology and Immunology and [2]Electron Microscopy Unit, Centro de Biología Molecular Severo Ochoa, Consejo Superior de Investigaciones Científicas and Universidad Autónoma de Madrid, 28049 Madrid, Spain
[3]Cell Biology and Neurobiology Branch, Eunice Kennedy Shriver National Institute of Child Health and Human Development, National Institutes of Health, Bethesda, MD 20892
[4]Centro Nacional de Biotecnología, Consejo Superior de Investigaciones Científicas, 28049 Madrid, Spain
[5]Department of Condensed Matter Physics, Instituto de Ciencias de Materiales Nicolás Cabrera and Instituto de Física de la Materia Condensada, Universidad Autónoma de Madrid, 28049 Madrid, Spain

The primary cilium is a membrane protrusion that is crucial for vertebrate tissue homeostasis and development. Here, we investigated the uncharacterized process of primary ciliogenesis in polarized epithelial cells. We show that after cytokinesis, the midbody is inherited by one of the daughter cells as a remnant that initially locates peripherally at the apical surface of one of the daughter cells. The remnant then moves along the apical surface and, once proximal to the centrosome at the center of the apical surface, enables cilium formation. The physical removal of the remnant greatly impairs ciliogenesis. We developed a probabilistic cell population–based model that reproduces the experimental data. In addition, our model explains, solely in terms of cell area constraints, the various observed transitions of the midbody, the beginning of ciliogenesis, and the accumulation of ciliated cells. Our findings reveal a biological mechanism that links the three microtubule-based organelles—the midbody, the centrosome, and the cilium—in the same cellular process.

Introduction

Most vertebrate cells have a primary cilium (PC) that projects from their surface as a single appendage (Gerdes et al., 2009; Bornens, 2012). The PC orchestrates important signaling pathways involved in development and cell proliferation, differentiation, survival, and migration (Singla and Reiter, 2006; Goetz and Anderson, 2010). Ciliary dysfunction produces a great variety of human developmental and degenerative disorders, collectively known as ciliopathies, which can affect nearly every major organ in the body (Hildebrandt et al., 2011).

In mammals, the PC consists of a specialized membrane protrusion that surrounds a structure known as the axoneme, which is organized in a ninefold symmetrical arrangement of microtubule doublets. In some cell types, the PC is deeply rooted in the cytoplasm in a membrane invagination referred to as the ciliary pocket, whereas in others the PC directly protrudes from the plasma membrane (Rohatgi and Snell, 2010; Benmerah, 2013). It has been postulated that the presence or absence of the ciliary pocket is a consequence of the use of two distinct pathways of primary ciliogenesis (Benmerah, 2013), distinguished by the position of the centrosome, either near the nucleus or close to the cell apex (Sorokin, 1968). In fibroblasts, which have a ciliary pocket and the centrosome near the nucleus, ciliogenesis follows the intracellular route, which begins inside the cell with the progressive formation of a large ciliary vesicle that encapsulates the distal end of the mother centriole. This vesicle is usually thought to be of Golgi origin, although, at least in embryonic neocortical stem cells, it appears that can also be derived from a previous ciliary membrane (Paridaen et al., 2013). After formation of an incipient axoneme by elongation of the two inner microtubules from each of the nine microtubule triplets of the mother centriole, the ciliary vesicle fuses with the plasma membrane and gives rise to the ciliary membrane and, probably, the ciliary pocket (Sorokin, 1962). In contrast, cells such as renal polarized epithelial cells (Latta et al., 1961), which lack a ciliary pocket and have their centrosome at the cell apex, assemble a PC once the centrosome is positioned at the cell apex. Despite its fundamental relevance, research on primary ciliogenesis has concerned itself almost

Correspondence to Miguel A. Alonso: maalonso@cbm.csic.es

Abbreviations used: IFT, intraflagellar transport; IMCD3, inner medullary collecting duct 3; MKLP1, mitotic kinesin-like protein 1; PC, primary cilium; PRC1, protein required for cytokinesis 1; RPE1, retinal pigment epithelial 1; TUSP, take-up by suction pressure.

The Rockefeller University Press $30.00
J. Cell Biol.
www.jcb.org/cgi/doi/10.1083/jcb.201601020

Published July 25, 2016

exclusively with the intracellular pathway, whereas the existence of an alternative route in polarized epithelial cells has remained largely unexplored.

Cytokinesis begins with ingression of the cleavage furrow that progressively constricts the cytoplasm and transforms spindle microtubules into the intercellular bridge connecting the two daughter cells (Chen et al., 2012; Fededa and Gerlich, 2012; Green et al., 2012). The midbody, or Flemming body, which is a 1.0- to 1.5-µm-electrodense structure characterized by dense packing of overlapping antiparallel microtubule bundles, forms in the middle of this bridge. Severing of the bridge membrane on one side of the midbody results in the physical separation of the two daughter cells. Once this process has taken place, if the bridge is severed on the other side, the postmitotic midbody is shed into the extracellular milieu and deteriorates with time. Alternatively, in the event that the second scission does not occur, the midbody is asymmetrically inherited by one of the daughter cells as a remnant, to be degraded or conserved over an extended period (Marzesco et al., 2005; Pohl and Jentsch, 2009; Kuo et al., 2011; Salzmann et al., 2014). The position of the remnant marks the site of formation of the first neurite in *Drosophila melanogaster* neurons in vivo (Pollarolo et al., 2011), defines the place of initiation of lumen formation in epithelial cells (Li et al., 2014), and constitutes a landmark for defining dorsoventral axis formation during the early development of *Caenorhabditis elegans* (Singh and Pohl, 2014). Although the exact role of the midbody remnant in these processes remains a mystery, its importance in cellular physiology and determination of cell fate is becoming apparent (Chen et al., 2013; Dionne et al., 2015).

Epithelial Madin-Darby canine kidney (MDCK) cells constitute a paradigm of renal tubular epithelial cells extensively used for investigating specialized membrane trafficking mechanisms and in vitro tubule formation (Rodriguez-Boulan et al., 2005). Here, we used MDCK cells to investigate the process of primary cilium formation in polarized renal epithelial cells. We show that the midbody remnant of MDCK cells is retained by one of the daughter cells and becomes located at the apical surface close to the cell junctions. The midbody remnant, which carries important machinery for primary cilium formation, such as Rab8 and intraflagellar transport (IFT) and exocyst subunits, then moves along the apical surface to the central zone, where the centrosome is situated. Once there, a primary cilium emerges. If the remnant is removed, primary ciliogenesis is greatly impaired. A mathematical simulation explains the dynamics of the process in terms of constraints on cell area brought about by cell proliferation and establishment of cell–cell contacts. Our work reveals a new biological mechanism for the process of primary ciliogenesis that directly implicates the postmitotic midbody.

Results

The effect of confluence and quiescence on primary ciliogenesis appears to depend on the cell type and cell culture conditions (Wheatley et al., 1994; Alieva and Vorobjev, 2004). MDCK cells form a PC at the center of the apical membrane when they are grown at high cell density, but unlike other cells, they do not form a PC in response to serum deprivation. The PC of MDCK cells does not contain a ciliary pocket (Zuo et al., 2009; Reales et al., 2015), and the centrosome of nonciliated cells localizes close to the apical membrane and is devoid of a large ciliary vesicle (Fig. 1, A and B). Therefore, as such, MDCK cells are an appropriate model for investigating the existence of an alternative pathway of ciliogenesis. The machinery for IFT (Rosenbaum and Witman, 2002), the Rab GTPase Rab8, and exocyst (a multi-subunit complex involved in tethering vesicles to the plasma membrane [Heider and Munson, 2012]) are important for the assembly of the PC (Nachury et al., 2007; Zuo et al., 2009; Das and Guo, 2011). To understand ciliogenesis in MDCK cells, we first examined the distribution at the apical zone of IFT20, a component of the IFT machinery. Interestingly, in addition to its expected ciliary localization, in nonciliated cells, IFT20 concentrated in a tubulin-rich structure positioned at the apical surface either peripherally, close to the cell junctions, or centrally, close to the centrosome (Fig. 1 C). Rab8 (Fig. 1 D) and Exo70 (Fig. S1 A; a subunit of the exocyst complex), but not podocalyxin (a PC-excluded transmembrane protein [Meder et al., 2005]; Fig. 1 E), also distributed in the three apical patterns. IFT88 followed the same distribution patterns (Fig. S1 B), but IFT81 (Fig. S1 C) was detected only in ciliary structures. Quantifying the number of cells with each of the three profiles in growing cells evolving from low to high confluence showed that cells with a peripheral profile emerged first, followed by the cell population with a central profile and then those with a cilium (Fig. 1 F). These dynamics and the observation that the PC shares IFT20, Rab8, Exo70, and α-tubulin with the central and peripheral structures prompted us to characterize these structures, examine their relationship, and investigate their involvement in ciliogenesis.

During cytokinesis, the intercellular bridge connecting newly formed daughter cells forms at the apical surface of MDCK cells (Reinsch and Karsenti, 1994; Fig. 2, A and B; and Video 1). The physical separation of the daughter cells then takes place by a process called abscission, which involves disassembly of the microtubules adjacent to the midbody and scission of the membrane bridge (Chen et al., 2012; Fededa and Gerlich, 2012; Mierzwa and Gerlich, 2014). After abscission, the postmitotic midbody was inherited as a midbody remnant by one of the daughter cells and localized at the apical surface close to the junction between them (Fig. 2 A and Video 1). The peripheral structure positive for IFT20 was identified as a midbody remnant by its colocalization with protein required for cytokinesis 1 (PRC1; Jiang et al., 1998; Fig. 2 C) and mitotic kinesin-like protein 1 (MKLP1; Mishima et al., 2002; Fig. S1 D), which were used as endogenous markers of the midbody, and with exogenous GFP-PRC1 (Fig. S1 E). The characteristic microtubular pattern and electrodense ultrastructure seen by EM analysis of the peripheral profiles confirmed this assignment (Figs. 2 D and Fig. S2, A and B). It is of note that detailed analysis of serial sections indicates that peripheral remnants are connected to the rest of the cell through tethers that appear continuous with the midbody (Fig. 2 D).

Consistent with previous observations in HeLa cells (Kaplan and Reiner, 2011), Rab8 was found in the intercellular bridge in MDCK cells, as was IFT88 (Fig. S1 F). IFT20 and IFT88 were also detected in the bridge in human telomerase reverse transcription–immortalized retinal pigment epithelial 1 (RPE1) cells (Fig. S1 G), which have a ciliary pocket and follow the intracellular route of ciliogenesis (Molla-Herman et al., 2010). Because IFT20 had not previously been detected in the bridge (Follit et al., 2006), its presence was confirmed by expression of GFP-IFT20 (Fig. S1 H). The localization of Rab8, IFT20, and IFT88 in the intercellular bridge explains their presence in peripheral remnants.

Published July 25, 2016

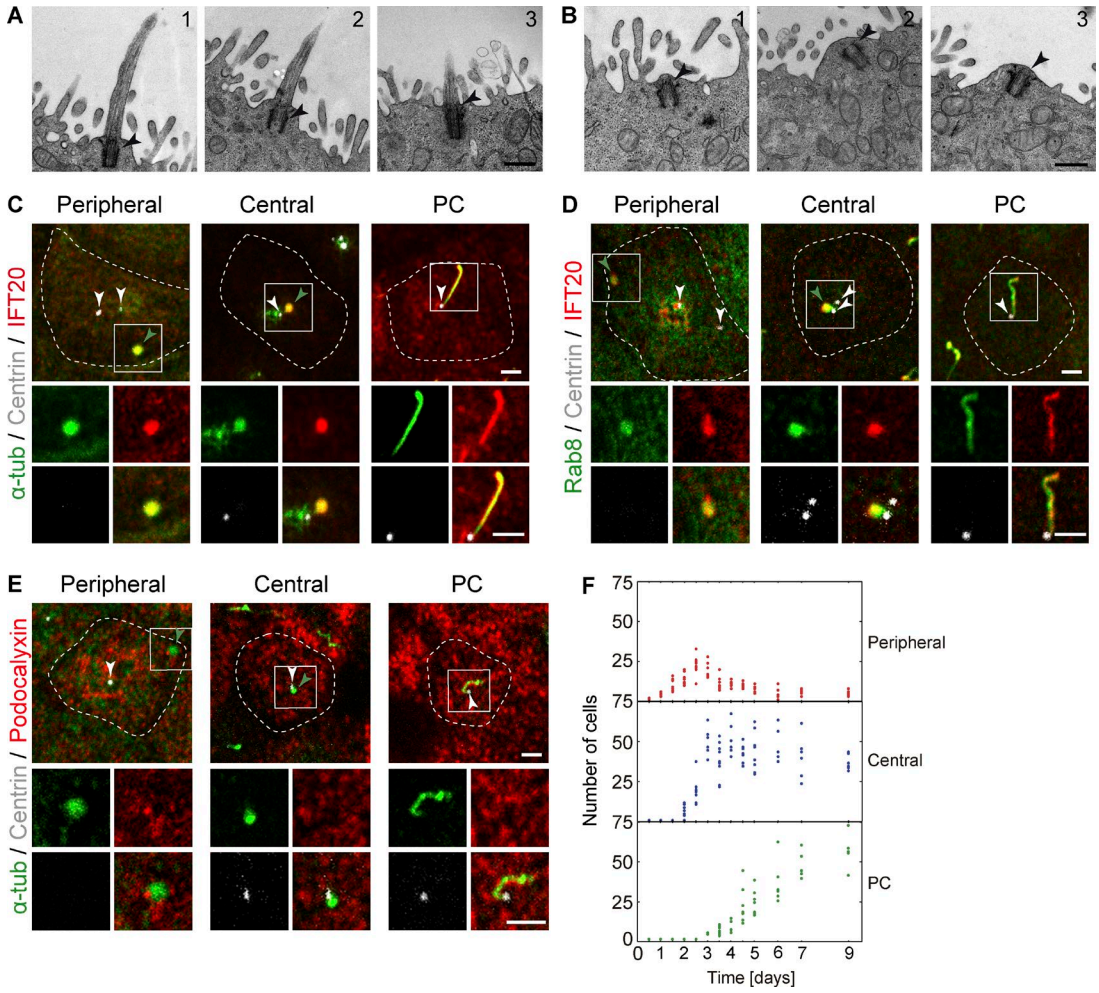

Figure 1. **IFT20 and Rab8 concentrate at peripheral and central structures in nonciliated MDCK cells.** (A and B) EM micrographs showing three representative examples of PCs (A) and apical centrosomes (B). No ciliary pocket (A) or vesicles surrounding the centrosome (B) were observed in 14 cilia and 16 apical centrosomes examined, respectively. The arrowhead marks the centrosome. Bars, 500 nm. (C–E) Cells grown for 4 d were stained for IFT20 and α-tubulin (C), Rab8 and IFT20 (D), and podocalyxin and α-tubulin (α-tub; E). The position of the centrosome was monitored by expression of dsRed-centrin. The projection of one to three apical planes of one representative example of each of the distributions patterns is shown. The dashed line indicates the cell contour. The enlargement shows the fluorescent signal in the boxed region for the proteins analyzed. White arrowheads point to the centrosome or to each of the two centrioles if they are separated, and green arrowheads point to the peripheral and central structures. Bars, 2 µm. (F) The number of cells with peripheral or central structures or a PC was measured at the indicated times after cell plating. Each dot represents the result from a microscope field. Three independent experiments were performed (n = 207–847 cells per time point; two to five fields per time point and per experiment).

To determine whether the central profile arises from translocation of the peripheral remnant, we tracked the dynamics of peripheral remnants labeled with GFP-PRC1 and cherry-tubulin. We observed that the remnant moved along the apical surface toward the center of the apical membrane (Fig. 3 A and Video 2). We also used cells expressing GFP-tubulin and dsRed-centrin to confirm that the remnant moves to be proximal to the centrosome (Fig. 3 B and Video 3). The transition to become cells with a central remnant occurred in ∼72% of cells that had a peripheral remnant, as measured 60–72 h after cell seeding, and the journey took 1–4 h, as assessed by videomicroscopic analysis of 40 cells. It is of note that the remnant reached a central position by climbing along the apical surface as the cell gradually grew in height and occupied less area (Fig. 3 C and Video 4). Similar to what was observed in peripheral remnants (Figs. 2 D and S2 A), EM analysis of serial longitudinal cell sections of a remnant in the proximity of the centrosome showed that the remnant is connected to the rest of the cell by a thin stalk (Fig. 3, D [section S2′] and E; and Fig. S3 B). In addition, the 3D reconstruction of serial EM sections showed that the midbody remnant is closely embraced by microvilli (Fig. 3 E and Video 5).

Rab8 localizes to the PC and is essential for efficient PC formation in RPE1 cells (Nachury et al., 2007; Westlake et al., 2011; Kuhns et al., 2013). The midbody remnant transports Rab8 to the center of the apical membrane in MDCK cells (Fig. S3 A). To investigate whether Rab8 is necessary for the movement of the remnant, we silenced Rab8 expression with specific siRNA (Fig. S4, A and B). Rab8 knockdown produced the accumulation of peripheral remnants in MDCK cells and, as in cells with a ciliary pocket, compromised PC formation (Fig. 4, A and B). This effect was impeded in cells expressing exogenously human Rab8 (Fig. 4, C and D). As a control of the specificity of the effect of Rab8 knockdown on the movement of the remnant, we observed that IFT88 knockdown (Fig. S4, C and D) did not produce the same effect (Fig. 4, E and F). Instead, IFT88 knockdown reduced the number not only of ciliated cells, but also of peripheral remnants, probably by favoring remnant release.

Published July 25, 2016

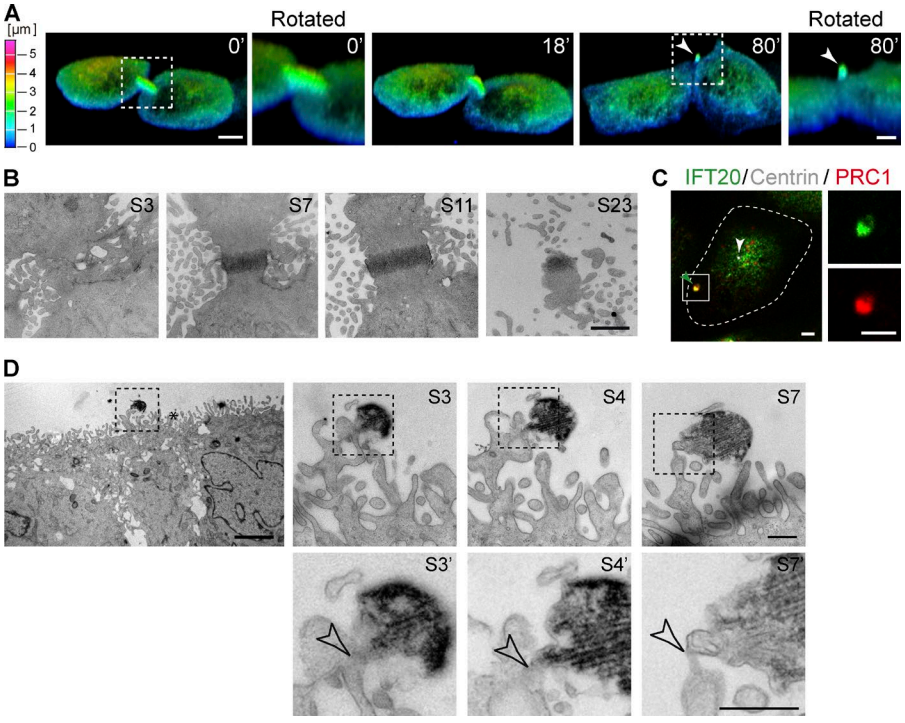

Figure 2. **The peripheral structure containing ciliary markers is a postmitotic midbody.** (A) The images correspond to 3D reconstructions of cells expressing cherry-tubulin that were filmed during cell division. The images were pseudocolored based on height, using the color scale on the left, to highlight that the intercellular bridge forms at the top of the cells and that the postmitotic midbody remnant localizes after abscission at a peripheral position at the apical surface. The arrowhead points to the postmitotic midbody. Bar, 5 µm. An enlargement of the boxed region at 0 and 80 min is also shown. Bars, 2 µm. (B) Serial EM sections of the apical region of MDCK cells during cytokinesis. The sections are numbered S1 onwards from the lower section to the top. Note the progressive loss of microvilli at the top sections. Bar, 1 µm. (C) Cells expressing dsRed-centrin were stained for IFT20 and PRC1. The enlargement of the boxed region shows the fluorescent signal for IFT20 and PRC1. The dashed line indicates the cell contour. The white and green arrowheads point to the centrosome and the peripheral structure, respectively. Bars, 2 µm. (D) EM micrograph of a cell with a peripheral midbody remnant (left panel) and enlargements of different serial sections (S3, S4, and S7, right). Note that in some of the sections it appears that the remnant is connected to the rest of the cell by a thin tether (empty arrowhead) as shown in the enlargements of the boxed regions of sections S3, S4, and S7 (S3′, S4′, and S7′, bottom). Asterisks indicate cell junctions. The images are orthogonal serial sections from the same cell. The sections were numbered S1 onwards from the back to the front. Bars: (panoramic view) 3 µm; (enlargements) 500 nm.

In addition, Rab8 knockdown did not grossly alter the process or duration of cytokinesis (Fig. S4, E and F). Although Rab8 regulates the establishment of apico-basal polarity and membrane trafficking, expression of dominant negative Rab8 does not produce loss of cell polarity in monolayers of already polarized cells (Ang et al., 2003). Similarly, we found that cell polarity, as assayed by the steady-state distribution of the apical podocalyxin and basolateral β-catenin markers and that of the tight junction ZO-1 protein, was apparently normal in the absence of Rab8 (Fig. S4 G). As in the case of peripheral remnants of normal cells, analysis of serial EM sections showed that the remnants of Rab8-knockdown cells were connected to the apical membrane by a thin stalk that appears continuous with the midbody (Fig. 4 G and Fig. S4 H). In summary, the results in Fig. 4 show that the midbody remnant moves along the apical membrane from a peripheral position toward the centrosome in a Rab8-dependent manner.

Having established that the central structure corresponded to the midbody remnant, we investigated the relationship between the central remnant and the cilium. Videomicroscopic analysis and 3D reconstruction of cells coexpressing GFP-tubulin and dsRed-centrin (Fig. 5 A and B; and Video 6) further revealed that a PC starts assembling once the remnant has encountered the centrosome. The observation of this encounter between the remnant and the centrosome could be reproducibly observed (n = 10 cells). A thin microtubular connection between the two structures preceded formation of a nascent cilium (Fig. 5 A). A second example of this microtubular extension is presented in Fig. 5 C. Afterward, the midbody remnant progressively separated from the centrosome and was eventually lost (Fig. 5 A). Similarly, movement of the midbody remnant to the cell center and PC formation were observed in inner medullary collecting duct 3 (IMCD3) cells (Fig. S4, I and J), where it is known that ∼90% of ciliated cells lack a ciliary pocket (Molla-Herman et al., 2010). In summary, the results in Figs. 3 and 5 are compatible with a sequential process by which the daughter cell that inherits the midbody remnant forms a PC by a process involving the movement of the remnant along the apical surface to become proximal to the centrosome.

Because of its dense structure and large size, the energy needed to destroy a midbody by laser ablation is so high that it causes extensive cell damage. Therefore, to investigate directly the requirement of the midbody remnant for PC biogenesis, we designed a gentle procedure to physically remove it. The procedure, which was named "take-up by suction pressure" (TUSP), uses patch-clamp equipment to aspirate the remnant (Fig. 6 A and Video 7). As a control, the same procedure was performed in cells with a remnant in a zone of the plasma membrane distant from it. Removal of the remnant by TUSP resulted in a fourfold reduction in the number of PCs relative to control cells (Fig. 6, B and C). Approximately 20% of the cells still formed a PC despite having their remnant removed, indicating that remnant removal might not have been complete in those cells, that the remnant had already enabled the centrosome to form a PC before removal, or that they formed a PC in a midbody remnant–independent manner. As controls of the TUSP procedure, we observed that cell polarity, as determined by the distribution of podocalyxin, β-catenin, and ZO-1 (Fig. 6 D) and F-actin and

Published July 25, 2016

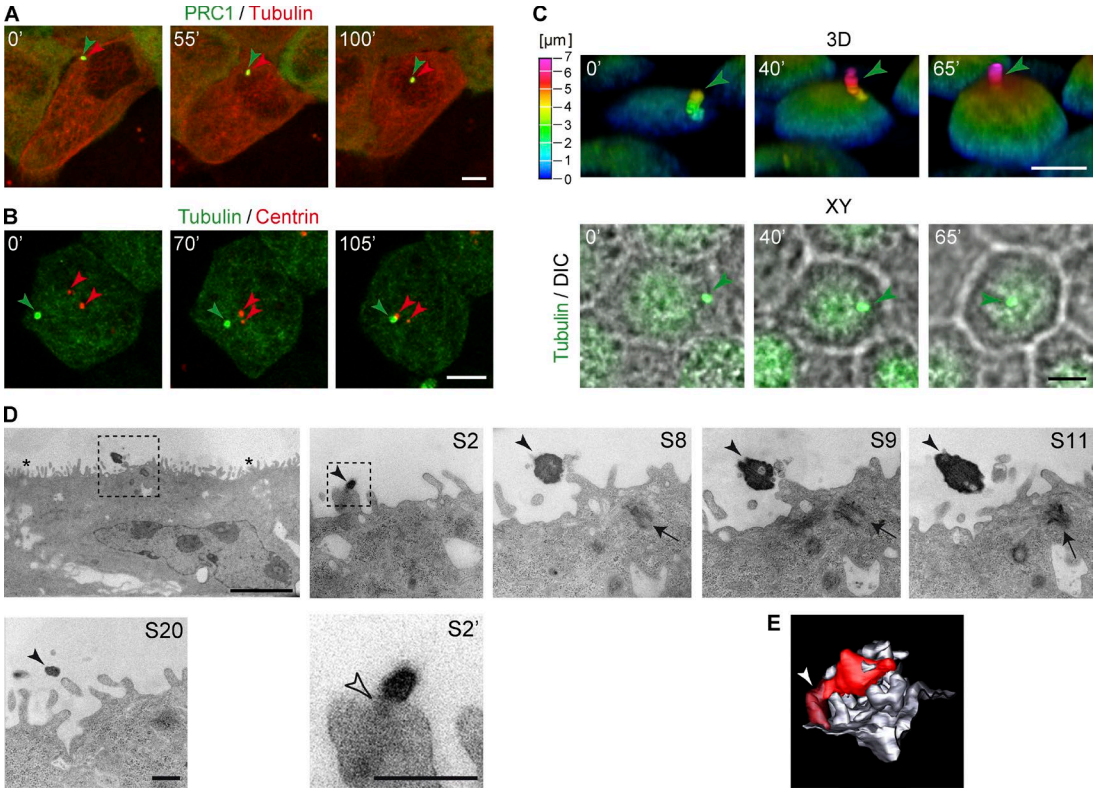

Figure 3. **The midbody remnant moves along the apical surface from a peripheral to a central position to encounter the centrosome.** (A and B) XY confocal stack of cells coexpressing GFP-PRC1 and cherry-tubulin (A) and GFP-tubulin and dsRed-centrin (B) during movement of the midbody remnant. In A, the green and red arrowheads point to the midbody remnant pools of PRC1 and tubulin, respectively. In B, the green and red arrowheads point to the remnant and the centrioles, respectively. (C) 3D reconstruction of cells expressing GFP-tubulin during remnant movement (top). The images were pseudocolored based on height, using the color scale on the left, to highlight that the remnant moved to the center of the apical surface as the cell gained height. The green arrowhead points to the midbody remnant. The differential interference contrast (DIC) images show that the cell occupied 25% less area at the end (bottom). Bars, 5 µm. (D) EM micrograph of a cell with the remnant in the vicinity of the centrosome at the center of the apical surface and enlargements of different sections. The images are orthogonal serial sections from the same cell. Asterisks indicate cell junctions, the black arrowhead points to the remnant, and the arrow indicates the centrosome. The sections were numbered S1 onwards from the back to the front. Note that it appears that the remnant is connected to the rest of the cell by a thin tether, indicated by an empty arrowhead (see S2′, which is an enlargement of the boxed region of S2). Bars: (panoramic view) 4 µm; (enlargements) 500 nm. (E) 3D reconstruction of the central remnant (red), the tether (dark red), and adjacent apical membrane (gray) obtained by manual tracing and stacking of their contours after alignment of the serial EM sections of Fig. S3 B. The arrowhead indicates the tether.

β-catenin (Fig. S5 A), and integrity of the plasma membrane, as assessed with a biotinylation reagent that does not permeate the plasma membrane (Fig. S5 B), were normal in cells in which TUSP was used for remnant removal. Cells remained viable as they responded to hepatocyte growth factor by undergoing cycles of extension-retraction of their plasma membrane, as did control cells in the same microscope field (Video 8). In summary, the results in Fig. 6 show that the midbody remnant is essential for efficient primary ciliogenesis.

Quantification of the area of the substrate occupied by the cells (hereafter referred to as the cell area) indicated that whereas the area of the cells with a peripheral remnant was not restricted, the cells with a central remnant or a primary cilium had areas less than 400 and 200 µm^2, respectively (Fig. 7 A). To investigate the possibility that constraints in the cell area regulate the process of PC formation, we developed a probabilistic population-based mathematical model in which cells are allowed to proliferate and transit between the different stages solely on the basis of the value of the cell area. In addition to the results in Fig. 7 A, the model was designed on the basis of parameters derived from measurements of the total cell number (Fig. 7 B), the single-cell area over time (Fig. S5, C–E), and the number of cells with a midbody remnant or a ciliary structure (Fig. 7 C). We defined the various transitions observed (cell cycle length, remnant conservation, movement of the remnant from a peripheral to a central position, and start of ciliogenesis) in the form of Hill functions of the cell area (Fig. 7 D and Materials and methods). The resulting simulations (Fig. 8 A) show that cells with a peripheral remnant emerged first, followed by the cell population with a central remnant and then those exhibiting a ciliary structure. This is consistent with our videomicroscopic analyses indicating a sequential relationship between the profiles. The simulations closely reproduced the experimental data of Fig. 1 F, as shown by their superimposition (Fig. 8 B). This finding indicates that constraints in the cell area explain all the experimentally observed transitions.

We used the micropatterning method to confirm that the cell area controls the different transitions of the midbody remnant and PC formation. A single cell was plated on disk micropatterns of 700, 1,100, and 1,600 µm^2 (Fig. 8 C), and the cell was left to divide to generate four or eight to 12 cells covering the entire available surface of the disks (Fig. 8 D). Consistent with the simulations, the percentage of cells with a midbody remnant or a PC increased as the cell area became smaller (Fig. 8 E). Moreover, the percentage of cells with either a central remnant or a PC increased with the degree of cell confinement (Fig. 8 F).

Published July 25, 2016

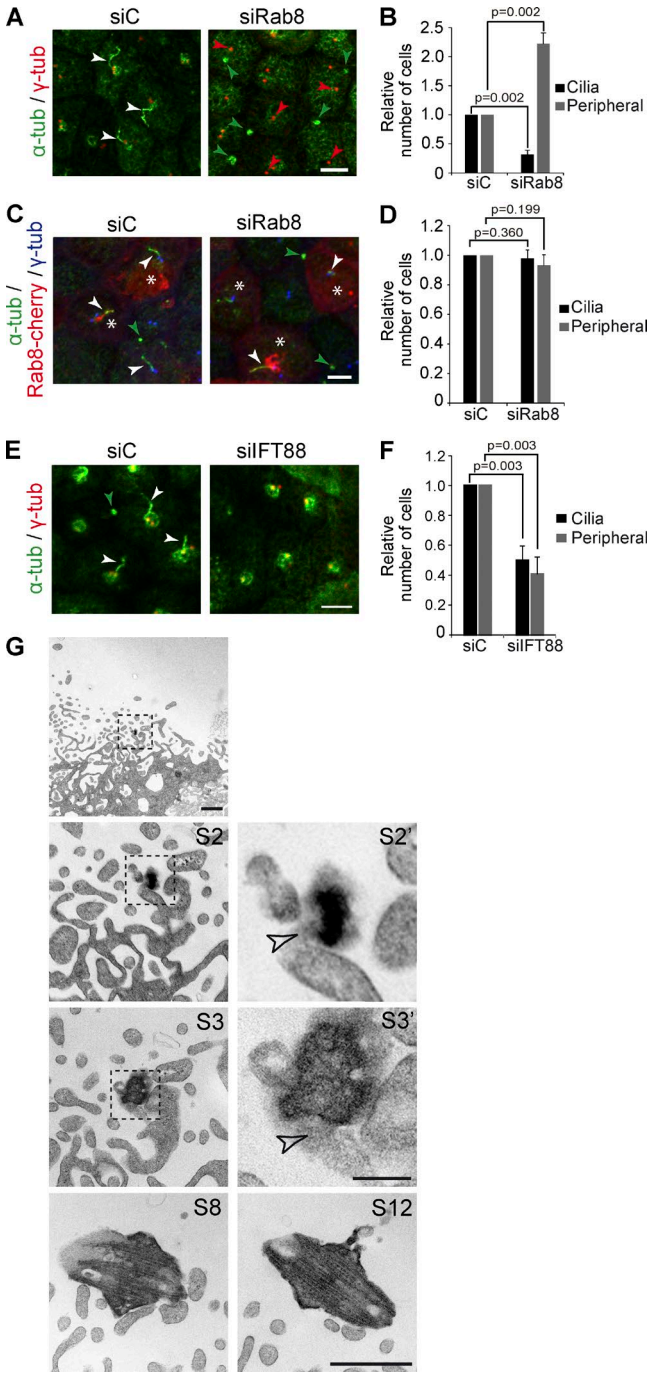

Figure 4. **Rab8 is necessary for the movement of the midbody remnant.** (A–D) Control cells (A and B) or cells stably expressing cherry-Rab8 (C and D) were transfected with siRNA control (siC) or targeted to Rab8 (siRab8). (A and C) Cells were stained for α- and γ-tubulin (α- and γ-tub). The green and red arrowheads point to the midbody remnant and the centrosome, respectively. The white arrowheads indicate the PCs. The asterisks in C mark the cells expressing cherry-Rab8. (B) The number of cells with a peripheral remnant or a PC was quantified in Rab8-knockdown cells and was expressed relative to that in siC-transfected cells. Data represent the mean + SEM from three independent experiments (n = 381 control cells and 354 Rab8-knockdown cells; two to three fields per experiment; Student's t test). (D) The number of cells with a peripheral remnant or a PC was quantified in siRab8-transfected cells expressing cherry-Rab8 and was expressed relative to that in siC-transfected cells. Data represent the mean + SEM from three independent experiments (n = 294 control cells and 322 Rab8-knockdown cells; three fields per experiment; Student's t test). (E and F) Cells were transfected with siC or siIFT88. (E) Cells were stained for α- and γ-tubulin. The green and white arrowheads point to the midbody remnant and the PC, respectively. (F) The number of cells with a peripheral remnant or a PC in IFT88-knockdown cells is expressed relative to that in siC-transfected cells. Data represent the mean + SEM from three independent experiments (n = 1,201 control cells and n = 1,329 IFT88-knockdown cells; three fields per experiment; Student's t test). (G) Panoramic EM image of an apical zone with a midbody remnant in a Rab8-knockdown cell (top) and enlargements of serial sections of the remnant region from the same cell. The sections were numbered S1 onwards from the bottom to the top. Panels S2′ and S3′ show an enlargement of the boxed regions in S2 and S3, respectively. Note that it appears that the remnant is connected to the rest of the cell by a thin tether, indicated by an empty arrowhead. Bars: (A, C, and E) 5 µm; (G, panoramic view and S2–S12) 1 µm; (G, S2′ and S3′) 200 nm.

It is of note that this increase did not affect all the cells on the disk in the same manner: cells at the edge had preferentially peripheral remnants, whereas those in an internal position exhibited most of the central remnants and PCs (Fig. 8 G). This observation is consistent with our measurements on cells grown on coverslips (Fig. 1 F), since in that analysis we ignored the cells at the edge of the coverslip. One interpretation of these findings is that, in addition to a reduced cell area, cell–cell contact favors the transitions of the midbody remnant and PC formation to occur efficiently.

Based on mathematical simulations, and supported by our experimental data, we propose a model of primary ciliogenesis that is mediated by the midbody remnant in which the transitions of the remnant (loss or movement to a central position) and the beginning of the ciliogenesis process are controlled in a cell area–dependent manner by two cell area thresholds (Fig. 9). It is of note that the first threshold (~400 µm^2), which marks the transition from a peripheral to a central remnant, approximately coincides with the area of cells reaching confluence (Fig. S5 F). The second threshold (~200 µm^2) marks the transitions to quiescence, full conservation of the remnant after cell division, and the beginning of ciliogenesis. Under our experimental conditions, most cells at day 9 (72.6 ± 10.2%) had a midbody remnant and hence had the potential to eventually form a PC, or had already formed a PC. Achieving higher percentages of ciliated cells requires an increase in the percentage of cells with one midbody remnant by new cycles of cell division or the elimination of the pool of cells without a remnant. Alternatively, the remaining cells simply might not be able to ciliate, as occurs with a pool of 10% of IMCD3 cells, or to assemble a PC by the intracellular route, which is probably the case of the pool of 10% of ciliated IMCD3 cells that have a ciliary pocket (Molla-Herman et al., 2010).

Discussion

Our understanding of the process of primary ciliogenesis in polarized epithelial cells has advanced little since the classic EM work of Sorokin nearly 50 years ago. In that seminal contribution, it was proposed that in polarized epithelial cells, primary ciliogenesis occurs on the plasma membrane, unlike in other cell types, such as fibroblasts and smooth muscle cells, in which cilium assembly starts intracellularly (Sorokin, 1968). In this article, we have analyzed the process of primary ciliogenesis in polarized MDCK epithelial cells. We show that, once the sister cells have separated, the postmitotic midbody locates peripherally at the apical surface for up to 4–10 h and concentrates machinery important for primary cilium growth, such as the Rab8,

Published July 25, 2016

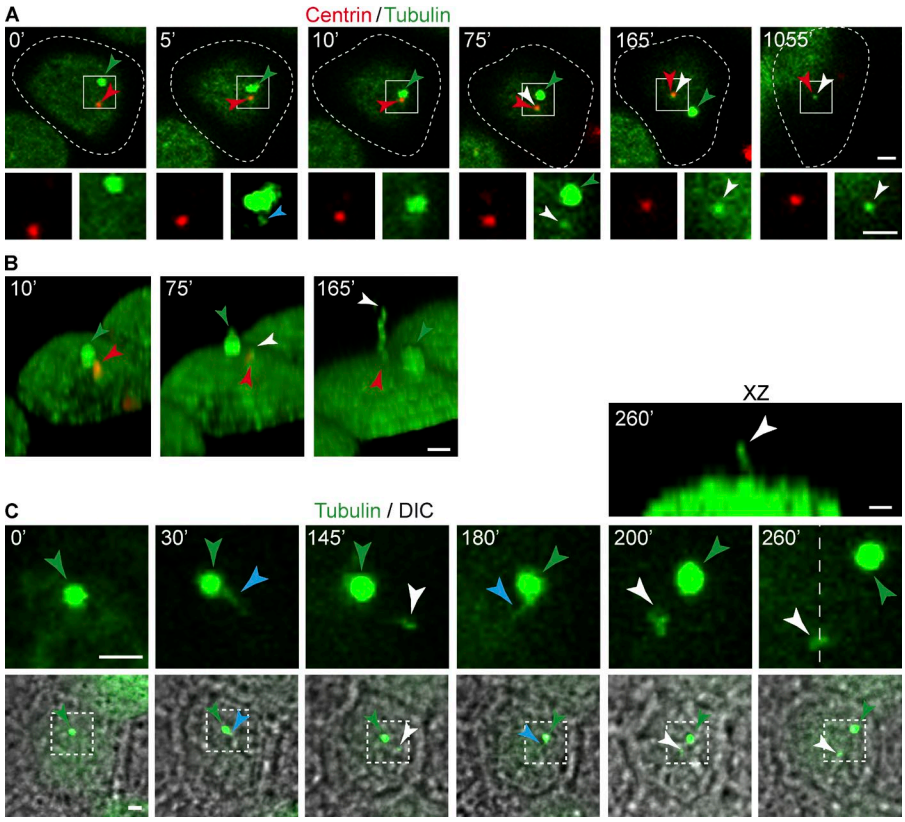

Figure 5. **A primary cilium forms once the midbody remnant becomes proximal to the centrosome.** (A–C) Videomicroscopic analysis of PC formation. (A) XY projection of GFP-tubulin and dsRed-centrin during PC formation (top). The enlargements show the fluorescent signal in the boxed region for the proteins analyzed (bottom). The blue and white arrowheads indicate a microtubular connection between the midbody remnant and the centrosome and a nascent cilium, respectively. The green and red arrowheads point to the midbody remnant and the centrosome, respectively. The dashed line indicates the cell contour. (B) 3D reconstruction of some of the images shown in A. (C) XY projection of GFP-tubulin and their corresponding differential interference contrast (DIC) images during PC formation (bottom). The enlargement of the boxed region shows the distribution of tubulin at apical planes (middle). Nascent cilia are visualized in the XY projections as dots because they are perpendicular to the substrate. Green arrowheads point to the midbody remnant. The blue and white arrowheads indicate a microtubular extension similar to that observed in A and a nascent cilium, respectively. An XZ image of the cells after 260 min is included to show that the new profile that appears close to the midbody remnant (white arrowhead) is a nascent cilium (top). The dotted line indicates the plane used for the confocal XZ image. Bars, 2 µm.

IFT, and exocyst components. The postmitotic midbody remnant then moves along the plasma membrane over 1–4 h carrying this machinery toward the center of the apical surface where the centrosome is situated. Primary cilium formation begins once the two organelles have been proximal for 2–6 h. Therefore, under our experimental conditions, the remnant remains associated with the cell membrane for 7–20 h before primary cilium assembly. Removal of the remnant greatly interferes

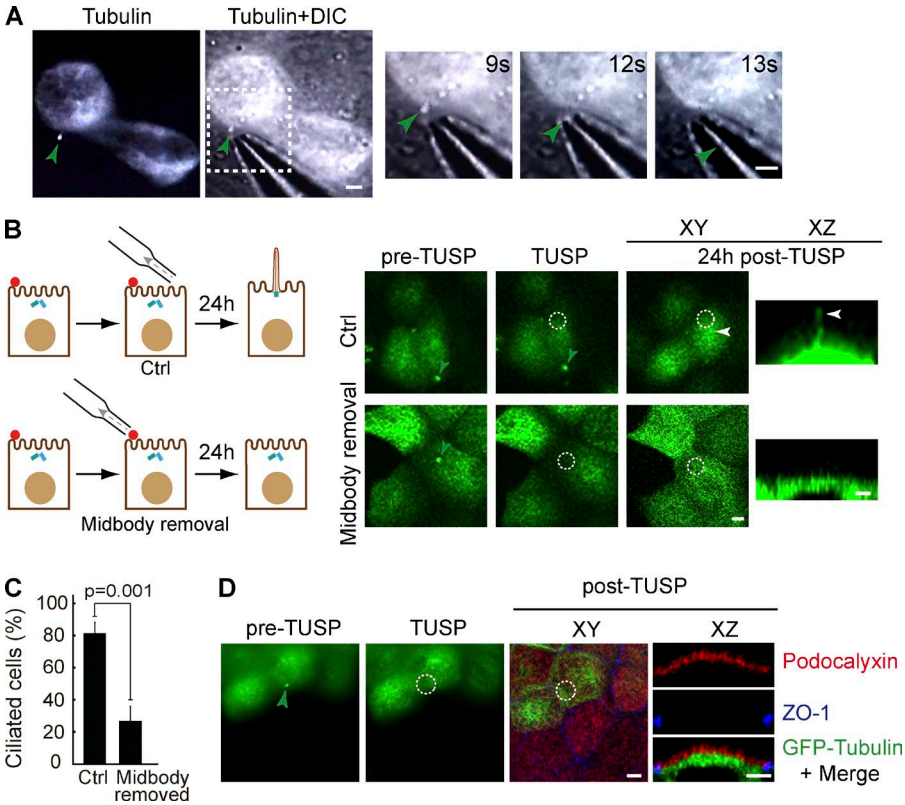

Figure 6. **Removal of the midbody remnant greatly interferes with PC formation in MDCK cells.** (A) Representative images of the TUSP procedure. DIC, differential interference contrast; (B and C) TUSP was used to remove the midbody remnant (B, bottom). As a control (Ctrl), TUSP was applied to cells with a remnant in a zone of the plasma membrane distant from it (B, top). After 24 h, the same cells were examined for the presence of a PC. The green and white arrowheads mark the midbody remnant and the PC, respectively. The circles indicate the plasma membrane zone subjected to TUSP. Bars, 3 µm. (C) The percentage of ciliated cells was quantified 24 h post-TUSP. Data represent the mean + SEM from six independent experiments (n = 26 control cells and 27 cells whose midbody remnant was removed; χ^2 test). (D) The distribution of podocalyxin, ZO-1, and GFP-tubulin was analyzed in cells in which the remnant was removed by TUSP. The arrowheads point to the midbody remnants, and the circles mark the plasma membrane zone subjected to TUSP. Bars, 5 µm.

Published July 25, 2016

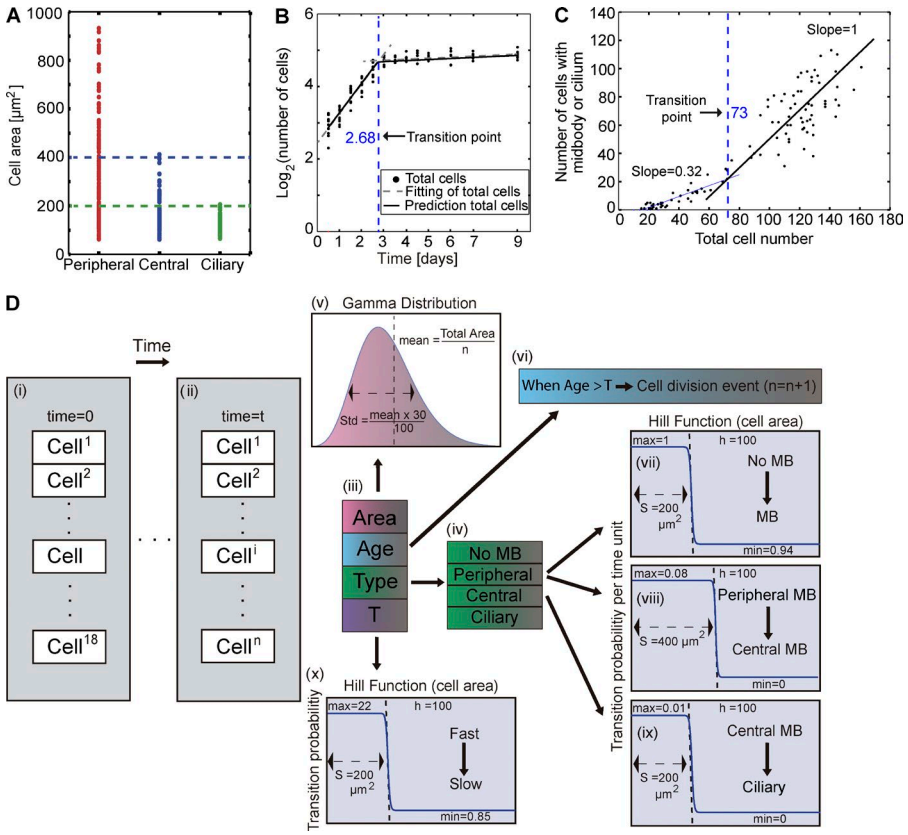

Figure 7. **Development of a mathematical model of primary ciliogenesis.** (A) Plot of the single-cell measures of cell area for peripheral, central, and ciliary profiles. Three independent experiments were performed (n = 406 cells; two to five fields per experiment were examined). (B) Plot of the total number of cells (black dots) over time. Fitting of "fast" and "slow" dynamics (gray dashed lines) intersects at the transition point (2.68 d). Prediction of the total number of cells by a Hill function of the cell cycle using a Hill coefficient of 100 (solid black line). (C) Plot of the number of cells with midbody remnant or PC versus the total number of cells. Two dynamic regimens that intersect at a total number of ∼73 cells are distinguished. Slope values less than 1 mean that a fraction of the new cells in the system does not conserve the remnant. Three independent experiments were performed (n = 207 to 847 cells per time point; two to five fields per time point and per experiment) in B and C. (D) Rationale of the probabilistic population-based mathematical model. (i and ii) An initial set of cells is allowed to proliferate and develop up to a given time t. (iii) Each individual cell in the population is defined as a numerical entity with four variables: its area, age, type, and cell cycle length (7). (iv) Cells can be in one of four distinct configurations depending on whether they lack or have a midbody remnant (MB) in a peripheral or central position or a ciliary structure. These configurations were named as no MB, peripheral, central, and ciliary, respectively. (v) The cell area for each individual cell in the population was obtained from a gamma distribution with standard deviation equal to 30% of the mean. (vi) When the age of a cell reaches the duration of its cell cycle, a division event occurs and a new cell with a peripheral remnant is generated. (vii) Based on the experimental data, we set the probability of conserving the remnant as a Hill function of the cell area, with a transition point at 200 μm². In the same way, the probability of transition from peripheral to central remnant (viii) and from central remnant to ciliary (ix) configurations were also set as Hill functions of the cell area at transition points of 400 and 200 μm², respectively. (x) The cell cycle length of each individual cell was obtained from a Hill function of the cell area with transition at 200 μm².

with PC biogenesis, indicating that the remnant is necessary for the latter to occur. Our model explains PC biogenesis in epithelial MDCK cells as a sequential process by which the daughter cell that inherits the midbody remnant forms a PC in a cell area–dependent manner. This process involves the movement of the remnant along the apical surface to enable the centrosome to form a primary cilium once the remnant and the centrosome become proximal. In addition to revealing the process of ciliogenesis in polarized epithelial cells, which was our primary objective, we made the unexpected but significant discovery that the postmitotic midbody is involved in this process.

Previous studies established that although the cleavage furrow in polarized epithelial cells initiates coincidently at the apical and basal surfaces, the rate of furrow ingression is more rapid from the basal surface. This difference in the rate of ingression causes the intercellular bridge to form close to the apical surface, near tight junctions (Reinsch and Karsenti, 1994; Morais-de-Sá and Sunkel, 2013). Consistent with these studies, we observed that cytokinesis does not occur at the middle region of the daughter cells but at the apical membrane of MDCK cells. Completion of cytokinesis requires both membrane and microtubule severing, the two processes being tightly correlated with abscission time (Steigemann et al., 2009; Chen et al., 2012). Severing the intercellular bridge can be symmetrical, when the abscission event takes place on both sides of the midbody, or asymmetrical, when it occurs only on one side. In the former case, the midbody is released, whereas the latter gives rise to asymmetrical midbody inheritance as one of the daughter cells receives the midbody remnant (Mierzwa and Gerlich, 2014; Dionne et al., 2015). A previous study showed that disassembly of the microtubule bundles of the intercellular bridge takes place on both sides of the midbody in epithelial MDCK cells (Elia et al., 2011). Although no large membrane bridge remnants were detected in that study by differential interference contrast microscopy, the technique cannot rule out the existence of a thin tether of plasma membrane connecting the midbody remnant to the rest of the cell. Our analysis of serial EM sections showed that this does occur in MDCK cells because peripheral and central remnants appear continuous with the tether, although the high contrast of the electrodense region with the density of the stalk might lead to the mistaken interpretation that they are discontinuous if only a few sections are examined. One possible explanation of this finding is that the severing of the membrane bridge on the side of the cell that inherits the remnant does not take place and that a thin tether with the rest of the cell is maintained during the movement of the remnant and in central remnants. A second scenario, which we consider less probable, is that severing of the plasma membrane is completed on both sides but that the midbody remnant remains on the cell surface and fuses thereafter with a thin protrusion of the cell.

The choice between release, conservation, or degradation of the midbody remnant depends on cell type and status (Marzesco

Published July 25, 2016

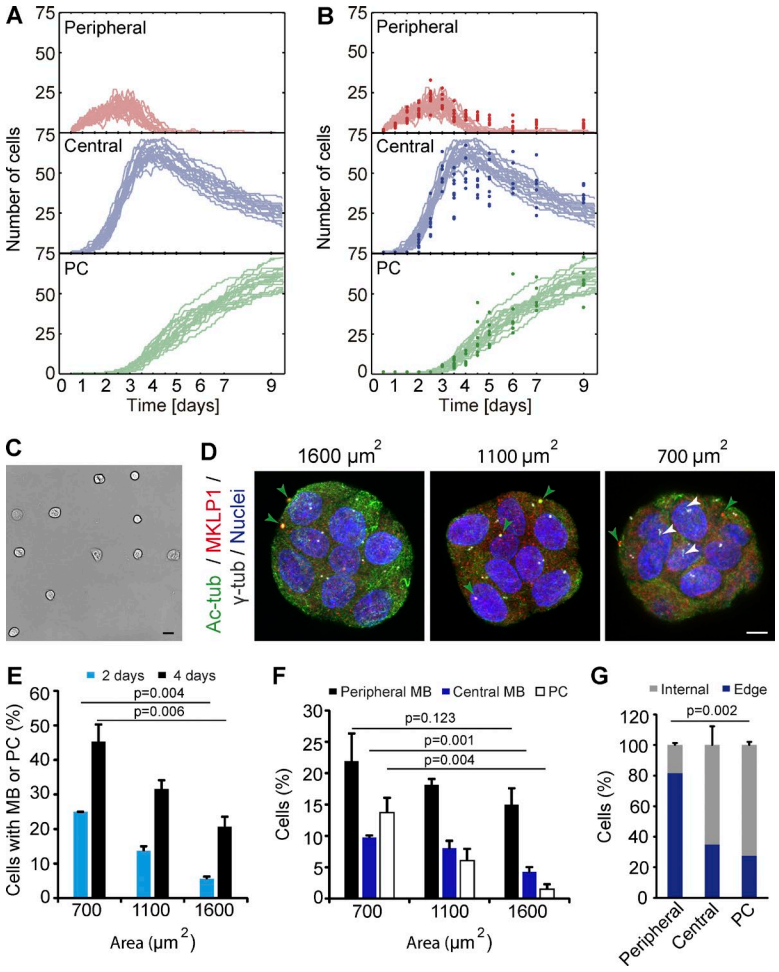

Figure 8. **Primary ciliogenesis in MDCK cells is governed by constraints in cell area at the single-cell level.** (A and B) Simulations (A) and superimposition of the experimental data (dots) shown in Fig. 1 F and the simulations (B). (C–E) A single cell per disk was seeded on disk micropatterns of 700, 1,100, and 1,600 μm² (C) and incubated for 2 or 4 d to allow the colony to reach a size of four or eight to 12 cells, respectively (D). (D) Cells were then processed for immunofluorescence analysis with antibodies to acetylated tubulin (Ac-tub), MKLP1, and γ-tubulin (γ-tub). Disk micropatterns with 8–12 cells are shown. The green and white arrowheads indicate the midbody remnant and PC, respectively. Nuclei were stained with DAPI. Bars: (C) 40 μm; (D) 6 μm. (E) The percentage of cells with either a midbody remnant or a PC relative to the total number of cells was determined after 2 or 4 d. Data represent the mean + SEM from three independent experiments (n = 180 cells grown for 2 d and n = 524 cells grown for 4 d were analyzed from 45 disk micropatterns each; Student's t test). (F) The percentage of cells with a peripheral remnant, a central remnant, or a PC relative to the total number of cells was determined after 4 d. (G) The cells at the edge or in internal positions on 700-μm² micropatterns were analyzed for the presence of peripheral or central midbody remnants or a PC after 4 d. The results are expressed as the percentage of internal or edge cells with peripheral or central remnants or a PC relative to the total number of cells with the corresponding structure. Data in F and G represent the mean + SEM from three independent experiments (n = 176 cells analyzed from 15 disk micropatterns; Student's t test).

et al., 2005; Pohl and Jentsch, 2009; Kuo et al., 2011; Salzmann et al., 2014), implying that its fate should be tightly regulated (Chen et al., 2013; Dionne et al., 2015). More than one remnant accumulates in subpopulations of stem cell–like populations and cancer cells, the frequency being higher in the latter (Ettinger et al., 2011; Kuo et al., 2011). Stem cells and cancer cells enriched in midbody remnants exhibit increased reprogramming efficiency and in vitro tumorigenicity, respectively (Kuo et al., 2011). We observed that partial remnant loss occurs in MDCK cells during the rapid regimen of cell division. In contrast, conservation takes place thereafter, coinciding with the switch to a slow regimen of cell proliferation. If the remnant is to be lost, the tether must be severed, whereas it can remain uncut in the case of conservation, as appears from our EM analysis of peripheral and central remnants. Therefore, according to our model, the cell area regulates the loss or conservation of the remnant and thereby the severing of the remnant stalk. Shedding of membranous particles with midbody markers has been observed in neural progenitors, although no relationship between those particles and PC biogenesis was established (Dubreuil et al., 2007). The endosomal sorting complex required for transport has a decisive role in the scission event of the intercellular bridge membrane that leads to daughter cell separation (Chen et al., 2012; Fededa and Gerlich, 2012; Agromayor and Martin-Serrano, 2013). The loss of the midbody remnants in the final stages of PC formation and during the rapid regimen of MDCK cell division implies scission of the thin stalk that connects the remnants to the rest of the cell. Therefore, it is plausible that the endosomal sorting complex required for transport machinery also mediates severing in both these occasions.

It was striking that, coinciding approximately with the establishment of cell–cell contacts, the midbody remnant moved along the apical membrane from the periphery to a central position in MDCK cells. Remnant movement in the plane of the plasma membrane has been observed after abscission in HeLa cells (Gromley et al., 2005). Because in MDCK cells a thin stalk appears to connect the peripheral and central remnants to the rest of the cell, it is feasible that the stalk mediates the movement of the remnant to encounter the centrosome. We observed that this movement was impaired in Rab8-knockdown cells. This observation does not necessarily means that Rab8 is directly involved in the process but rather that Rab8 expression is required for it to take place. Although we cannot rule out other possibilities such as a role of Rab8 controlling the cytoskeleton, since the best known function of Rab8 relates to membrane trafficking (Peränen, 2011; Barr, 2013), one possibility is that the effect of Rab8 knockdown on the movement of the remnant is likely caused by defects in the transport of proteins and/or lipids to the remnant zone that facilitate its movement.

We have observed accumulation of IFT subunits at the intercellular bridge, and previous studies have established the presence of exocyst subunits (Gromley et al., 2005) and Rab8 (Kaplan and Reiner, 2011). Because postmitotic midbodies contain these and other proteins known to be important in ciliogenesis and because the proteomes of midbodies (Skop et al., 2004) and PCs (Ishikawa et al., 2012) have a high degree of

Published July 25, 2016

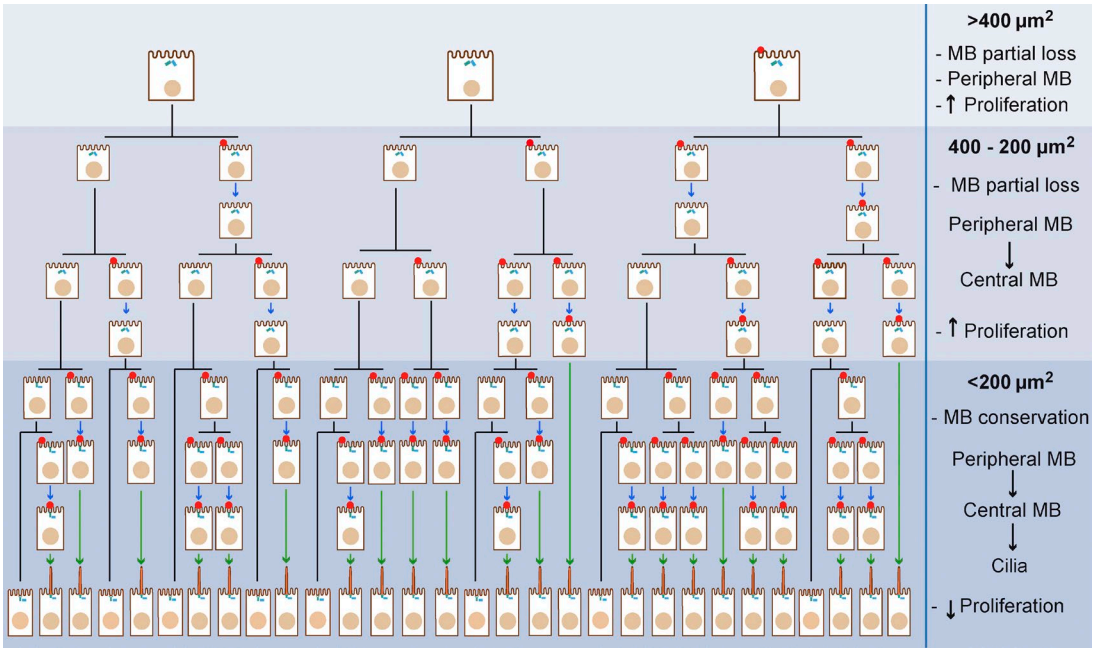

Figure 9. **Schematic of the proposed model of primary ciliogenesis in polarized epithelial cells.** The transitions of the midbody remnant (release or movement to a central position) and the beginning of the ciliogenesis process are controlled in a cell area–dependent manner by two cell area thresholds: a first threshold of ∼400 and a second of ∼200 µm². For cell areas above the second threshold, the remnant is only partially conserved, whereas it is fully conserved for cell areas below it. With regard to the remnant location, it locates peripherally in the apical surface at cell areas above a first threshold. When the area of the cell is between the first and a second threshold, it moves toward the center of the apical membrane to meet the centrosome, and this transition generates a pool of cells ready to start ciliogenesis. When the area of the cells falls below the second threshold, cells continue dividing and generating new midbody remnants that move to the cell center and enable ciliogenesis. Successive cycles of cell division (only one cycle is represented) increase the number of cells with a midbody remnant and, subsequently, the number of ciliated cells. In this way, the percentage of nonciliated cells becomes progressively smaller. Cell area reduction is produced by occupancy of the room of the mother cell by the daughter cells or compression of a cell by cells that divide in its proximity. Black lines represent cell divisions; blue and green arrows represent midbody remnant transitions (loss or peripheral to central movement) and PC formation, respectively.

overlap (Smith et al., 2011), one interesting possibility is that the connection of the remnant through the stalk facilitates the transfer of relevant material to the centrosome, once they are proximal. We have detected the establishment of a thin microtubular connection between the remnant and the centrosome when the two organelles meet at the center of the apical surface (Fig. 5 A). This connection can facilitate transport of material or can be itself the means by which the midbody remnant enables the centrosome for PC formation. A second possibility for the role of the remnant in ciliogenesis is that, because the PC has compact membranes at the ciliary base (Vieira et al., 2006) and these specialized membranes are required for PC formation (Reales et al., 2015), the stalk zone constitutes a compact membrane domain used to form the ciliary base. A third possibility is that the presence of the remnant proximal to the centrosome promotes the signaling required for primary ciliogenesis.

We focused on the cell area in our analysis because it is easily and directly measured. Cells sense their chemical and mechanical context and divide when they sense space is available (Puliafito et al., 2012). Such behavior appears to be achieved by coupling cell division to cell distortion and to changes in the balance of mechanical forces within the cell (Huang and Ingber, 1999). In subconfluent cell culture conditions, cells are not physically constrained by their neighbors, the cells are extended and subjected to tensile stress, and no PC is formed (Pitaval et al., 2010). However, under conditions of limited cell area brought about by cell proliferation, cells become progressively constrained by their neighbors and compressive stress replaces tensile stress (Trepat et al., 2009; Bazellières et al., 2015). In accordance with this, we observe that the movement of the midbody remnant from a peripheral position to a central position takes place as the cell grows in height and reduces its area (Fig. 3 C). We also demonstrate that cells grown on disk micropatterns show a greater percentage of PCs and central remnants in cells occupying an internal position relative to the cells at the disk edge. This observation shows the importance of cell–cell contacts in the transitions of the remnants and the formation of a PC. In contrast, primary ciliogenesis by the intracellular route takes place efficiently in RPE1 cells in the absence of cell–cell contact (Pitaval et al., 2010). The events leading to reduction in cell area, increase in cell height, and movement of the midbody remnant as well as cell polarization and junction formation are probably related with a common cause in a way that becomes evident only when tight cell–cell contacts are established. We propose that the change from tensile to compressive forces caused by cell–cell contacts in highly confluent MDCK cells (Ishikawa and Marshall, 2014), rather than the cell area per se, is the trigger at least for the conservation of the midbody remnant, its transition to a central position, and the beginning of ciliogenesis.

A relationship between the mother centriole and the intercellular bridge has been documented (Piel et al., 2001; Jonsdottir et al., 2010). In HeLa cells and L929 fibroblasts, the mother centriole moves transiently to the cell periphery to become proximal to the intercellular bridge before abscission and then moves back to the cell center (Piel et al., 2001). Centriole movement

Published July 25, 2016

was found to be highly dependent on cell line (Jonsdottir et al., 2010). Under certain conditions, the mother centriole was found even inside the intercellular bridge, very proximal to the midbody. The exocyst (Gromley et al., 2005), Rab8 (Kaplan and Reiner, 2011), and IFT subunits (Fig. S1, F–H) are present in the intercellular bridge. Therefore, it is plausible that, in addition to enabling cytokinesis completion as was originally proposed (Piel et al., 2001), the mother centriole recruits these or other materials from the midbody in some cell types. These materials could work in conjunction with membranes obtained from the Golgi or, as reported in neuroepithelial cells (Paridaen et al., 2013), with remnants of the ciliary membrane of the mother cell to form the ciliary vesicle in cells relying on the intracellular pathway of ciliogenesis. In cells in which the postmitotic midbody follows the autophagic route, materials from the remnant could also contribute to form the ciliary vesicle.

Our model of cilium formation is tightly linked to cell division, a process so inherent to life that the same basic mechanism of ciliogenesis that we propose could conceivably have operated early on in ciliary evolution using remnants of a primitive, microtubule-containing intercellular bridge. This view is somehow reminiscent of the model of Satir et al. (2007), which proposes that the evolutionary origin of the cilium is a microtubule-containing virus instead of the bridge remnant, as in our model.

The three microtubule-based organelles—the centrosome, the cilium, and the midbody—were discovered in the second half of the 19th century. The link between the centrosome and cell division was soon realized and subsequently thoroughly investigated, whereas research into the other two organelles has intensified only in recent years. Our finding that the postmitotic midbody enables PC formation reveals an unexpected role of the midbody in primary ciliogenesis and highlights a new biological mechanism that functionally links the midbody with the other two microtubule-based organelles.

Materials and methods

Antibodies and reagents

The sources of the antibodies to the different markers were as follows. IFT20 (rabbit polyclonal; used at 1/200; HPA021376), γ-tubulin (rabbit polyclonal; used at 1/2,000; T3559); mouse mAb IgG1 (clone GTU-88; used at 1/2,000; T6557), total α-tubulin (mouse mAb IgG1, clone DM1A; used at 1/500; T9026), and Rab8 (rabbit polyclonal; used at 1/500; R5530) used in immunoblotting experiments were obtained from Sigma-Aldrich. Rab8 (mouse mAb IgG2b, clone 4/Rab4; used at 1/100; 610844) used for immunofluorescence analysis was obtained from BD. Tyrosinated α-tubulin (rat mAb IgG2a, clone YL1/2; used at 1/500; MA1-80017) was purchased from Thermo Fisher Scientific. Exo70 (mouse mAb IgG2b, clone 70X13F3; used at 1/200) was purchased from Kerafast. Podocalyxin/gp135 (mouse mAb IgG1; used at 1/500; 3F2/D8) and ZO-1 (rat mAb IgG1; used at 1/500; R26.4C) were purchased from Developmental Studies Hybridoma Bank. MKLP1 (rabbit polyclonal; used at 1/500; sc-867) and β-catenin (rabbit polyclonal; used at 1/500; sc-7199) were obtained from Santa Cruz Biotechnology, Inc. PRC1 (mouse mAb IgG2b, clone 16F2; used at 1/200; MA1-846), IFT88 (rabbit polyclonal; used at 1/100; 13967-1-AP), and IFT81 (rabbit polyclonal; used at 1/100; 11744-1-AP) were obtained from Proteintech. Hepatocyte growth factor (product GF116) was obtained from EMD Millipore. DAPI stain was purchased from Thermo Fisher Scientific. Fluorescent phalloidin and secondary antibodies conjugated to Alexa Fluor 488, 594, or 647 were purchased from Invitrogen.

Cell culture

Epithelial canine MDCK II (CRL2936), IMCD3 (CRL2123), and RPE1 (CRL4000) cells were obtained from ATCC. Cells were grown in MEM supplemented with 5% FBS (Sigma-Aldrich) at 37°C in an atmosphere of 5% CO_2. Mycoplasma testing was regularly performed. For immunofluorescence analysis, 5.0×10^5 cells were seeded on 12-mm polycarbonate membranes of 0.2-µm pore size (Costar Transwell; Corning). For the quantitative analyses in Figs. 1 F, 7 (A–C), and S5 (C–E), 2.5×10^4 MDCK cells were plated onto coverslips maintained in 24-well multiwell plates and grown for the indicated times. Under these conditions, a mean of 18 cells per field were visualized with a 63× objective under our microscope 12 h after plating. Cells were then analyzed for α- and γ-tubulin staining and by differential interference contrast microscopy. Cells with both a PC and midbody remnant were assigned to the PC group. We cannot rule out that a small fraction of short PCs were scored as central midbody remnants in Fig. 1 F.

DNA constructs, siRNA, and transfection conditions

The DNA constructs expressing dsRed-centrin2 (Tanaka et al., 2004; plasmid 29523; Addgene) and GFP-PRC1 (Hu et al., 2012) were gifts from J. Gleeson (University of California, San Diego, La Jolla, CA) and C.-K. Hu (University of Stanford, Stanford, CA), respectively. The constructs expressing GFP- or cherry-tubulin were obtained from Takara Bio Inc. For transient transfection of DNA constructs, cells were transfected with Lipofectamine 2000 (Thermo Fisher Scientific) according to the manufacturer's recommendations. The construct expressing GFP-IFT20 was generated by cloning the IFT20 coding sequence, which was obtained by PCR using specific primers and human IFT20 cDNA (IMAGE clone 3907361; Source Bioscience) as template, in the pEGFP-C1 expression vector (Takara Bio Inc.). Stably transfected cells were generated by transfection and selection with 1 mg/ml G-418 (Thermo Fisher Scientific). The resulting clones were screened under a fluorescence microscope. 1.0×10^6 cells were transfected with 20 nM siRNA negative control (siC) Hi GC (product 12935-500) or 20 nM siRNA targeted to Rab8a (siRab8, 5′-GACAAGUUUCCA AGGAACG-3′) or IFT88 (siIFT88, 5′-UCGUCUAAGGCAAAU GGAACGUGAA-3′; Thermo Fisher Scientific) by electroporation in an Amaxa apparatus running the L-005 program. After overnight incubation, cells were washed three times and resuspended in fresh medium. Rab8 and IFT88 knockdown was verified by immunoblotting 72 h after transfection.

Immunofluorescence and time-lapse microscopic analyses

Cells were fixed in formalin for 20 min, rinsed, and treated with 10 mM glycine in PBS for 5 min to quench the aldehyde groups. Cells were then washed, permeabilized or not with 0.1% Triton X-100 in PBS at 4°C for 10 min, rinsed, incubated with 3% (wt/vol) BSA for 15 min, and incubated with the primary antibody. For γ-tubulin staining, cells were fixed with cold methanol for 5 min. After 1 h at room temperature, cells were washed and incubated with the appropriate fluorescent secondary antibody. For double-labeling experiments, the same procedure was repeated for the second primary antibody. Cells were mounted in coverslips using ProLong Gold antifade reagent (Thermo Fisher Scientific). For selective labeling of the apical surface, 0.25 mg/ml sulfo-NHS-biotin (Thermo Fisher Scientific) were added to confluent monolayers of MDCK cells. After 30 min at 4°C, the solution was removed and the remaining unreacted biotin was quenched by incubation with ice-cold serum-free MEM. The biotin groups were detected by incubation with streptavidin–Alexa Fluor 555 (Thermo Fisher Scientific) for 30 min. Images were obtained using an LSM 710 confocal microscope (ZEISS) with a 63× oil objective and a numerical aperture of 1.4. The projection of one to three apical planes is shown in the XY

Published July 25, 2016

images of cells grown on Transwells. For time-lapse fluorescence microscopy, we used a Nikon A1R confocal microscope with 60× water objective and a numerical aperture of 1.2. For 3D reconstruction, we used NIS-Elements microscope imaging software (Nikon). Cells were plated onto 35-mm glass-bottom dishes (MatTek) and maintained at 37°C in MEM without phenol red supplemented with 0.25% fetal bovine serum during the recording. Immunofluorescence and time-lapse experiments were performed at least four independent times, and images shown are representative from samples that were used for quantification. Brightness and contrast were optimized with ImageJ (National Institutes of Health) and Photoshop (Adobe Systems). Quantifications were performed using ImageJ.

Electron microscopy and 3D reconstruction

Cells grown on Transwell filters were fixed with 4% paraformaldehyde and 2% glutaraldehyde for 90 min at RT. Cell samples were then processed for embedding in Epoxy, TAAB 812 Resin (TAAB Laboratories) according to standard procedures. The samples were processed for sequential 80-nm ultrathin sections perpendicular to the plane of the cell monolayer. The obtained sections were numbered as S1 onwards. Sections were stained with saturated uranyl acetate and lead citrate by standard procedures. Samples were examined at 80 kV in an electron microscope (JEM-1010; Jeol). Pictures were taken with a TemCam-F416 (4,000 by 4,000-pixel) digital camera (TVIPS). For 3D reconstruction (Fig. 3 E and Video 5), EM images from a stack of 21 sequential sections (Fig. S3 B) were binned twice to give an effective pixel size at the specimen level of 4 nm. The EM image series were aligned with the IMOD software tool (Kremer et al., 1996). Structural features that were unequivocally identified in adjacent sections, with a particular focus on microvilli and discernible cytoplasmic structures, were manually selected and used as fiducial markers to guide the alignment. Full linear transformation was used to align each pair of successive sections independently. The 3D reconstruction was finalized by transforming each section into a common alignment in which the section located in the middle of the stack acted as a reference. The 3D reconstruction was modeled with IMOD by manually tracing the contour of the features of interest, particularly midbody remnants, plasma membrane, and microvilli along the sections of the EM stack (Fig. S3 B). The modeled reconstruction was visualized in 3D by surface rendering (Fig. 3 E and Video 5). As individual sections had a nominal thickness of 80 nm and we used a stack of 21 sections, the total thickness of the 3D reconstruction was ∼1.68 µm.

Midbody remnant removal

A mixed population of cells stably expressing or not expressing GFP-tubulin, which was used to visualize the midbody remnant, were grown for 4 d to generate a confluent monolayer. By using a glass pipette hitched to a patch-clamp equipment, remnants were removed by aspiration by TUSP (Video 7). Cell visualization was performed with a microscope (BX51; Olympus), using bright field and epifluorescence illumination. TUSP was assisted with Sutter MP-225 motorized micromanipulators. As a control, TUSP was applied to cells in a zone of the plasma membrane distant from the remnant. Cells were fixed 24 h post-TUSP and analyzed for the presence of PC. TUSP was performed on cells within areas previously labeled in the coverslips. The fluorescence pattern of the cells in the same area served to unambiguously identify TUSP-treated cells.

Micropatterned cell culture

MDCK cells were cultured on micropatterned glass coverslips (CYTOOchips; CYTOO). Disk-shaped micropatterns of different area (700, 1,100, and 1,600 µm^2) were used. 35,000 cells/chip were seeded and then washed and incubated according to the manufacturer's instructions.

Statistical analysis

In Fig. 6 C, χ^2 test was used because of the categorical nature of the data. Data in the rest of the figures were analyzed using Student's *t* test.

Mathematical model

Calculation of cell cycle duration and Hill coefficient for the mean proliferation dynamics of the population. The number of cells over time follows the equation

$$A(t) = A(0)2^{t/T(t)}, \quad (1)$$

where $A(t)$ is the number of cells at any given time t, $A(0)$ is the initial number of cells, and $T(t)$ is the mean cell cycle in the population that can change over time. Plot of the total number of cells over time (Fig. 7 B, black dots) from multiple experiments showed two distinct regimes of cell proliferation dynamics with a transition of 2.5–3.0 d. These "fast" and "slow" regimes can be fitted to Eq. 1 for constant values of the duration of the cell cycle of 0.85 and 22 d, respectively (Fig. 7 B, dashed gray lines). The long duration of the cell cycle calculated for this regimen can be explained in biological terms by assuming that all the cells divided slowly instead of a small proportion doing so at a normal rate. For the cell population model, cell cycle length $T(t)$ is assumed to follow a Hill function of the form

$$T(t) = \frac{T_{\max} + (T_{\min} - T_{\max})}{1 + \left(\frac{t}{S}\right)^h} \quad (2)$$

between minimum ($T_{\min}$ = 0.85 d) and maximum ($T_{\max}$ = 22 d) values, where S is the transition point. The transition point (2.68 d) was calculated as the intersection between the two dashed gray lines. The cell area at the transition point (212 µm^2) was estimated by dividing the total cell area (15,647 µm^2; see next paragraph) by the number of cells in the system predicted by Eq. 1 at 2.68 d. The Hill coefficient h (a measure of the sharpness of the transition between the fast- and slow-proliferating regimes shown in Fig. 7 B) was calculated by directly fitting Eq. 1 to the experimental value of the total number of cells for different values of h. The calculated number of cells (Fig. 7 B, solid black line) provided a good fit of the experimental data for values of $h > 100$, which corresponds to a very sharp transition in the mean cell cycle duration of the cell population. For simplicity, the same value (h = 100) of the Hill coefficient was used for the other Hill functions in the cell population–based simulation.

Calculation of the individual cell area in the simulations. The effective total area occupied by the cells was estimated from data from single-cell area measurements at days 6, 7, and 9 by multiplying the mean cell area at each time by the total number of cells present at those times. The mean of the three values was used to calculate the total area (15,647 µm^2) occupied by the cells (Fig. S5 D). The single-cell measurements of cell area for a population of cells at any time fitted to a gamma distribution with a 30% SD from the mean value at each time (as an example, see Fig. S5 E for day 2). Based on this observation, we set the area of each cell in the simulation as a random value sampled from a theoretical gamma distribution calculated for each time point by dividing the total area occupied by the number of cells at each time point (Fig. S5 C, small dots). The experimental mean cell area was calculated by dividing the effective area of the system by the mean number of cells at each time point (Fig. S5 C, large dots).

Calculation of the number of cells that conserve the midbody remnant. A newly formed midbody remnant with a peripheral distribution is inherited by one of the daughter cells after cell division. However, our time-lapse microscopic analysis showed that cells could lose the remnant (Video 9). We also observed that cell divisions of a mother

Published July 25, 2016

cell with one remnant generated two daughter cells with one remnant each (Video 10). To estimate the number of cells that have a remnant, we plot the number of cells with a remnant or a PC versus the total number of cells in the population. The plot revealed the existence of two linear regimens (Fig. 7 C). For low total cell numbers, the slope of the linear fitting was 0.32, suggesting that a fraction of newly generated cells did not conserve the remnant. For high cell numbers, the slope is practically 1.0, which means that all the new cells conserved the remnant. The point where the two linear fittings cross (73 cells) gives the transition point between the two regimens. The cell area corresponding to this transition (214 μm^2) was obtained by dividing the effective total area occupied by the cells (15,647 μm^2) by the number of cells (73 cells). The value of 214 μm^2 for this transition was used for the numerical simulation of the system.

Cell population-based simulations of the system. Simulations were performed using a Matlab (MathWorks) script developed in-house. Each simulation proceeded as follows: an initial number of 18 cells (this value was obtained from the mean of the initial number of cells in the microscope field in the experiments of Fig. 1 F) without a midbody remnant are plated on day 0 of the simulation (Fig. 7 D, i). For each cell in the population, we set a value of its individual area as explained in "Calculation of the individual cell area in the simulations" (Fig. 7 D, v). Each given cell in the simulation undergoes mitosis as soon as its age exceeds its cell cycle duration (Fig. 7 D, vi).

Based on the experimental data, we set the various transitions observed (cell cycle length, midbody remnant conservation, movement of the remnant from a peripheral to a central position, and the start of ciliogenesis) in the form of Hill functions of the cell area. In this way, we eliminated the dependence of the transitions on the time elapsed since cells were plated.

For the cell cycle length, Eq. 2 was rewritten as

$$T(A) = \frac{T_{max} + (T_{min} - T_{max})}{1 + \left(\frac{A}{S}\right)^h},$$

where the inflection of the curve was set as the cell area at 2.68 d (S = 212 μm^2) and the Hill coefficient calculated earlier (h = 100; Fig. 7 D, x).

The probability that cells have a midbody remnant was also set as a Hill function of the cell area in the form

$$P(A) = \frac{P_{max} + (P_{min} - P_{max})}{1 + \left(\frac{A}{S}\right)^h},$$

where $P(A)$ is the probability of conserving the remnant per time step, and P_{max} and P_{min} are the maximum and minimum probability, respectively. The transition point was set as the cell area when the system contains 73 cells (S = 214 μm^2). The probability of conserving the remnant before the transition point was set as 0.3, based on the value of the slope of the linear fitting (value per time step = $0.3^{1/T}$ = 0.943). As time goes by, the increasing number of cells results in a reduction in the cell area (Fig. S5 C). After the transition point (that is, when the mean cell area is less than 214 μm^2), cells conserved the remnant (P_{max} = 1). The Hill coefficient was also assumed as being h = 100 (Fig. 7 D, vii).

Based on our experimental data (Fig. 7 A), the transition from a peripheral to a central remnant can take place if the cell area is less than 400 μm^2. In addition, cells with a central remnant can become ciliated if their area is less than 200 μm^2. The probabilities of these two transitions were also defined as Hill functions of the cell area, from a zero value to a constant probability that is modulated to fit the final number of cells in each configuration (Fig. 7 D, viii and ix). Each simulation produces a slightly different outcome in the population of cells because we introduce variability in the value of the cell area to represent the experimental distribution of cell areas (Fig. 8 A, solid lines). For the sake of simplicity, for the simulation the calculated values for the transition for cell cycle (212 μm^2) and the probability of conserving the remnant (214 μm^2) were set as 200 μm^2 (same the value of the cell area where the first cells with a PC appear). In this way, we simplified the system by using just two transition points: 200 and 400 μm^2.

Online supplemental material

Fig. S1 shows the distribution of ciliary markers in MDCK cells during interphase and in cytokinesis. Fig. S2 shows a complete series of EM sections of a peripheral midbody remnant and a second example of peripheral remnant. Fig. S3 shows a complete series of EM sections of a remnant proximal to the centrosome at the middle of the apical membrane. Fig. S4 shows controls of cell polarization of Rab8-knockdown cells, a complete series of EM sections of a remnant in Rab8-knockdown cells, and the dynamics of the remnant in IMCD3 cells. Fig. S5 shows controls of membrane integrity of TUSP-treated cells and measures of cell area over time. Video 1 shows the formation of the intercellular bridge at the apical surface and the inheritance of the postmitotic midbody. Videos 2–4 show the movement of the midbody remnant to the center of the cell. Video 5 shows a 3D reconstruction of the midbody remnant at the center of the apical membrane. Video 6 shows the dynamics of the remnant during PC formation. Video 7 shows an example of the TUSP procedure. Video 8 shows that cells whose midbody remnant is removed by TUSP remain viable. Videos 9 and 10 show examples of a cell that loses the remnant and of cells that conserve it and divide to give rise to two daughter cells with a remnant each. Online supplemental material is available at http://www.jcb.org/cgi/content/full/jcb.201601020/DC1. Additional data are available in the JCB DataViewer at http://dx.doi.org/10.1083/jcb.201601020.dv.

Acknowledgments

The expert technical advice of the Optical and Confocal Microscopy and Electron Microscopy Units of the Centro de Biología Molecular Severo Ochoa is gratefully acknowledged. We thank Laura Fernández-Martín for her excellent technical help and Milagros Guerra for her invaluable assistance in the preparation of the EM sections. We also thank Minerva Bosch-Fortea for helpful comments. We express our gratitude to Dr. D.A. Hoffman (National Institute of Child Health and Human Development, Bethesda, MD) and Dr. J.A. Esteban (Centro de Biología Molecular Severo Ochoa, Madrid, Spain) for the use of their patch-clamp equipment.

This work was supported by the following grants from the Spanish Ministerio de Economía y Competitividad/Fondo Europeo de Desarrollo Regional: BFU2012-32532 and BFU2015-67266-R to M.A. Alonso, BFU2014-53299-P to D.G. Miguez, and TIN2012-37483-C03-02 to J.F. Fernández. Grants from the Comunidad de Madrid (S2010/BMD-2305) to I. Correas and from Instituto de Investigaciones Sanitarias Jiménez Díaz to J. Millán are also acknowledged. M. Bernabé-Rubio and D.G. Miguez are the holders of a fellowship and a Ramón y Cajal contract (RYC-2010-07450), respectively, from the Ministerio de Economía y Competitividad. G. Andrés was supported by the Amarouto Program from the Comunidad de Madrid.

The authors declare no competing financial interests.

Submitted: 7 January 2016
Accepted: 29 June 2016

Published July 25, 2016

References

Agromayor, M., and J. Martin-Serrano. 2013. Knowing when to cut and run: Mechanisms that control cytokinetic abscission. *Trends Cell Biol.* 23:433–441. http://dx.doi.org/10.1016/j.tcb.2013.04.006

Alieva, I.B., and I.A. Vorobjev. 2004. Vertebrate primary cilia: A sensory part of centrosomal complex in tissue cells, but a "sleeping beauty" in cultured cells? *Cell Biol. Int.* 28:139–150. http://dx.doi.org/10.1016/j.cellbi.2003.11.013

Ang, A.L., H. Fölsch, U.-M. Koivisto, M. Pypaert, and I. Mellman. 2003. The Rab8 GTPase selectively regulates AP-1B-dependent basolateral transport in polarized Madin-Darby canine kidney cells. *J. Cell Biol.* 163:339–350. http://dx.doi.org/10.1083/jcb.200307046

Barr, F.A. 2013. Review series: Rab GTPases and membrane identity: Causal or inconsequential? *J. Cell Biol.* 202:191–199. http://dx.doi.org/10.1083/jcb.201306010

Bazellières, E., V. Conte, A. Elosegui-Artola, X. Serra-Picamal, M. Bintanel-Morcillo, P. Roca-Cusachs, J.J. Muñoz, M. Sales-Pardo, R. Guimerà, and X. Trepat. 2015. Control of cell-cell forces and collective cell dynamics by the intercellular adhesome. *Nat. Cell Biol.* 17:409–420. http://dx.doi.org/10.1038/ncb3135

Benmerah, A. 2013. The ciliary pocket. *Curr. Opin. Cell Biol.* 25:78–84. http://dx.doi.org/10.1016/j.ceb.2012.10.011

Bornens, M. 2012. The centrosome in cells and organisms. *Science.* 335:422–426. http://dx.doi.org/10.1126/science.1209037

Chen, C.-T., H. Hehnly, and S.J. Doxsey. 2012. Orchestrating vesicle transport, ESCRTs and kinase surveillance during abscission. *Nat. Rev. Mol. Cell Biol.* 13:483–488. http://dx.doi.org/10.1038/nrm3395

Chen, C.-T., A.W. Ettinger, W.B. Huttner, and S.J. Doxsey. 2013. Resurrecting remnants: The lives of post-mitotic midbodies. *Trends Cell Biol.* 23:118–128. http://dx.doi.org/10.1016/j.tcb.2012.10.012

Das, A., and W. Guo. 2011. Rabs and the exocyst in ciliogenesis, tubulogenesis and beyond. *Trends Cell Biol.* 21:383–386. http://dx.doi.org/10.1016/j.tcb.2011.03.006

Dionne, L.K., X.-J. Wang, and R. Prekeris. 2015. Midbody: from cellular junk to regulator of cell polarity and cell fate. *Curr. Opin. Cell Biol.* 35:51–58. http://dx.doi.org/10.1016/j.ceb.2015.04.010

Dubreuil, V., A.-M. Marzesco, D. Corbeil, W.B. Huttner, and M. Wilsch-Bräuninger. 2007. Midbody and primary cilium of neural progenitors release extracellular membrane particles enriched in the stem cell marker prominin-1. *J. Cell Biol.* 176:483–495. http://dx.doi.org/10.1083/jcb.200608137

Elia, N., R. Sougrat, T.A. Spurlin, J.H. Hurley, and J. Lippincott-Schwartz. 2011. Dynamics of endosomal sorting complex required for transport (ESCRT) machinery during cytokinesis and its role in abscission. *Proc. Natl. Acad. Sci. USA.* 108:4846–4851. http://dx.doi.org/10.1073/pnas.1102714108

Ettinger, A.W., M. Wilsch-Bräuninger, A.-M. Marzesco, M. Bickle, A. Lohmann, Z. Maliga, J. Karbanová, D. Corbeil, A.A. Hyman, and W.B. Huttner. 2011. Proliferating versus differentiating stem and cancer cells exhibit distinct midbody-release behaviour. *Nat. Commun.* 2:503. http://dx.doi.org/10.1038/ncomms1511

Fededa, J.P., and D.W. Gerlich. 2012. Molecular control of animal cell cytokinesis. *Nat. Cell Biol.* 14:440–447. http://dx.doi.org/10.1038/ncb2482

Follit, J.A., R.A. Tuft, K.E. Fogarty, and G.J. Pazour. 2006. The intraflagellar transport protein IFT20 is associated with the Golgi complex and is required for cilia assembly. *Mol. Biol. Cell.* 17:3781–3792. http://dx.doi.org/10.1091/mbc.E06-02-0133

Gerdes, J.M., E.E. Davis, and N. Katsanis. 2009. The vertebrate primary cilium in development, homeostasis, and disease. *Cell.* 137:32–45. http://dx.doi.org/10.1016/j.cell.2009.03.023

Goetz, S.C., and K.V. Anderson. 2010. The primary cilium: A signalling centre during vertebrate development. *Nat. Rev. Genet.* 11:331–344. http://dx.doi.org/10.1038/nrg2774

Green, R.A., E. Paluch, and K. Oegema. 2012. Cytokinesis in animal cells. *Annu. Rev. Cell Dev. Biol.* 28:29–58. http://dx.doi.org/10.1146/annurev-cellbio-101011-155718

Gromley, A., C. Yeaman, J. Rosa, S. Redick, C.-T. Chen, S. Mirabelle, M. Guha, J. Sillibourne, and S.J. Doxsey. 2005. Centriolin anchoring of exocyst and SNARE complexes at the midbody is required for secretory-vesicle-mediated abscission. *Cell.* 123:75–87. http://dx.doi.org/10.1016/j.cell.2005.07.027

Heider, M.R., and M. Munson. 2012. Exorcising the exocyst complex. *Traffic.* 13:898–907. http://dx.doi.org/10.1111/j.1600-0854.2012.01353.x

Hildebrandt, F., T. Benzing, and N. Katsanis. 2011. Ciliopathies. *N. Engl. J. Med.* 364:1533–1543. http://dx.doi.org/10.1056/NEJMra1010172

Hu, C.-K., M. Coughlin, and T.J. Mitchison. 2012. Midbody assembly and its regulation during cytokinesis. *Mol. Biol. Cell.* 23:1024–1034. http://dx.doi.org/10.1091/mbc.E11-08-0721

Huang, S., and D.E. Ingber. 1999. The structural and mechanical complexity of cell-growth control. *Nat. Cell Biol.* 1:E131–E138. http://dx.doi.org/10.1038/13043

Ishikawa, H., and W.F. Marshall. 2014. Mechanobiology of ciliogenesis. *Bioscience.* 64:1084–1091. http://dx.doi.org/10.1093/biosci/biu173

Ishikawa, H., J. Thompson, J.R. Yates III, and W.F. Marshall. 2012. Proteomic analysis of mammalian primary cilia. *Curr. Biol.* 22:414–419. http://dx.doi.org/10.1016/j.cub.2012.01.031

Jiang, W., G. Jimenez, N.J. Wells, T.J. Hope, G.M. Wahl, T. Hunter, and R. Fukunaga. 1998. PRC1: A human mitotic spindle-associated CDK substrate protein required for cytokinesis. *Mol. Cell.* 2:877–885. http://dx.doi.org/10.1016/S1097-2765(00)80302-0

Jonsdottir, A.B., R.W. Dirks, J. Vrolijk, H.M. Ögmundsdottir, H.J. Tanke, J.E. Eyfjörd, and K. Szuhai. 2010. Centriole movements in mammalian epithelial cells during cytokinesis. *BMC Cell Biol.* 11:34. http://dx.doi.org/10.1186/1471-2121-11-34

Kaplan, A., and O. Reiner. 2011. Linking cytoplasmic dynein and transport of Rab8 vesicles to the midbody during cytokinesis by the doublecortin domain-containing 5 protein. *J. Cell Sci.* 124:3989–4000. http://dx.doi.org/10.1242/jcs.085407

Kremer, J.R., D.N. Mastronarde, and J.R. McIntosh. 1996. Computer visualization of three-dimensional image data using IMOD. *J. Struct. Biol.* 116:71–76. http://dx.doi.org/10.1006/jsbi.1996.0013

Kuhns, S., K.N. Schmidt, J. Reymann, D.F. Gilbert, A. Neuner, B. Hub, R. Carvalho, P. Wiedemann, H. Zentgraf, H. Erfle, et al. 2013. The microtubule affinity regulating kinase MARK4 promotes axoneme extension during early ciliogenesis. *J. Cell Biol.* 200:505–522. http://dx.doi.org/10.1083/jcb.201206013

Kuo, T.-C., C.-T. Chen, D. Baron, T.T. Onder, S. Loewer, S. Almeida, C.M. Weismann, P. Xu, J.-M. Houghton, F.-B. Gao, et al. 2011. Midbody accumulation through evasion of autophagy contributes to cellular reprogramming and tumorigenicity. *Nat. Cell Biol.* 13:1214–1223. http://dx.doi.org/10.1038/ncb2332

Latta, H., A.B. Maunsbach, and S.C. Madden. 1961. Cilia in different segments of the rat nephron. *J. Biophys. Biochem. Cytol.* 11:248–252. http://dx.doi.org/10.1083/jcb.11.1.248

Li, D., A. Mangan, L. Cicchini, B. Margolis, and R. Prekeris. 2014. FIP5 phosphorylation during mitosis regulates apical trafficking and lumenogenesis. *EMBO Rep.* 15:428–437. http://dx.doi.org/10.1002/embr.201338128

Marzesco, A.-M., P. Janich, M. Wilsch-Bräuninger, V. Dubreuil, K. Langenfeld, D. Corbeil, and W.B. Huttner. 2005. Release of extracellular membrane particles carrying the stem cell marker prominin-1 (CD133) from neural progenitors and other epithelial cells. *J. Cell Sci.* 118:2849–2858. http://dx.doi.org/10.1242/jcs.02439

Meder, D., A. Shevchenko, K. Simons, and J. Füllekrug. 2005. Gp135/podocalyxin and NHERF-2 participate in the formation of a preapical domain during polarization of MDCK cells. *J. Cell Biol.* 168:303–313. http://dx.doi.org/10.1083/jcb.200407072

Mierzwa, B., and D.W. Gerlich. 2014. Cytokinetic abscission: Molecular mechanisms and temporal control. *Dev. Cell.* 31:525–538. http://dx.doi.org/10.1016/j.devcel.2014.11.006

Mishima, M., S. Kaitna, and M. Glotzer. 2002. Central spindle assembly and cytokinesis require a kinesin-like protein/RhoGAP complex with microtubule bundling activity. *Dev. Cell.* 2:41–54. http://dx.doi.org/10.1016/S1534-5807(01)00110-1

Molla-Herman, A., R. Ghossoub, T. Blisnick, A. Meunier, C. Serres, F. Silbermann, C. Emmerson, K. Romeo, P. Bourdoncle, A. Schmitt, et al. 2010. The ciliary pocket: an endocytic membrane domain at the base of primary and motile cilia. *J. Cell Sci.* 123:1785–1795. http://dx.doi.org/10.1242/jcs.059519

Morais-de-Sá, E., and C. Sunkel. 2013. Adherens junctions determine the apical position of the midbody during follicular epithelial cell division. *EMBO Rep.* 14:696–703. http://dx.doi.org/10.1038/embor.2013.85

Nachury, M.V., A.V. Loktev, Q. Zhang, C.J. Westlake, J. Peränen, A. Merdes, D.C. Slusarski, R.H. Scheller, J.F. Bazan, V.C. Sheffield, and P.K. Jackson. 2007. A core complex of BBS proteins cooperates with the GTPase Rab8 to promote ciliary membrane biogenesis. *Cell.* 129:1201–1213. http://dx.doi.org/10.1016/j.cell.2007.03.053

Paridaen, J.T.M.L., M. Wilsch-Bräuninger, and W.B. Huttner. 2013. Asymmetric inheritance of centrosome-associated primary cilium membrane directs ciliogenesis after cell division. *Cell.* 155:333–344. http://dx.doi.org/10.1016/j.cell.2013.08.060

Peränen, J. 2011. Rab8 GTPase as a regulator of cell shape. *Cytoskeleton (Hoboken).* 68:527–539. http://dx.doi.org/10.1002/cm.20529

Piel, M., J. Nordberg, U. Euteneuer, and M. Bornens. 2001. Centrosome-dependent exit of cytokinesis in animal cells. *Science.* 291:1550–1553. http://dx.doi.org/10.1126/science.1057330

Pitaval, A., Q. Tseng, M. Bornens, and M. Théry. 2010. Cell shape and contractility regulate ciliogenesis in cell cycle–arrested cells. *J. Cell Biol.* 191:303–312. http://dx.doi.org/10.1083/jcb.201004003

Pohl, C., and S. Jentsch. 2009. Midbody ring disposal by autophagy is a post-abscission event of cytokinesis. *Nat. Cell Biol.* 11:65–70. http://dx.doi.org/10.1038/ncb1813

Pollarolo, G., J.G. Schulz, S. Munck, and C.G. Dotti. 2011. Cytokinesis remnants define first neuronal asymmetry in vivo. *Nat. Neurosci.* 14:1525–1533. http://dx.doi.org/10.1038/nn.2976

Puliafito, A., L. Hufnagel, P. Neveu, S. Streichan, A. Sigal, D.K. Fygenson, and B.I. Shraiman. 2012. Collective and single cell behavior in epithelial contact inhibition. *Proc. Natl. Acad. Sci. USA.* 109:739–744. http://dx.doi.org/10.1073/pnas.1007809109

Reales, E., M. Bernabé-Rubio, J. Casares-Arias, C. Rentero, J. Fernández-Barrera, L. Rangel, I. Correas, C. Enrich, G. Andrés, and M.A. Alonso. 2015. The MAL protein is crucial for proper membrane condensation at the ciliary base, which is required for primary cilium elongation. *J. Cell Sci.* 128:2261–2270. http://dx.doi.org/10.1242/jcs.164970

Reinsch, S., and E. Karsenti. 1994. Orientation of spindle axis and distribution of plasma membrane proteins during cell division in polarized MDCKII cells. *J. Cell Biol.* 126:1509–1526. http://dx.doi.org/10.1083/jcb.126.6.1509

Rodriguez-Boulan, E., G. Kreitzer, and A. Müsch. 2005. Organization of vesicular trafficking in epithelia. *Nat. Rev. Mol. Cell Biol.* 6:233–247. http://dx.doi.org/10.1038/nrm1593

Rohatgi, R., and W.J. Snell. 2010. The ciliary membrane. *Curr. Opin. Cell Biol.* 22:541–546. http://dx.doi.org/10.1016/j.ceb.2010.03.010

Rosenbaum, J.L., and G.B. Witman. 2002. Intraflagellar transport. *Nat. Rev. Mol. Cell Biol.* 3:813–825. http://dx.doi.org/10.1038/nrm952

Salzmann, V., C. Chen, C.Y.A. Chiang, A. Tiyaboonchai, M. Mayer, and Y.M. Yamashita. 2014. Centrosome-dependent asymmetric inheritance of the midbody ring in *Drosophila* germline stem cell division. *Mol. Biol. Cell.* 25:267–275. http://dx.doi.org/10.1091/mbc.E13-09-0541

Satir, P., C. Guerra, and A.J. Bell. 2007. Evolution and persistence of the cilium. *Cell Motil. Cytoskeleton.* 64:906–913. http://dx.doi.org/10.1002/cm.20238

Singh, D., and C. Pohl. 2014. Coupling of rotational cortical flow, asymmetric midbody positioning, and spindle rotation mediates dorsoventral axis formation in *C. elegans*. *Dev. Cell.* 28:253–267. http://dx.doi.org/10.1016/j.devcel.2014.01.002

Singla, V., and J.F. Reiter. 2006. The primary cilium as the cell's antenna: Signaling at a sensory organelle. *Science.* 313:629–633. http://dx.doi.org/10.1126/science.1124534

Skop, A.R., H. Liu, J. Yates III, B.J. Meyer, and R. Heald. 2004. Dissection of the mammalian midbody proteome reveals conserved cytokinesis mechanisms. *Science.* 305:61–66. http://dx.doi.org/10.1126/science.1097931

Smith, K.R., E.K. Kieserman, P.I. Wang, S.G. Basten, R.H. Giles, E.M. Marcotte, and J.B. Wallingford. 2011. A role for central spindle proteins in cilia structure and function. *Cytoskeleton (Hoboken).* 68:112–124. http://dx.doi.org/10.1002/cm.20498

Sorokin, S. 1962. Centrioles and the formation of rudimentary cilia by fibroblasts and smooth muscle cells. *J. Cell Biol.* 15:363–377. http://dx.doi.org/10.1083/jcb.15.2.363

Sorokin, S.P. 1968. Reconstructions of centriole formation and ciliogenesis in mammalian lungs. *J. Cell Sci.* 3:207–230.

Steigemann, P., C. Wurzenberger, M.H.A. Schmitz, M. Held, J. Guizetti, S. Maar, and D.W. Gerlich. 2009. Aurora B-mediated abscission checkpoint protects against tetraploidization. *Cell.* 136:473–484. http://dx.doi.org/10.1016/j.cell.2008.12.020

Tanaka, T., F.F. Serneo, C. Higgins, M.J. Gambello, A. Wynshaw-Boris, and J.G. Gleeson. 2004. Lis1 and doublecortin function with dynein to mediate coupling of the nucleus to the centrosome in neuronal migration. *J. Cell Biol.* 165:709–721. http://dx.doi.org/10.1083/jcb.200309025

Trepat, X., M.R. Wasserman, T.E. Angelini, E. Millet, D.A. Weitz, J.P. Butler, and J.J. Fredberg. 2009. Physical forces during collective cell migration. *Nat. Phys.* 5:426–430. http://dx.doi.org/10.1038/nphys1269

Vieira, O.V., K. Gaus, P. Verkade, J. Fullekrug, W.L.C. Vaz, and K. Simons. 2006. FAPP2, cilium formation, and compartmentalization of the apical membrane in polarized Madin-Darby canine kidney (MDCK) cells. *Proc. Natl. Acad. Sci. USA.* 103:18556–18561. http://dx.doi.org/10.1073/pnas.0608291103

Westlake, C.J., L.M. Baye, M.V. Nachury, K.J. Wright, K.E. Ervin, L. Phu, C. Chalouni, J.S. Beck, D.S. Kirkpatrick, D.C. Slusarski, et al. 2011. Primary cilia membrane assembly is initiated by Rab11 and transport protein particle II (TRAPPII) complex-dependent trafficking of Rabin8 to the centrosome. *Proc. Natl. Acad. Sci. USA.* 108:2759–2764. http://dx.doi.org/10.1073/pnas.1018823108

Wheatley, D.N., E.M. Feilen, Z. Yin, and S.P. Wheatley. 1994. Primary cilia in cultured mammalian cells: detection with an antibody against detyrosinated alpha-tubulin (ID5) and by electron microscopy. *J. Submicrosc. Cytol. Pathol.* 26:91–102.

Zuo, X., W. Guo, and J.H. Lipschutz. 2009. The exocyst protein Sec10 is necessary for primary ciliogenesis and cystogenesis in vitro. *Mol. Biol. Cell.* 20:2522–2529. http://dx.doi.org/10.1091/mbc.E08-07-0772

Bernabé-Rubio et al., http://www.jcb.org/cgi/content/full/jcb.201601020/DC1

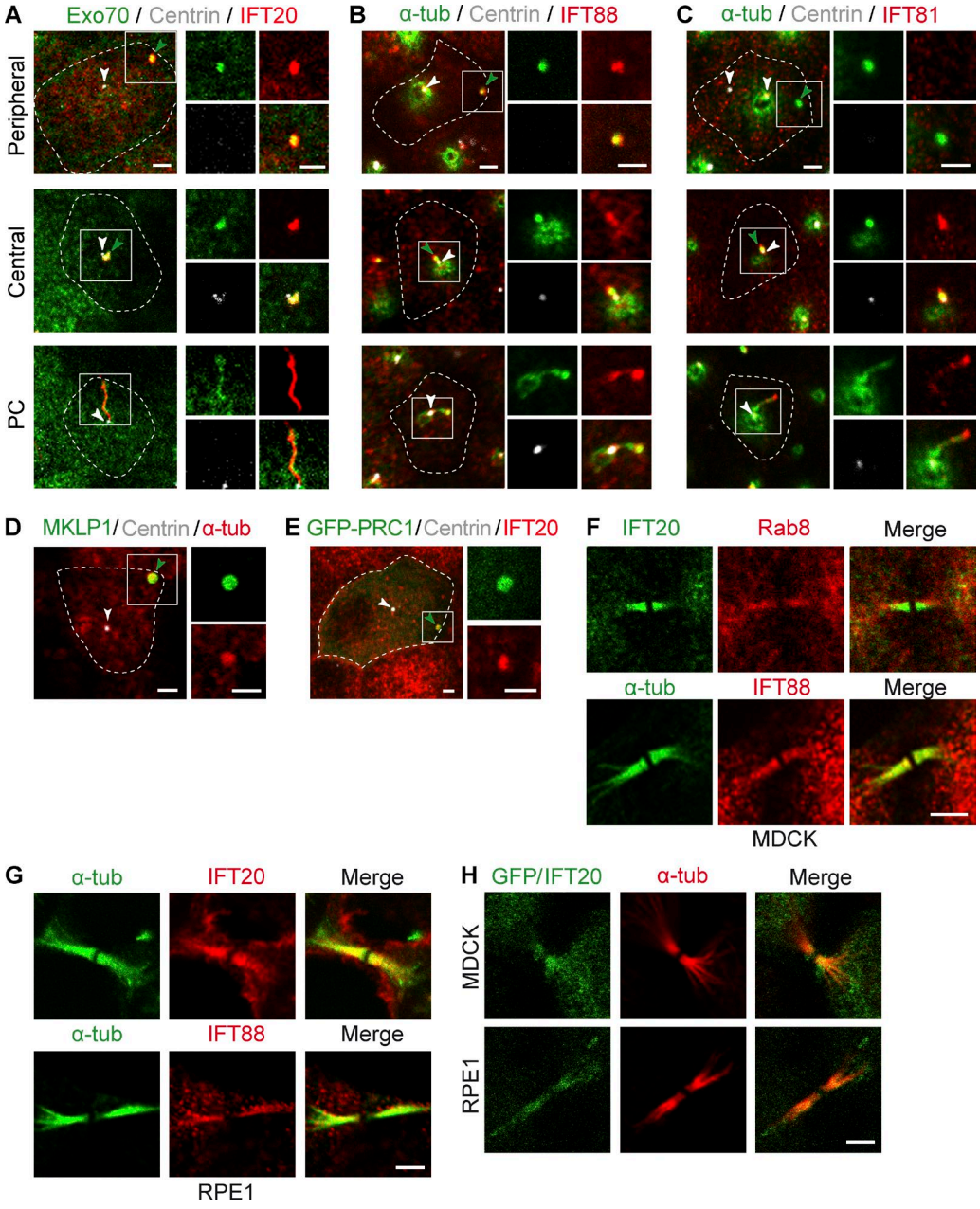

Figure S1. **Distribution of different ciliary markers in interphase cells and during cytokinesis.** MDCK cells stably expressing dsRed-centrin grown for 4 d were stained for IFT20 and Exo70 (A) and for α-tubulin (α-tub) and IFT88 (B) or IFT81 (C). Shown is the projection of one to three apical planes of one representative example of each of the discrete distributions patterns found. The enlargement shows the fluorescent signal in the boxed region of the different proteins analyzed. White arrowheads point to the centrioles, and green arrowheads point to the peripheral and central structures. Bars, 2 µm. (D) Cells expressing dsRed-centrin were stained for α-tubulin and MKLP1. The enlargements show the fluorescent signal for α-tubulin and MKLP1 in the boxed region. (E) Cells with a peripheral profile expressing dsRed-centrin and GFP-PRC1 were stained for IFT20. The enlargements show the fluorescent signal for IFT20 and GFP-PRC1 in the boxed region. The white and green arrowheads in D and E indicate the centrosome and the midbody remnant, respectively. The dashed line in A–E indicates the cell contour. (F and G) MDCK (F) and RPE1 (G) cells in cytokinesis were processed for immunofluorescence analysis with antibodies to the indicated markers. (H) MDCK cells (top) and RPE1 cells (bottom) expressing GFP-IFT20 were fixed and stained for α-tubulin. Only the intercellular bridge is shown in F–H. Bars: (A–E) 2 µm; (F–H) 3 µm.

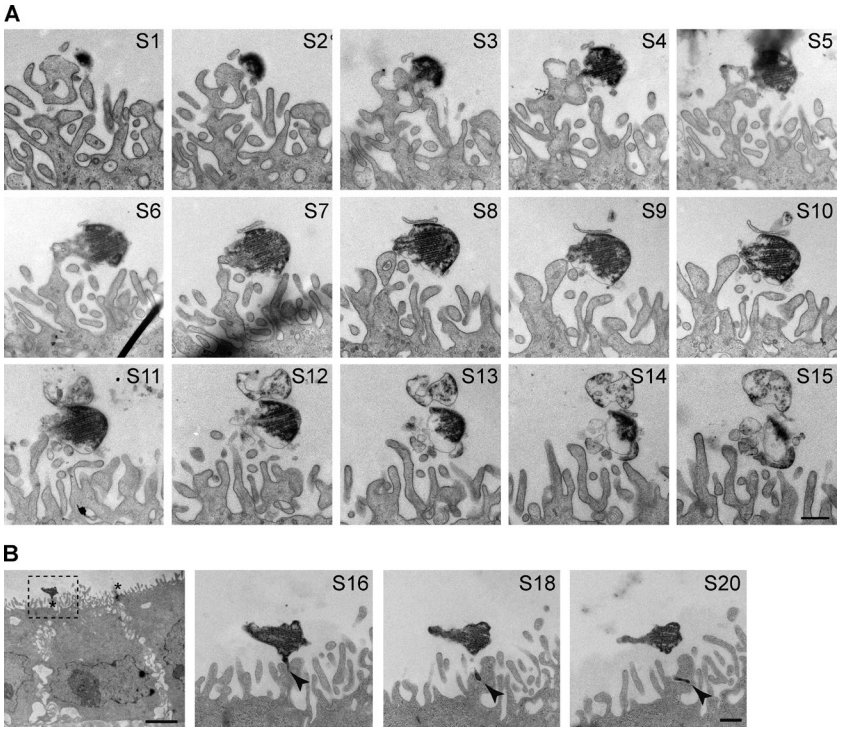

Figure S2. **EM analysis of peripheral midbody remnants.** (A) Orthogonal EM section series of the peripheral midbody remnant shown in Fig. 2 D. The images are serial sections from the same cell. The sections are numbered sequentially S1 onwards from the back to the front. The midbody remnant was identified by characteristic microtubular pattern and electrodense ultrastructure. Bar, 500 nm. (B) EM micrograph of second example of a cell with a peripheral midbody remnant and enlargements of serial sections of the same remnant. Asterisks indicate the cell junctions. The sections were numbered S1 onwards from the back to the front. Bars: (panoramic view) 3 µm; (enlargements) 500 nm.

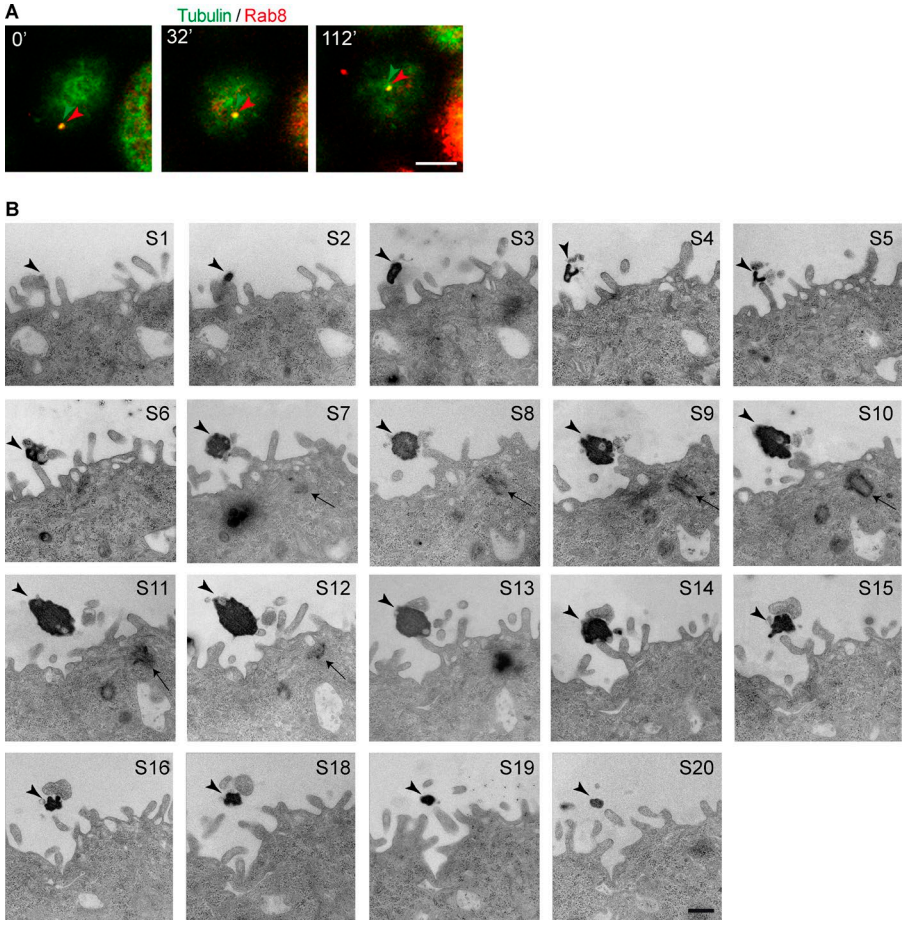

Figure S3. **EM analysis of a central midbody remnant.** (A) XY confocal stack of cells coexpressing GFP-tubulin and cherry-Rab8 during the movement of the midbody remnant. The green and the red arrowheads point to the midbody remnant pool of tubulin and Rab8, respectively. Bar, 5 µm. (B) EM analysis of a midbody remnant proximal to the centrosome. The sections are numbered sequentially S1 onwards from the front to the back. These images were used for the 3D reconstruction shown in Fig. 3 E and Video 5. The images are serial sections from the same cell. The black arrowhead indicates the midbody remnant, and the arrow marks the mother centriole, which was identified by the presence of characteristic distal appendages. Bar, 500 nm.

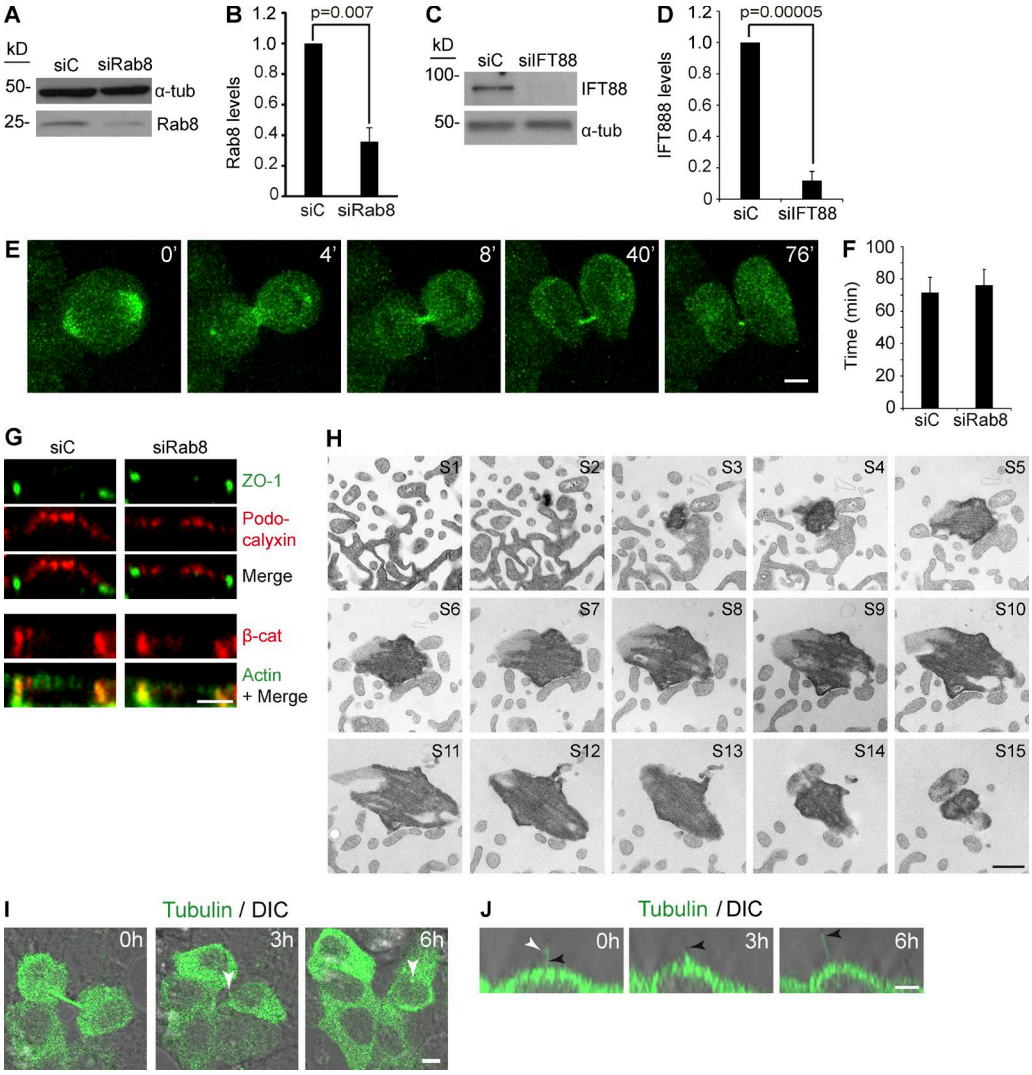

Figure S4. **Rab8 knockdown affects neither the duration of the cell cycle nor cell polarity.** (A–D) MDCK cells were transfected with siC or siRab8 (A and B) or IFT88 (C and D). Total cell extracts (A) or IFT88 immunoprecipitates (C) were analyzed by immunoblotting with antibodies to α-tubulin (α-tub) and Rab8 or IFT88 as indicated. The position of molecular mass markers is shown on the left of each blot. The levels of Rab8 (B) and IFT88 (D) were quantified. Data represent the mean + SEM from three independent experiments (Student's *t* test). (E and F) Videomicroscopic analysis of Rab8-knockdown cells expressing GFP-tubulin during cytokinesis (E). The duration of cytokinesis was measured in control and Rab8-knockdown cells (F). Data represent the mean + SD from at least three independent experiments (n = 16 cells from each type). (G) The distribution of ZO-1 and podocalyxin (top) and of β-catenin (β-cat) and F-actin (bottom) was analyzed in control and Rab8-knockdown cells. (H) Horizontal EM section series of the midbody remnant of Rab8-knockdown cells shown in Fig. 4 G. The images are serial sections from the same cell. The sections are numbered sequentially S1 onwards from the bottom to the top. Note the progressive loss of microvilli at the top sections. Bar, 500 nm. (I and J) Videomicroscopic analysis of IMCD3 cells transiently expressing GFP-tubulin during cell division (I) or primary cilium elongation (J). The corresponding differential interference contrast (DIC) images are shown superimposed to the fluorescence images. White and black arrowheads indicate the midbody remnant and the axoneme, respectively. Bars, 5 µm.

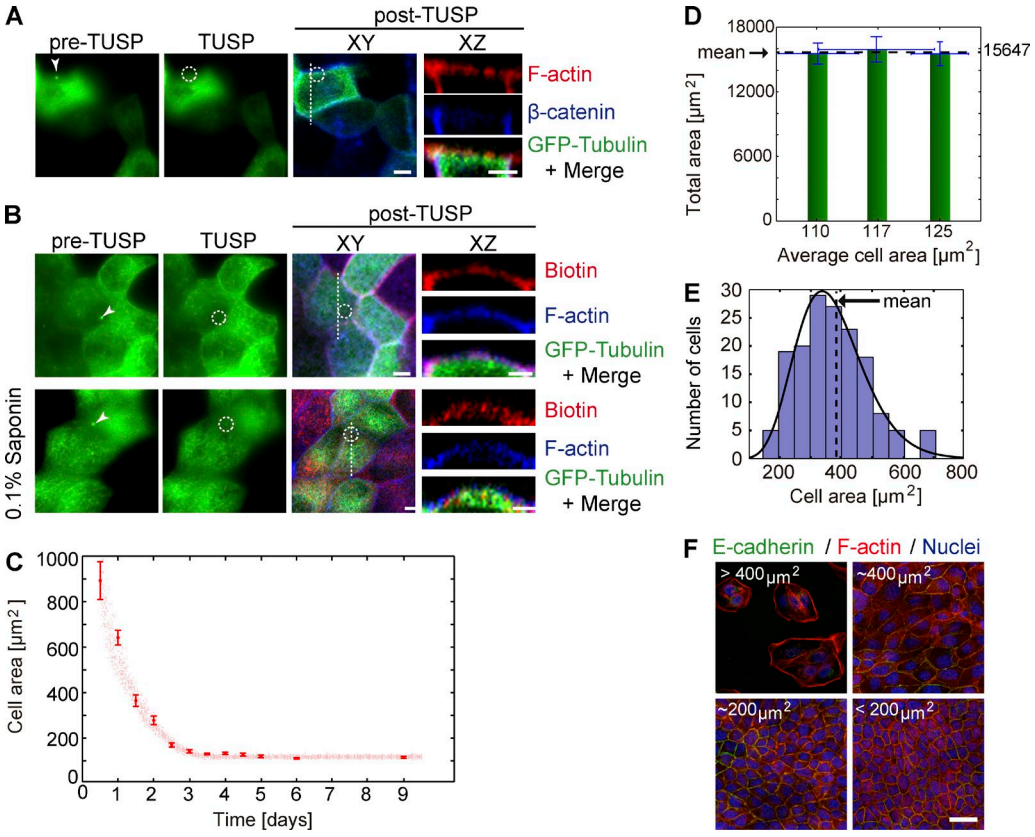

Figure S5. **Cell polarity and integrity of the plasma membrane are normal after midbody removal.** (A) The distribution of F-actin, β-catenin, and GFP-tubulin was analyzed in cells grown in coverslips in which the midbody remnant was removed by TUSP. (B) Cells expressing GFP-tubulin grown on coverslips were subjected to TUSP to remove the remnant and were left untreated (top) or, as a control, were permeabilized with 0.1% saponin (bottom). Cells were then incubated with a non–membrane-permeant protein biotinylation reagent and stained for F-actin and with fluorescent streptavidin to detect biotinylated proteins. XY and XZ projections are shown. Note that internal biotinylation is detected only in permeabilized cells. In A and B, the dotted lines indicate the plane used for the confocal XZ images shown on the right. The arrowheads point to midbody remnants, and the circles mark the plasma membrane zone subjected to TUSP. Bars, 5 μm. (C) Comparison of experimental and predicted values of cell area over time. Small dots represent the cell area resulting from 20 independent simulations. Large dots represent the experimental mean cell area, calculated by dividing the effective area of the system by the mean number of cells at each time point. Error bars represent SEM. (D) To estimate the effective total area occupied by the cells in the field of our microscope, we first calculated the mean area obtained from single-cell area measurements at days 6, 7, and 9 and multiplied it by the total number of cells at those times. The mean value of the 3 d (15,647 μm^2), which corresponds to the dashed line, was then used as the effective total area occupied by the cells in the simulations. Data represent the mean ± SEM from three independent experiments (n = 35 peripheral, 35 central, and 36 ciliary cells; two fields per experiment were analyzed). (E) Histogram of single-cell area distribution at day 2. The cell areas were individually measured and represented in 50-μm^2 intervals. The dashed line indicates the mean value. The continuous line represents the gamma distribution of the mean and 30% SD. Pooled data from three independent experiments (n = 159 cells) were used. (F) MDCK cells were stained for E-cadherin and F-actin, and the mean cell area was measured. Bar, 30 μm.

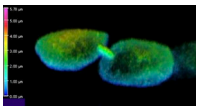

Video 1. **3D reconstruction of the intercellular bridge at the apical surface and inheritance of the midbody.** Cherry-tubulin was transiently expressed in MDCK cells. The images were pseudocolored based on height using the color scale on the left. Images were captured every 2 min. Arrowheads point to the postmitotic midbody.

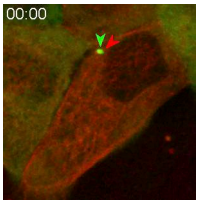

Video 2. **Movement of the midbody remnant from a peripheral position to the center of the apical surface.** Cherry-tubulin was transiently expressed in MDCK cells stably expressing GFP-PRC1. Images were captured every 5 min. Green and red arrowheads point to the GFP-PRC1 and the cherry-tubulin label within the midbody remnant, respectively.

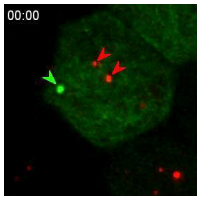

Video 3. **Encounter of the midbody remnant and the centrosome at the cell apex.** MDCK cells stably coexpressing GFP-tubulin and dsRed-centrin were used. Images were captured every 5 min. Green and red arrowheads point to the midbody and the two centrioles, respectively.

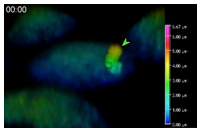

Video 4. **3D reconstruction of the movement of the midbody remnant from a peripheral position to the center of the apical surface.** MDCK cells stably expressing GFP-tubulin were used. The images were pseudocolored based on height using the color scale on the right. Images were captured every 5 min.

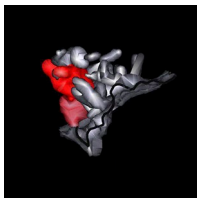

Video 5. **3D reconstruction showing a central midbody remnant embraced by microvilli.** The reconstruction was done using the EM images shown in Fig. S3 B. The midbody remnant is colored in red, the tether is highlighted in dark red, and the adjacent apical membrane is in gray.

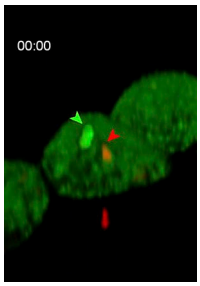

Video 6. **3D reconstruction of the dynamics of PC formation.** MDCK cells stably expressing GFP-tubulin and dsRed-centrin were used. Images were captured every 5 min during the first 90 min and every 15 min afterward. Green and red arrowheads point to the midbody remnant and centrioles, respectively. The white arrowhead points to a nascent PC.

Video 7. **Videomicroscopy of the TUSP procedure.** MDCK cells were stably transfected with GFP-tubulin. Different confocal planes of the same cell before and after TUSP are shown to visualize the presence or absence of the midbody remnant. DIC images are shown superimposed to the fluorescence images during the process of aspiration of the remnant. Images were captured in real time. The arrowhead marks the midbody remnant.

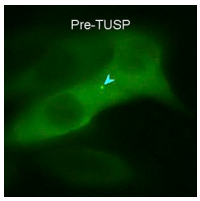

Video 8. **Cells whose midbody is removed by TUSP remain viable.** Confluent monolayers of pools of MDCK cells stably expressing or not expressing GFP-PRC1 were grown. The midbody remnant indicated by a white arrowhead was removed by TUSP. Cells are shown before and after TUSP. Cells were then incubated in the presence of 30 ng/ml hepatocyte growth factor and subjected to videomicroscopy for 11 h and 53 min. Images were captured every 23 min. The black arrowhead marks the cell whose midbody remnant was removed.

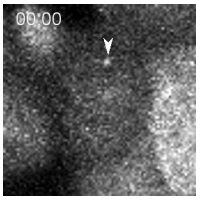

Video 9. **Midbody remnant loss.** MDCK cells stably expressing GFP-tubulin were subjected to time-lapse videomicroscopy. Note the loss of the midbody remnant. Images were captured every 1 h. The arrowhead points to the midbody remnant.

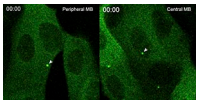

Video 10. **Division of cells with a peripheral or a central midbody remnant generates two daughter cells with a peripheral remnant each.** MDCK cells stably expressing GFP-PRC1 were subjected to time-lapse videomicroscopy. Images were captured every 23 min. The arrowheads point to midbody remnants.

Physical removal of the midbody remnant from polarised epithelial cells using take-up by suction pressure (TUSP)

Miguel Bernabé-Rubio, David C. Gershlick, Miguel A. Alonso.

Publicado en abril de 2017 en Bio-protocol *7(8)*: e2244.
doi: https://doi.org/10.21769/BioProtoc.2244

RESUMEN

El cuerpo medio o el cuerpo de Flemming es la estructura central del puente intercelular que conecta las dos células hijas durante la citocinesis. Una vez roto el puente en un proceso conocido como abscisión, el remanente del cuerpo medio puede ser heredado por una de las dos células si el corte se da en un solo sitio del puente. Además de su conocida función en la regulación del proceso de citocinesis, diversos estudios han empezado a desvelar que el remanente del cuerpo medio está implicado en procesos post-mitóticos. Se ha demostrado que este remanente es crucial para la formación del cilio primario en células epiteliales polarizadas, y que es un determinante tanto de la polaridad como de la diferenciación celular. Para demostrar la implicación del remanente del cuerpo medio en diversos procesos celulares, hemos diseñado un método para eliminarlo físicamente de la superficie apical de las células, y así poder evaluar las consecuencias de su pérdida. Este nuevo método consiste en la utilización de un equipo de *patch-clamp* conectado a una micropipeta de cristal, a través de la cual se aplica presión negativa para aspirar el remanente del cuerpo medio y así eliminarlo de la célula.

bio-protocol www.bio-protocol.org/e2244 Vol 7, Iss 08, Apr 20, 2017
DOI:10.21769/BioProtoc.2244

Physical Removal of the Midbody Remnant from Polarised Epithelial Cells Using Take-Up by Suction Pressure (TUSP)

Miguel Bernabé-Rubio[1], David C. Gershlick[2] and Miguel A. Alonso[1, *]

[1]Department of Cell Biology and Immunology, Centro de Biología Molecular Severo Ochoa, Consejo Superior de Investigaciones Científicas and Universidad Autónoma de Madrid, Madrid, Spain; [2]Cell Biology and Neurobiology Branch, Eunice Kennedy Shriver National Institute of Child Health and Human Development, National Institutes of Health, Bethesda, USA
*For correspondence: maalonso@cbm.csic.es

[Abstract] In polarised epithelial cells the midbody forms at the apical cell surface during cytokinesis. Once severed, the midbody is inherited by one of the daughter cells remaining tethered to the apical plasma membrane where it participates in non-cytokinetic processes, such as primary ciliogenesis. Here, we describe a novel method to physically remove the midbody remnant from cells and assess the possible effects caused by its loss (Bernabé-Rubio *et al.*, 2016).
Keywords: Epithelial cells, Midbody remnant, Primary cilium, Suction pressure, Patch-clamp equipment

[Background] The midbody or the Flemming body is the central part of the intercellular bridge formed between daughter cells during the final stages of mitosis. The abscission on either side of the bridge by the endosomal sorting complexes required for transport (ESCRT) machinery, results in the physical separation of the two daughter cells (Green *et al.*, 2012). In addition to its known function in the regulation of mitosis, recent studies have begun to elucidate post-mitotic roles for the midbody. Due to its role in the initiation of lumen formation in kidney cells, the midbody has been postulated to serve as a polarity cue (Li *et al.*, 2014). More recently, it has been demonstrated that the midbody remnant is directly involved in primary ciliogenesis by polarised Madin-Darby canine kidney (MDCK) cells (Bernabé-Rubio *et al.*, 2016). It has been also found to have a role in formation of the dorsoventral axis during the development of *Caenorhabditis elegans* (Singh and Pohl, 2014), and in defining cell fate and differentiation (Kuo *et al.*, 2011). Previous studies have used laser ablation to impair the function of the midbody remnant. When performed in cultured cell lines, however, laser ablation can result in cell death due to damage of the plasma membrane and proximal cytosolic elements. Accordingly, we have designed a gentle procedure, which we have called ‘take-up by suction pressure’ (TUSP). TUSP allows non-deleterious midbody remnant removal from the cell surface of epithelial cells. The fundamental principle is based on using a fine-aperture glass pipette attached to patch-clamp apparatus to physically remove the midbody with applied negative pressure (Figure 1).

Vol 7, Iss 08, Apr 20, 2017
DOI:10.21769/BioProtoc.2244

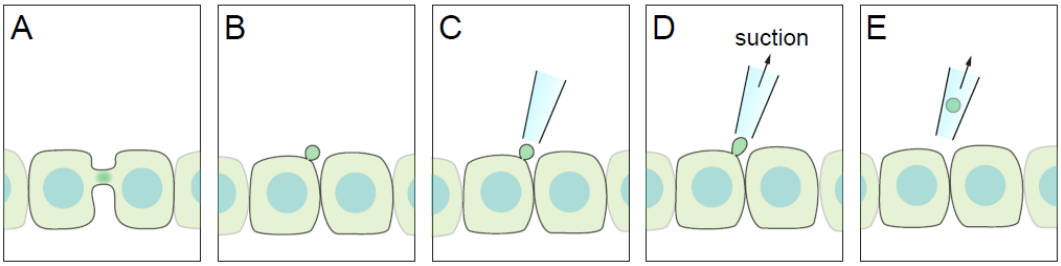

Figure 1. Diagram of the TUSP procedure. A. An apical intercellular bridge forms during cytokinesis in polarised epithelial cells. B. After abscission, one of the daughter cells inherits the midbody as a remnant, which will be positioned over the apical cell surface. C-E. By using a glass pipette connected to path-clamp apparatus, the midbody remnant can be removed from cells if suction pressure is applied.

Materials and Reagents

1. 12 mm glass coverslips #1 (VWR, catalog number: 631-0713)
2. Gridded coverslips (optional) (Electron Microscopy Sciences, catalog number: 72265-12)
3. Falcon 24-well plates (Corning, catalog number: 353047)
4. Permanent marker (Faber-Castell Multimark 1523) (CultPens, catalog number: FC19628)
5. 1 mL syringe (BD, catalog number: 303172)
6. 25 G 1 ½ needle (BD, catalog number: 305127)
7. Epithelial Madin-Darby canine kidney (MDCK II) from ATCC (ATCC, catalog number: CRL2936)
8. DNA construct expressing a fluorescent midbody localised protein (*e.g.*, Cherry-tubulin, Addgene, catalog number: 49149)
9. Dulbecco's modified Eagle's medium (DMEM) (Sigma-Aldrich, catalog number: D5796)
10. Fetal bovine serum (Sigma-Aldrich, catalog number: F7524)
11. Penicillin-streptomycin solution (Sigma-Aldrich, catalog number: P4333)
12. Lipofectamine 2000 (Thermo Fisher Scientific, Invitrogen™, catalog number: 11668027)
13. Hank's balanced salt solution (HBSS) without phenol red (Sigma-Aldrich, catalog number: H8264)
14. 1 M HEPES solution (Thermo Fisher Scientific, Gibco™, catalog number: 15630080)

Equipment

1. Autoclave
2. Tweezers (Fine Science Tools, catalog number: 11251-20)
3. LSM 710 confocal microscope (ZEISS, model: LSM 710) or any other inverted confocal microscope with 25x and 40x oil objectives and a numerical aperture of 0.8 and 1.3, respectively
4. Patch clamp equipment (Axon Instruments)
5. Microscope BX51 (Olympus, model: BX51)

Vol 7, Iss 08, Apr 20, 2017
DOI:10.21769/BioProtoc.2244

6. Borosilicate glass with filament for pipette fabrication. Outer diameter: 1.5 mm, inner diameter: 0.86 mm, 10 cm length (Linton Instrumentation, catalog number: BF150-86-10)
7. CO_2 cell culture incubator (Thermo Electron Corporation)
8. P-97 Flaming/Brown micropipette puller (Sutter Instruments, model: P-97)
9. Sutter MP-225 motorised micromanipulators (Sutter Instruments, model: MP-225)

Software

1. ImageJ (https://imagej.nih.gov/ij, National Institutes of Health)

Procedure

1. Using permanent marker, label a round coverslip with a small circle and one extra mark to keep the same orientation of the coverslip when moving between different equipment (Figure 2). Autoclave the coverslips to avoid contaminations.
   Note: Instead of using coverslips labelled with permanent marker, gridded coverslips can be used for subconfluent cell cultures. In confluent fully polarised monolayers, however, the grids can be hard to visualise.

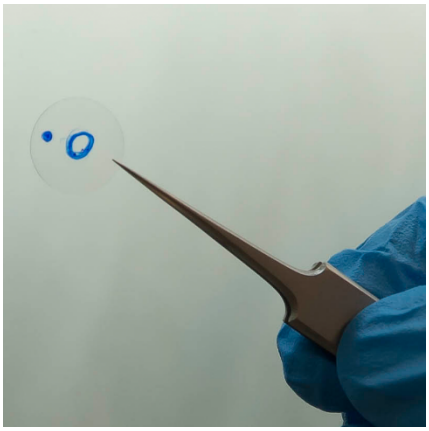

Figure 2. Round coverslip labelled with permanent marks for generation of cell maps

2. Place the coverslip into a 24-well plate and seed 200,000 MDCK cells onto the coverslip, which should be oriented so that the unmarked side is on top. Grow the cells in DMEM supplemented with 5% fetal bovine serum, 50 U/ml penicillin, and 50 µg/ml streptomycin.
3. The following day transfect MDCK cells with a midbody localised protein (*e.g.*, PRC1, MKLP1, or tubulin) genetically fused to a fluorescent protein such as GFP or mCherry. If using stably transfected cells, between 20-60% should be expressing the transgene. Cells can be diluted with untransfected cells to achieve this. It is important to have between 20-60% of cells expressing the transgene in order to have a distinctive cell map allowing easy orientation of the

Vol 7, Iss 08, Apr 20, 2017
DOI:10.21769/BioProtoc.2244

cell map at the later stages. Leave cells to grow for at least two days to allow cells to divide and subsequently generate new midbodies.

Note: We recommend using Lipofectamine 2000 reagent according to the manufacturers' instructions for transfection of MDCK cells. In this protocol we use 200,000 cells, 1 µg of DNA, and 1 µl of Lipofectamine 2000 per well.

4. For the cell map, image the cells situated inside the circle using a confocal microscope at low magnification (Figure 3). Print out the images allowing them to be used for reference in the later steps.

   Note: For the generation of cell maps, we use a 25x objective.

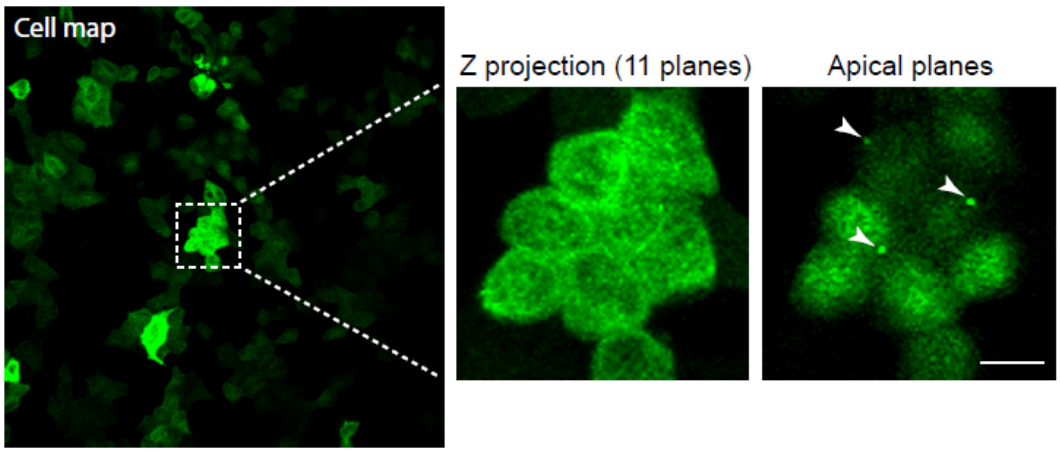

Figure 3. Generation of a cell map and midbody visualisation. Cells stably expressing GFP-tubulin were used. Cell map is represented on the far left using a 25x objective. The boxed region shows a magnification with a 40x objective, and was used for localising cells exhibiting midbodies. Note that the midbodies are localised on the apical surface. The white arrowheads mark the midbody remnants. Scale bar = 10 µm.

5. Subsequently, choose some cells to image at higher resolution to document the presence of the midbody remnants before manipulation with patch-clamp apparatus. Cells that are amenable to midbody remnant removal will have the remnants positioned over the apical cell surface (Figure 3; Video 1). Using a pen, make a note of the cells imaged on the printed image.

   Note: Be careful to avoid photobleaching. Move focal plane to the apical surface of the cell monolayer to find midbody remnants.

Vol 7, Iss 08, Apr 20, 2017
DOI:10.21769/BioProtoc.2244

Video 1. Z-stack images of MDCK cells stably expressing GFP-tubulin before TUSP. Images are shown from the basolateral to apical membranes (*i.e.*, bottom to the top). The white arrowheads point to the midbody remnants. Note that the remnants are localised at the apical cell surface.

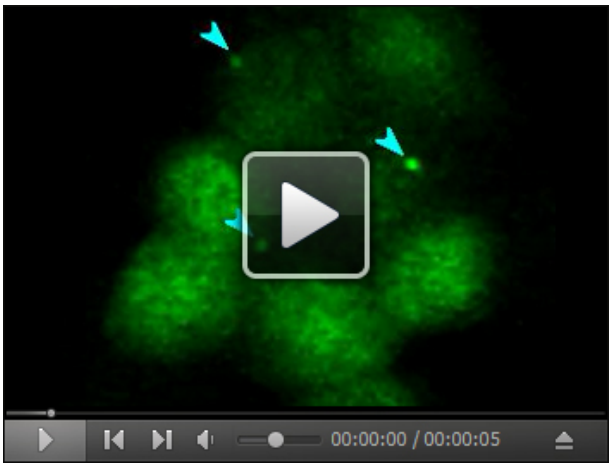

6. Transfer samples to the patch-clamp apparatus (Figure 4). Fill the chamber of the patch-clamp apparatus with HBSS medium supplemented with 0.5% fetal bovine serum, HEPES 20 mM, pH 7.2-7.5, 50 U/ml penicillin, and 50 µg/ml streptomycin, and place the coverslip into the chamber. To allow easier detection of previously imaged areas, use the marked position on the coverslip to position the sample in the same orientation as was previously used to generate the cell map.

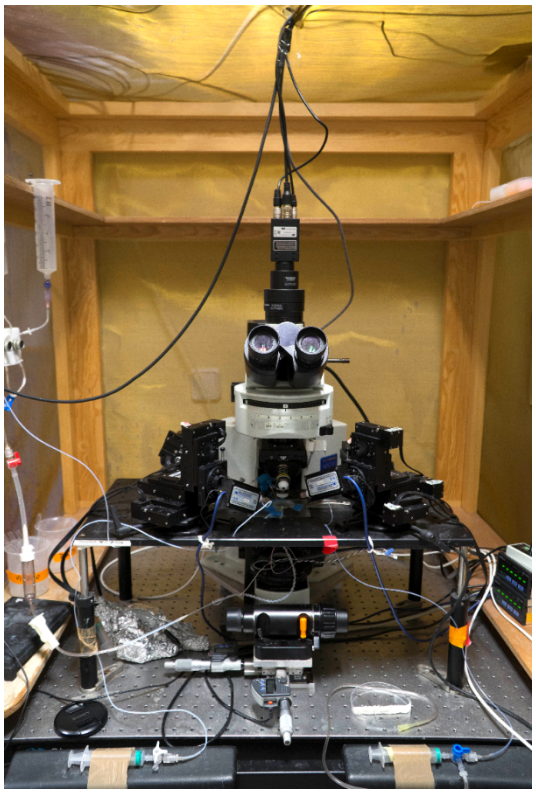

Figure 4. Patch-clamp apparatus coupled to an epifluorescence microscope

Vol 7, Iss 08, Apr 20, 2017
DOI:10.21769/BioProtoc.2244

7. Using the printed cell maps as a reference, identify the cells previously imaged inside the circle under the epifluorescence microscope coupled to the patch-clamp apparatus.
   Note: In this step, use a low magnification objective.
8. Once the cell map has been correctly oriented, use an objective of higher magnification and move along the XY axis to the position where the cells whose midbody remnants were documented before, are situated. Double-check for the presence of remnants.
   Note: In our epifluorescence microscope this step is performed with a 60x objective. Take a quick look to observe the remnants and turn off the fluorescence channel to avoid photobleaching.
9. Move the objective to allow the glass pipette to be between the objective and the monolayer.
10. For fabricating a glass pipette, load a borosilicate glass pipette of 1.5 mm in outer diameter, 0.86 mm in inner diameter, and 10 cm in length into a micropipette puller (Figure 5). Ramp value = 515-535; Pull = 0; Velocity = 15-25; 4 heating cycles.

Figure 5. Puller used for creating glass pipettes

11. Once generated, take the glass pipette, and fill it with HBSS medium using a syringe with a 25 G 1 ½ needle.
12. Fit the glass pipette to the pipette holder, and move it under the objective (Figure 6).

Vol 7, Iss 08, Apr 20, 2017
DOI:10.21769/BioProtoc.2244

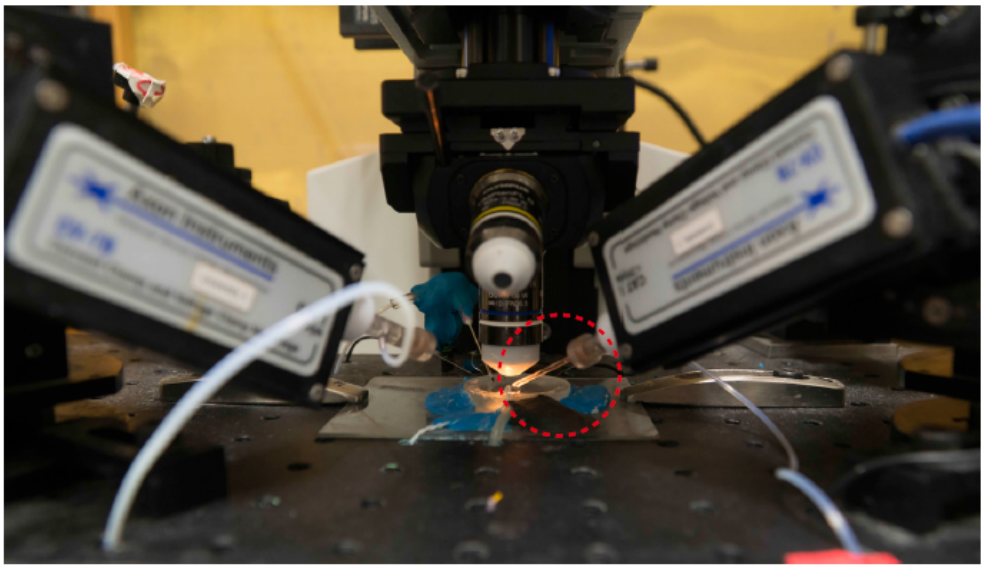

Figure 6. Glass pipette fitted to the pipette holder of the patch-clamp apparatus should be positioned in between the objective and the sample. The red circle indicates the glass pipette.

13. Use brightfield illumination to focus on the tip of the glass pipette.
14. Simultaneously move down the pipette and the objective of the microscope on the z axis until the monolayer comes into the focal plane. Do not let the glass pipette contact the monolayer at this stage.
15. Once the monolayer is in focus, use fluorescence to detect the midbody remnants (Figure 7; Video 2; Bernabé-Rubio *et al*., 2016).

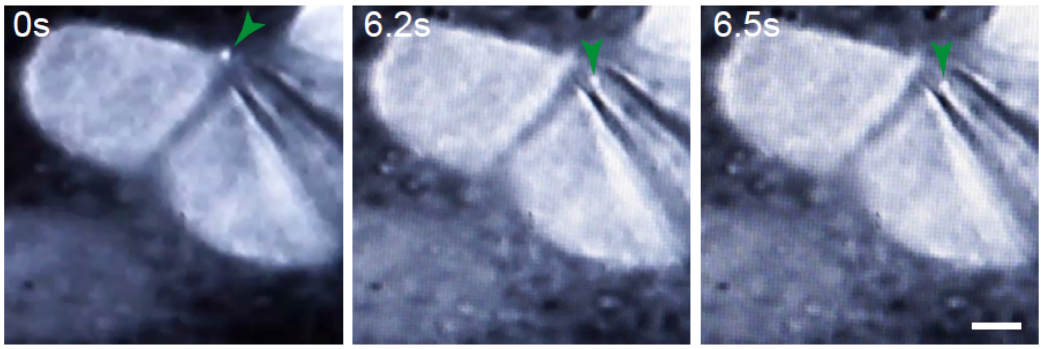

Figure 7. Representative example of cells subjected to TUSP. MDCK cells expressing GFP-tubulin were imaged at real time under an epifluorescence microscope. Green arrows indicate the midbody remnant. Scale bar = 5 μm.

Vol 7, Iss 08, Apr 20, 2017
DOI:10.21769/BioProtoc.2244

Video 2. Videomicroscopy of the TUSP procedure. MDCK cells stably expressing GFP-tubulin were subjected to TUSP. Images were captured in real time. Brightfield and fluorescence channels are shown superimposed. The green arrow indicates the position of the midbody remnant.

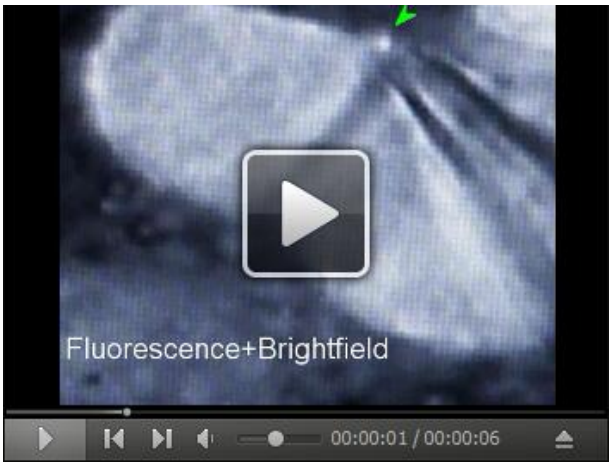

16. Select a midbody remnant for removal and slowly move the glass pipette closer to the remnant using the brightfield illumination. Once proximal to each other, keep the brightfield channel and the fluorescence superimposed. Using the mouth to apply negative pressure to the pipette via a tube, draw the midbody remnant from the cell surface (Figures 1 and 7; Video 2; Bernabé-Rubio *et al*., 2016).
17. After midbody remnant removal, image the cells under a confocal microscope acquiring different planes of the cell to ensure that removal of the whole midbody has occurred (Figure 8; Video 3).

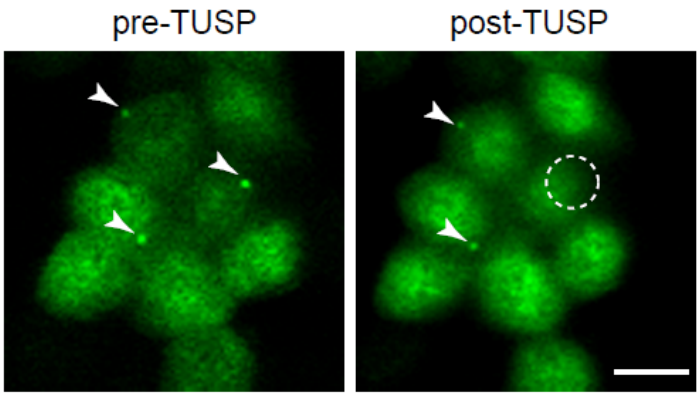

Figure 8. Midbody remnants from cells expressing GFP-tubulin were removed by TUSP. Cells exhibiting midbodies are shown before (pre-TUSP) and after TUSP (post-TUSP). Note that the remnants are localised at the apical surface. The white arrowheads mark the midbody remnants. Since cells continuously move, it is often difficult to have several cells in-focus while imaging a cell field. The circle indicates the zone subjected to TUSP. Note that the midbody remnant of the cell exposed to TUSP was removed. Scale bar = 10 μm.

Vol 7, Iss 08, Apr 20, 2017
DOI:10.21769/BioProtoc.2244

Video 3. Z-stack images of MDCK cells stably expressing GFP-tubulin before (pre-TUSP) and after TUSP (post-TUSP). Images are shown from the basolateral to apical membranes (*i.e.*, bottom to the top). The white arrowheads point to the midbody remnants. The circle indicates the zone subjected to TUSP. Note that the remnant of the cell subjected to TUSP was completely removed.

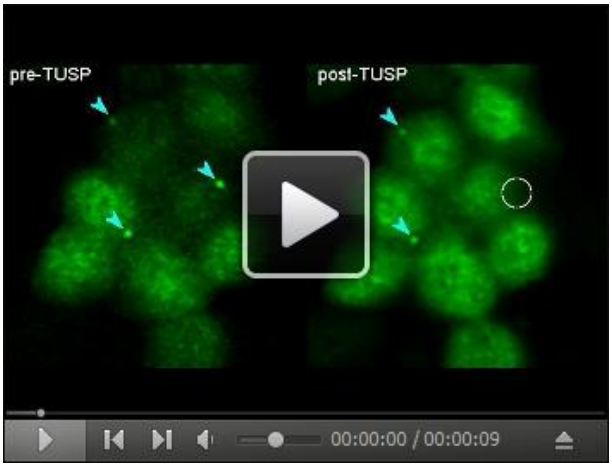

18. Place cells in an incubator at 37 °C in DMEM supplemented with 5% fetal bovine serum, 50 U/ml penicillin, and 50 µg/ml streptomycin under an atmosphere of 5% CO_2/95% air.
19. Various readouts can be used to assess possible biological effects of midbody removal using appropriate experimental setups. For example, we have studied the role of the midbody remnant in primary ciliogenesis using fluorescence microscopy (Bernabé-Rubio *et al.*, 2016).

Data analysis

For qualitative analysis of effects of midbody removal live-cell videomicroscopy can be used. This procedure can also be used to quantitatively address the absence or presence of the cilium 24 h after midbody removal, as used previously (Bernabé-Rubio *et al*., 2016). Cells should be fixed after 24 h and imaged to detect the presence of the cilium. In this case the data is categorical and as such a chi-squared analysis is appropriate after a minimum of 3 experimental repetitions with controls.

Notes

This protocol is highly reproducible as long as there is no phototoxicity/photobleaching of cells, and cell maps are clearly defined. A short exposure time to light is recommended to reduce phototoxicity/photobleaching.

Vol 7, Iss 08, Apr 20, 2017
DOI:10.21769/BioProtoc.2244

Recipes

1. HBSS medium to fill the chamber of the patch-clamp apparatus
   Hank's balanced salt solution (HBSS) without phenol red
   20 mM HEPEs (pH 7.2-7.5)
   50 U/ml penicillin, 50 µg/ml streptomycin
   0.5% fetal bovine serum
2. DMEM for MDCK cell culture
   Dulbecco's modified Eagle's medium (DMEM)
   50 U/ml penicillin, 50 µg/ml streptomycin
   5% fetal bovine serum

Acknowledgments

We thank Dr. José A. Esteban (Centro de Biología Molecular Severo Ochoa, Madrid, Spain) for the use of his patch-clamp equipment. We express our gratitude to Laura Rangel for taking some of the pictures shown in this protocol, and for recording the video of TUSP procedure. We also thank Minerva Bosch-Fortea for critical reading of the protocol. D.C.G. would like to thank Juan Bonifacino and the Bonifacino Lab for support whilst developing this protocol, and Laura Pellegrini for critically reading the protocol. The expert technical advice of the Optical and Confocal Microscopy Unit of the Centro de Biología Molecular Severo Ochoa is gratefully acknowledged. This work was supported by grant BFU2015-67266-R from the Spanish Ministerio de Economía y Competitividad/Fondo Europeo de Desarrollo Regional (MINECO/FEDER) to M.A. Alonso. M. Bernabé-Rubio is the holder of a fellowship from the Ministerio de Economía y Competitividad.

References

1. Bernabé-Rubio, M., Andres, G., Casares-Arias, J., Fernandez-Barrera, J., Rangel, L., Reglero-Real, N., Gershlick, D. C., Fernandez, J. J., Millan, J., Correas, I., Miguez, D. G. and Alonso, M. A. (2016). Novel role for the midbody in primary ciliogenesis by polarized epithelial cells. *J Cell Biol* 214(3): 259-273.
2. Green, R. A., Paluch, E. and Oegema, K. (2012). Cytokinesis in animal cells. *Annu Rev Cell Dev Biol* 28: 29-58.
3. Kuo, T. C., Chen, C. T., Baron, D., Onder, T. T., Loewer, S., Almeida, S., Weismann, C. M., Xu, P., Houghton, J. M. and Gao, F. B., Daley, G. Q. and Doxsey, S. (2011). Midbody accumulation through evasion of autophagy contributes to cellular reprogramming and tumorigenicity. *Nat Cell Biol* 13: 1214-1223.
4. Li, D., Mangan, A., Cicchini, L., Margolis, B. and Prekeris, R. (2014). FIP5 phosphorylation during mitosis regulates apical trafficking and lumenogenesis. *EMBO Rep* 15(4): 428-437.

Vol 7, Iss 08, Apr 20, 2017
DOI:10.21769/BioProtoc.2244

5. Singh, D. and Pohl, C. (2014). Coupling of rotational cortical flow, asymmetric midbody positioning, and spindle rotation mediates dorsoventral axis formation in *C. elegans*. *Dev Cell* 28(3): 253-267.

The MAL protein is crucial for proper membrane condensation at the ciliary base, which is required for primary cilium elongation

Elena Reales*, **Miguel Bernabé-Rubio***, Javier Casares-Arias, Carles Rentero, Jaime Fernández-Barrera, Laura Rangel, Isabel Correas, Carlos Enrich, Germán Andrés, Miguel A. Alonso.

* Contribución equivalente

Publicado en junio de 2015 en The Journal of Cell Science *128*; págs 2261-2270.
doi: 10.1242/jcs.164970

RESUMEN

La base del cilio primario contiene una zona especializada de membranas condensadas que se ha postulado que podría funcionar como una barrera para el movimiento de lípidos y proteínas entre la membrana apical y la ciliar. Sin embargo, los mecanismos moleculares por los cuales se establece esta zona de dominios de membrana condensados en la base del cilio se desconocen. En este trabajo estudiamos el papel de la proteína MAL, una proteína transmembrana que se asocia exclusivamente a dominios de membrana condensados, y que está implicada en transporte apical, en la formación del cilio primario. Observamos que la proteína MAL se concentra en la base del cilio primario de las células epiteliales polarizadas MDCK. Mediante su silenciamiento observamos que la compactación de membranas en la base del cilio disminuye específicamente sin que se vea alterada la condensación lipídica de la membrana apical. Esta disminución en el orden de membranas en la base del cilio resulta en una reducción significativa tanto en el número de células ciliadas como en la longitud de los cilios. Además, aprovechamos esta reducción en la compactación de membranas causada por la pérdida de MAL para examinar un posible defecto en el reclutamiento de proteínas importantes para la ciliogénesis, en el anclaje del centriolo materno a la membrana plasmática, así como un posible defecto en la ultraestructura ciliar. En este análisis observamos que el reclutamiento de proteínas necesarias para la formación del cilio como Rab8, IFT20 o IFT88 a la base del mismo, no se perturba por la ausencia de MAL, así como el anclaje del centriolo materno a la membrana plasmática o la ultraestructura de los cilios. Además, examinamos si esta perturbación del orden lipídico resultaba en la difusión de proteínas de membrana que normalmente residen en la membrana apical, como la podocalyxina, p75 o CD59, al compartimento ciliar, no observándose alteraciones

evidentes. Estos resultados sugieren que la organización de los lípidos de la base ciliar regulada por la proteína MAL es crucial para que el crecimiento del cilio primario tenga lugar de forma eficiente, y que esta zona especializada de membranas no actúa como barrera general para la entrada de proteínas de membrana al cilio. En este trabajo, por tanto, establecemos una función hasta la fecha desconocida para esta región de dominios de membrana condensados localizados en la base del cilio primario de las células epiteliales polarizadas.

© 2015. Published by The Company of Biologists Ltd | Journal of Cell Science (2015) 128, 2261-2270 doi:10.1242/jcs.164970

RESEARCH ARTICLE

The MAL protein is crucial for proper membrane condensation at the ciliary base, which is required for primary cilium elongation

Elena Reales[1,*], Miguel Bernabé-Rubio[1,*], Javier Casares-Arias[1], Carles Rentero[2], Jaime Fernández-Barrera[1], Laura Rangel[1], Isabel Correas[1], Carlos Enrich[2], Germán Andrés[3] and Miguel A. Alonso[1,‡]

ABSTRACT

The base of the primary cilium contains a zone of condensed membranes whose importance is not known. Here, we have studied the involvement of MAL, a tetraspanning protein that exclusively partitions into condensed membrane fractions, in the condensation of membranes at the ciliary base and investigated the importance of these membranes in primary cilium formation. We show that MAL accumulates at the ciliary base of epithelial MDCK cells. Knockdown of MAL expression resulted in a drastic reduction in the condensation of membranes at the ciliary base, the percentage of ciliated cells and the length of the cilia, but did not affect the docking of the centrosome to the plasma membrane or produce missorting of proteins to the pericentriolar zone or to the membrane of the remaining cilia. Rab8 (for which there are two isoforms, Rab8A and Rab8b), IFT88 and IFT20, which are important components of the machinery of ciliary growth, were recruited normally to the ciliary base of MAL-knockdown cells but were unable to elongate the primary cilium correctly. MAL, therefore, is crucial for the proper condensation of membranes at the ciliary base, which is required for efficient primary cilium extension.

KEY WORDS: Primary ciliogenesis, Centrosome, Condensed membranes, MAL

INTRODUCTION

The primary cilium is a single appendage that projects from the cell surface in most vertebrate cells. It is made up of a ciliary membrane that surrounds a microtubule-based structure, termed the axoneme, which is nucleated from the older of the two centrioles in the centrosome. Primary cilia sense a diverse range of environmental signals in the extracellular milieu and relay these to the cell body through surface receptors specifically localized on the ciliary membrane (Gerdes et al., 2009; Goetz and Anderson, 2010; Ishikawa and Marshall, 2011). Defects in primary cilium functioning are associated with a growing list of human developmental and degenerative disorders, collectively referred to as ciliopathies, that simultaneously affect many organs in the body (Hildebrandt et al., 2011; Novarino et al., 2011).

[1]Department of Cell Biology and Immunology, Centro de Biología Molecular Severo Ochoa, Consejo Superior de Investigaciones Científicas and Universidad Autónoma de Madrid, Cantoblanco, Madrid 28049, Spain. [2]Departament de Biologia Cel·lular, Immunologia i Neurociències, Institut d'Investigacions Biomèdiques August Pi i Sunyer (IDIBAPS), Facultat de Medicina, Universitat de Barcelona, Barcelona 08036, Spain. [3]Electron Microscopy Unit, Centro de Biología Molecular Severo Ochoa, Consejo Superior de Investigaciones Científicas and Universidad Autónoma de Madrid, Cantoblanco, Madrid 28049, Spain.
*These authors contributed equally to this work

[‡]Author for correspondence (maalonso@cbm.csic.es)

Received 27 October 2014; Accepted 30 April 2015

By assessing the degree of lipid condensation, it has been found that the base of cilia is more condensed than the surrounding apical membrane of epithelial Madin–Darby canine kidney (MDCK) cells (Vieira et al., 2006). Possible functions postulated for the condensed membranes at the ciliary base include that it acts to facilitate the docking of the basal body to the plasma membrane, that it modulates the elongation of the ciliary membrane, that it has a structural role or that it functions as a barrier for controlling the composition of the ciliary membrane (Reiter and Mostov, 2006; Vieira et al., 2006). Previous studies have revealed that knockdown(KD) of phosphatidylinositol-4-phosphate adaptor protein-2 (FAPP2, also known as PLEKHA8) alters the condensation of the apical membrane and reduces primary cilium formation suggesting that there is a link between apical membrane condensation and primary ciliogenesis (Vieira et al., 2006). However, the importance and role of the condensed membranes specifically found at the ciliary base in the process of primary cilium assembly are still unclear.

MAL, a 17-kDa tetraspanning membrane protein, partitions into detergent-insoluble membrane fractions (Cheong et al., 1999; Puertollano et al., 1999), which are enriched in condensed membranes also known as membrane rafts (Gaus et al., 2003; Lingwood and Simons, 2010). MAL was initially characterized as a component of the specialized machinery that regulates the rate of transport of proteins to the apical surface of MDCK cells (Cheong et al., 1999; Puertollano et al., 1999). MAL levels are important for primary ciliogenesis in MDCK cells (Takiar et al., 2012; Torkko et al., 2008), but the role of MAL in this process has remained unexplored. In this work, we show that MAL, which localizes at the base of the primary cilium, is important for membrane condensation at the ciliary base. Using MAL KD cells, we characterized the stage at which the ciliogenesis process is impacted by reduced condensation of membranes at the ciliary base. We found that the centrosome docked efficiently to the plasma membrane and that the ciliary base still controlled the access of membrane proteins and recruited machinery for primary cilium growth but, without proper membrane condensation, the ciliary base was unable to elongate the cilium efficiently. MAL and periciliary condensed membranes, therefore, appear to be required for efficient functioning of the machinery of primary cilium growth.

RESULTS

MAL expression is induced with cell confluence

Renal epithelial MDCK cells assemble a primary cilium when they reach confluence and become quiescent. To establish whether MAL expression is regulated by cell confluence, MDCK cells were grown for different times and the levels of MAL were analyzed by immunoblotting. The formation of primary cilia and the expression of the adhesion protein E-cadherin, which is known to be upregulated with increased cell–cell contacts, were examined in

Journal of Cell Science (2015) 128, 2261-2270 doi:10.1242/jcs.164970

parallel. MAL levels increased with cell confluence similar to E-cadherin levels and concomitantly with the number of ciliated cells, whereas the expression of caveolin-1, which was used as the control for the experiment, remained unaltered (Fig. 1A,B). The increase of MAL levels upon cell confluence correlated with the upregulation of MAL mRNA, as determined by quantitative real-time PCR analysis (qRT-PCR) (supplementary material Fig. S1A). In conclusion, MAL expression accompanies cell polarization, including primary cilium formation.

MAL is crucial for efficient primary cilia formation

MDCK cells segregate apical and basolateral domains and assemble a primary cilium at the center of the apical surface. To investigate the requirement for MAL in primary ciliogenesis we compared primary cilium formation in MDCK cells transfected with a control small interfering RNA (siRNA) (siC) or with siRNAs (si1 MAL and si2 MAL) targeting the sequences surrounding the AUG translation initiation site or the 3′ untranslated region, respectively, of canine MAL mRNA. The extent of endogenous MAL KD was 90–95% in the case of si1 MAL and 70% in the case of si2 MAL, as assessed by immunoblotting (Fig. 2A,B, supplementary material Fig. S1B). MAL KD produced an important decrease in the number of cilia and in the length of the remaining cilia in these cells (Fig. 2C–E, supplementary material Fig. S1C). Given that si1 MAL was more effective than si2 MAL, we used si1 MAL in all subsequent experiments. We used MDCK cells that express the intact coding sequence of human MAL mRNA (denoted MDCK-MAL cells) as an additional control. This sequence exhibited one mismatch with si1 MAL, and therefore the expression of human MAL in these cells was predicted to be less sensitive to si1 MAL than is endogenous dog MAL, as indeed proved to be the case (Fig. 2A,B). Cilia number and ciliary length were not affected in MDCK-MAL cells in which the endogenous protein was knocked down with si1 MAL (Fig. 2C–E). In summary, MAL, whose expression is induced by the time primary ciliogenesis starts, is essential for normal primary ciliogenesis.

The docking of the centrosome to the center of the apical membrane, as visualized with GFP–centrin (Fig. 3A) and the presence of the centriole subdistal and distal appendage protein marker Odf2 at the centrosome were not perturbed in MAL KD cells (Fig. 3B). The distribution of basolateral (β-catenin) and tight junction (ZO-1, also known as TJP1) markers were also unaffected (Fig. 3C), as was the periciliary ring delimiting the ciliary base visualized by galectin-3 staining (Fig. 3D). Consistent with our confocal microscopic studies, electron microscopic analysis showed that MAL KD cells exhibited stunted cilia compared with control cells (Fig. 4A, supplementary material Fig. S2). In addition, the older centriole, which is referred to as the basal body when it is docked to the plasma membrane to form a cilium, was correctly apposed to the plasma membrane and its transition fibers were apparently normal in MAL KD cells (Fig. 4, supplementary material Fig. S2). No apparent accumulation of vesicles was detected in the vicinity of the basal body in MAL KD cells (Fig. 4A, supplementary material Fig. S2). The analysis of sequential longitudinal sections confirmed that cilia in MAL KD cells were shorter than in control cells (supplementary material Fig. S2). Examination of sequential cross-sections below the transition fibers showed that the basal body had the typical triplet microtubule structure in MAL KD cells (Fig. 4B). The analysis of sequential cross-sections above the basal body revealed that the appearance of microtubule singlets occurred close to the basal body in the case of MAL KD cells (Fig. 4B). In summary, Figs 3, 4 and supplementary material Fig. S2 indicate that the effect of MAL silencing in primary ciliogenesis is not a consequence of defects in centrosome structure, basal body docking, periciliary ring assembly, fusion of transport vesicles or cell polarization.

MAL is important for membrane condensation at the ciliary base

We next analyzed the distribution of MAL relative to the primary cilium. As the current antibodies available to canine MAL are not of use in immunofluorescence studies, we used our anti-human MAL mAb 6D9 and the MDCK-MAL cell clone previously used in the rescue-of-function experiments (Fig. 2C–E). Consistent with previous observations (Martin-Belmonte et al., 1998), the 6D9 mAb recognized exogenous human MAL, but not endogenous canine protein (Fig. 5A). As revealed by double labeling with antibodies to MAL and α-tubulin, exogenous MAL was found to concentrate predominantly at the base of the cilium relative to the surrounding apical membrane in moderately confluent cell cultures (Fig. 5A, middle panel; Fig. 5B) and also at the primary cilium at high cell confluency (Fig. 5A, bottom panel; Fig. 5C). The distribution of MAL indicates that it could play a role at the ciliary base during primary ciliogenesis and at the primary cilium.

The packing density of biological membranes can be directly measured using the Laurdan fluorescent membrane dye (Gaus et al., 2006). The Laurdan dye penetrates the cell membrane and aligns parallel to the phospholipids (Bagatolli et al., 2003), undergoing a shift in its peak emission wavelength from 500 nm in fluid membranes to 440 nm in ordered membranes. A normalized ratio of the two emission regions, given by the general polarization

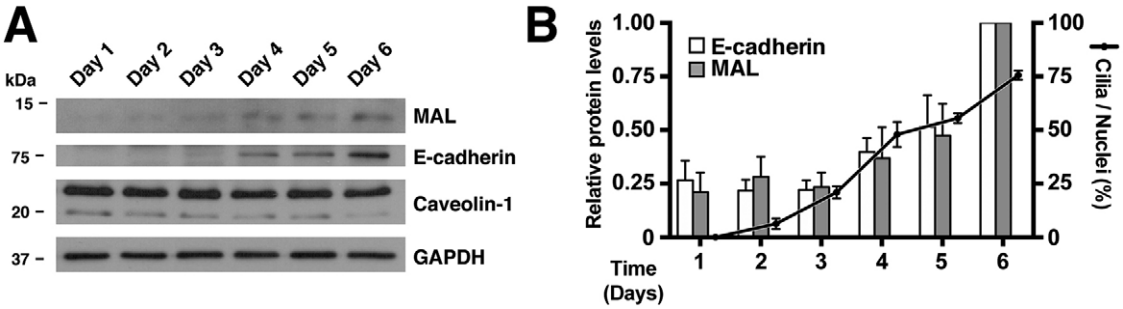

Fig. 1. MAL expression is induced with cell confluence and regulates primary ciliogenesis. (A,B) Extracts of MDCK cells grown for different times were immunoblotted for the indicated proteins. The levels of MAL and E-cadherin were quantified and normalized to those of glyceraldehyde 3-phosphate dehydrogenase (GAPDH), which was used as loading control (left *y*-axis). The number of cilia was determined in parallel experiments (right *y*-axis). The histogram illustrates the levels of MAL and the number of cilia relative to the values on day 6 (B). Data are the mean±s.e.m. from at least three independent experiments.

Journal of Cell Science (2015) 128, 2261-2270 doi:10.1242/jcs.164970

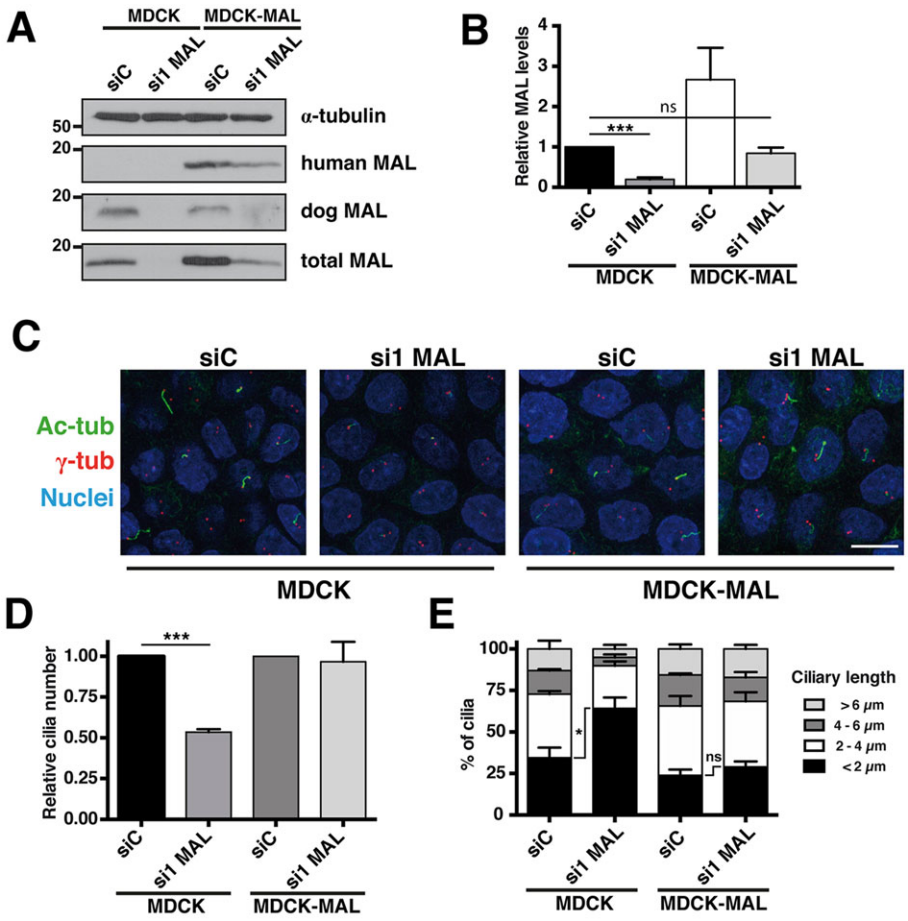

Fig. 2. MAL regulates primary ciliogenesis. (A–E) Control or MDCK cells stably expressing human MAL (MDCK-MAL) were transfected with the indicated siRNA. Cell extracts were immunoblotted for α-tubulin or for human (mAb 6D9), dog (mAb 2E5) or total (goat polyclonal) MAL, as indicated (A). The intensity of the MAL bands obtained with the antibody to total MAL was quantified. The values obtained for MAL were corrected using those of α-tubulin and represented relative to those in control cells (B). Cells grown in Transwell inserts for 72 h were stained for acetylated-tubulin (Ac-tub), γ-tubulin and nuclei (C). The number of primary cilia was determined and expressed relative to that in control cells transfected with siC (D). The length of the cilia was measured and the values were grouped in the indicated size ranges. The results represent the percentage of cilia in each range relative to the total number of cilia present in each condition (E). Scale bar: 10 μm. Data in B, D and E are the mean±s.e.m. from at least three independent experiments. **P*<0.05; ****P*<0.001; ns, not significant.

index provides a relative measure of membrane order. This experimental approach was previously used to demonstrate the existence of condensed membranes at the ciliary base of MDCK cells (Vieira et al., 2006). To investigate whether MAL regulates membrane condensation at this important zone, we stained the cells with Laurdan and measured membrane order at the ciliary base, which was visualized by galectin-3 labeling. Membrane condensation at the ciliary base was dramatically diminished in MAL KD cells, whereas it was not significantly affected in the rest of the apical membrane (Fig. 5D,E). This result indicates that MAL expression is crucial for membrane condensation at the ciliary base.

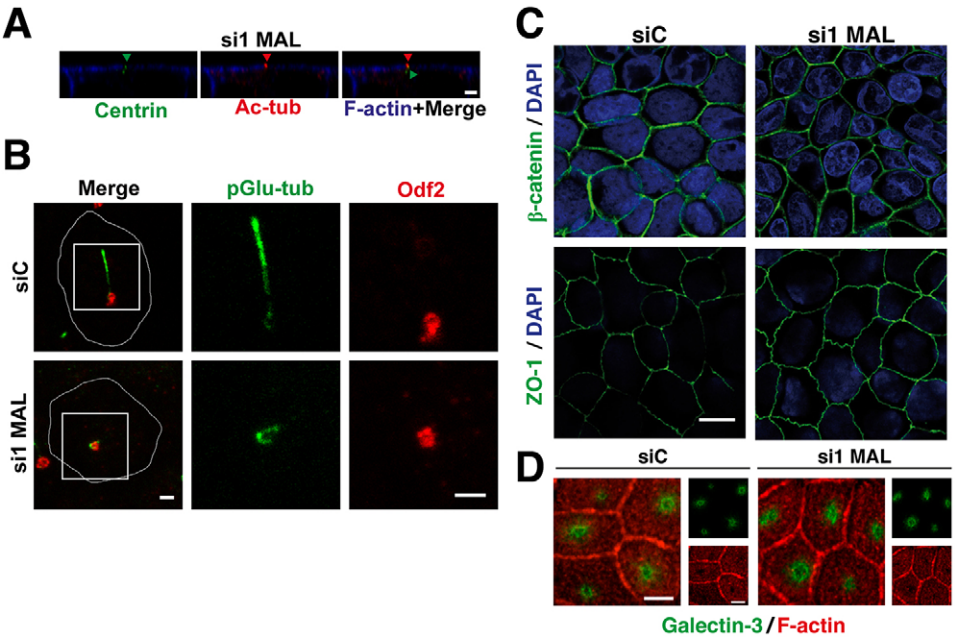

Fig. 3. Effect of MAL knockdown on the distribution of a range of protein markers. (A) MAL KD cells stably expressing GFP–centrin (green arrowhead) grown on Transwell inserts were stained for acetylated tubulin (Ac-tub, red arrowhead) and F-actin. The *xz* projection shows that the centrosome was correctly positioned at the center of the apical membrane. Scale bar: 2 μm. (B) Cells were stained for the subdistal and distal appendage marker Odf2 (red) and polyglutamylated tubulin (pGlu-tub, green), which stains the axoneme. The white line indicates the cell contour. The merged image is shown on the left. The right panels show the separate stainings. Scale bars: 3 μm. (C) Cells were grown in Transwell inserts for 72 h. Cells were labeled with DAPI to visualize the nuclei and stained for β-catenin or ZO-1, as indicated. Scale bar: 10 μm. (D) Cells were stained for galectin-3 and F-actin. The merged image is shown on the left. The right panels show the separate stainings. Scale bar: 3 μm.

Journal of Cell Science (2015) 128, 2261-2270 doi:10.1242/jcs.164970

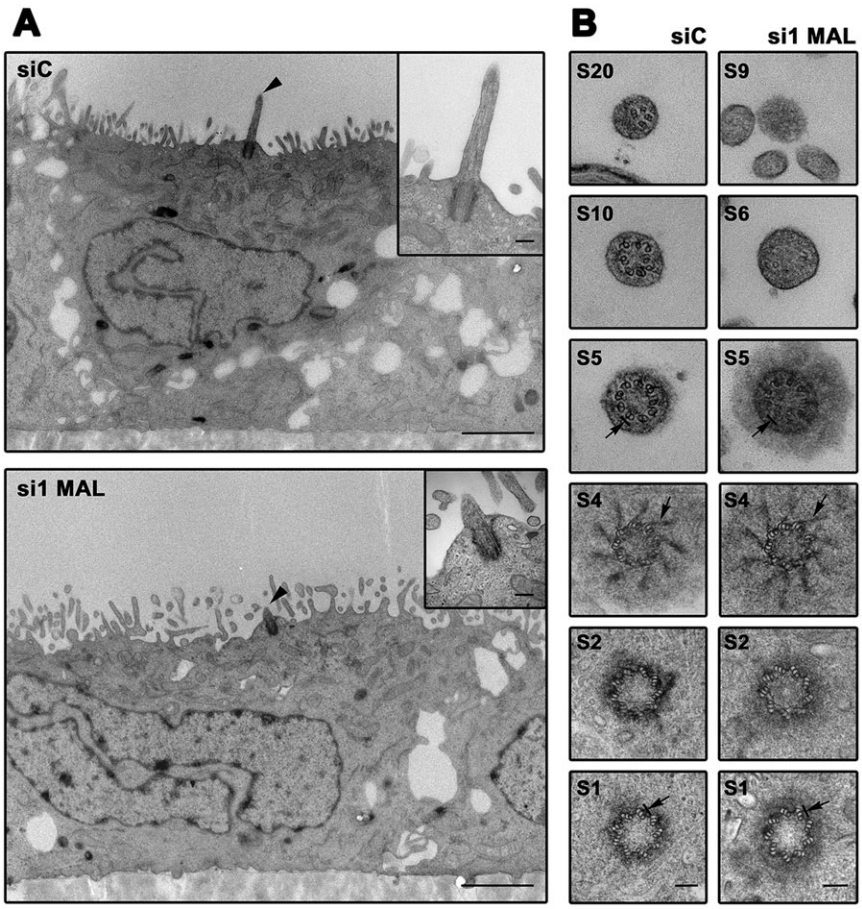

Fig. 4. Ultrastructural analysis of the primary cilium in control and MAL-knockdown cells. MDCK cells grown on Transwell filters for 5 days were fixed, embedded in resin and sectioned orthogonally to or in parallel with the supporting substrate.
(A) Representative image of a primary cilium in control and MAL KD cells. Note that the primary cilium (arrowhead), which appears longitudinally sectioned, is shorter in MAL-KD cells than in control cells. The insets show the primary cilium at higher magnification.
(B) Representative images of a cross-sectioned primary cilium of control and MAL KD cells. The sections are numbered from the basal body (S1 to S4) to the tip of the cilium (S5 onwards). Note that although the cilium ends prematurely the overall ultrastructure of the basal body and the beginning of the cilium in MAL KD cells are similar to those in control cells. Arrows in S1 point to the microtubule triplets of the basal body, in S4 to the transition filaments (S4), and in S5 to the axoneme doublets. Scale bars: 1 µm (A); 50 nm (B, insets in A).

Machinery of primary cilium growth is efficiently recruited to the ciliary base in MAL knocked-down cells

One of the functions postulated for the condensed membranes of the ciliary base is that it serves as a fence to separate the ciliary membrane from the surrounding apical membrane proteins (Reiter and Mostov, 2006; Vieira et al., 2006). If this were the case, disruption of the condensed membranes at the ciliary base would allow the entry to the pericentriolar zone and the ciliary membrane of proteins that are normally excluded. We compared the distribution of several apical membrane proteins normally excluded from the ciliary base and ciliary membrane in control and MAL KD cells (Fig. 6). We did not detect in MAL KD cells a significant increase in the access to the pericentriolar zone of the p75 neurotrophin receptor (also known as NGFR) fused to GFP (p75–GFP) (Kreitzer et al., 2003), Smoothened (Smo), a seven-pass transmembrane protein that functions in the Hedgehog signaling pathway (Chen et al., 2002), endogenous podocalyxin (Meder et al., 2005) or exogenous CD59, chosen as a representative of glycophosphatidylinositol (GPI)-anchored proteins (Lisanti et al., 1990; Lisanti and Rodriguez-Boulan, 1990). In summary, Fig. 6 shows that the condensed membranes of the ciliary base do not appear to function as a general barrier to the entry of membrane proteins into the primary cilium.

The small GTPases Rab8 (for which there are two isoforms, Rab8a and Rab8b) and Rab10 (Knodler et al., 2010) and the machinery for intraflagellar transport (IFT) are necessary for primary cilium growth (Rosenbaum and Witman, 2002). Stunted or absent cilia, as seen in MAL KD cells, have been described in cells with deficient expression of Rab8 (Westlake et al., 2011), which regulates exocytosis of ciliary components to the ciliary base, or IFT machinery, which transports proteins along the ciliary membrane (Rosenbaum and Witman, 2002). It is of note that Rab8 and two components of the IFT machinery, IFT88 and IFT20 (Follit et al., 2006; Pazour et al., 2000), distributed along the primary cilium and the pericentriolar region in control cells, whereas the three proteins localized to the pericentriolar region of MAL KD cells lacking a primary cilium (Fig. 7A–C). Smo resides outside the primary cilium under basal conditions and translocates to the primary cilium in response to Hedgehog or the Smo agonist (Milenkovic et al., 2009). Whereas Smo–GFP distributed along the ciliary membrane in control cells after agonist stimulation, we found that it accumulated at the pericentriolar region in MAL KD cells (Fig. 7D). The quantitative analysis indicated a marked increase in the presence of all the markers analyzed at the pericentriolar area in MAL KD cells (Fig. 7E). The remaining cilia of MAL KD cells were as positive as those of control cells for the four ciliary markers (Fig. 7F). The results illustrated in Fig. 7 rule out the possibility that the impairment of ciliary growth observed in MAL KD cells is due to a defect in the recruitment of Rab8 or IFT machinery to the ciliary base, or to a general defect in protein targeting to the periciliary compartment, and point to a failure in primary cilia elongation caused by the reduced condensation of membranes at the ciliary base.

DISCUSSION

A zone of highly condensed membranes of unknown importance exists at the ciliary base of epithelial MDCK cells (Vieira et al., 2006). We observed that depletion of MAL, a protein that selectively partitions into condensed membrane fractions, reduced membrane condensation at the ciliary base and inhibited primary ciliogenesis. We used MAL KD cells to test several hypothesized

Journal of Cell Science (2015) 128, 2261-2270 doi:10.1242/jcs.164970

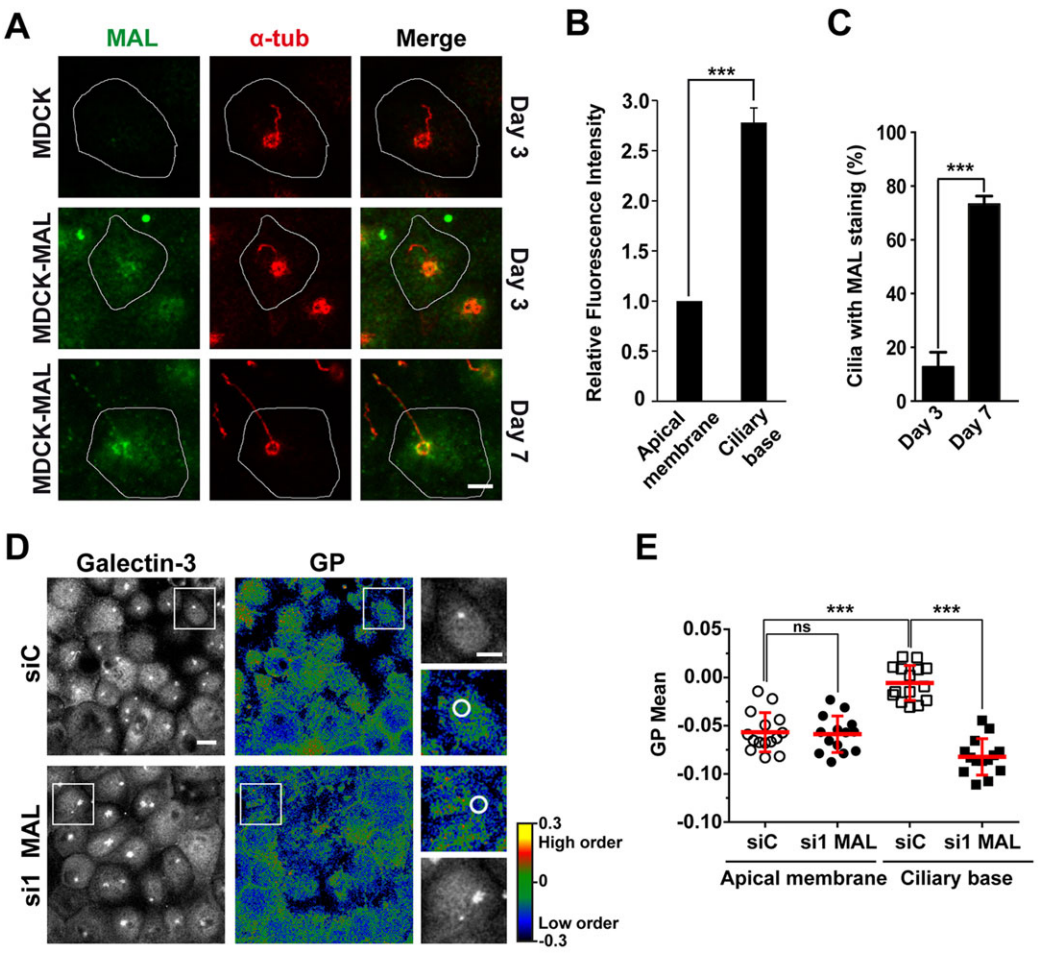

Fig. 5. MAL concentrates at the base of the primary cilium and is important for membrane condensation at the ciliary base. (A–C) Control (top panels) or MDCK-MAL cells (middle and bottom panels) grown on Transwell inserts for 3 or 7 days were immunolabeled for exogenous MAL and α-tubulin. The white line indicates the cell periphery. Scale bar: 3 µm (A). The intensity of MAL staining at day 3 was quantified in rings enclosing the ciliary base. The values are expressed relative to the mean of three identical rings chosen at random from the surrounding apical surface (B). The percentages of cilia immunolabeled for MAL at day 3 and day 7 were determined (C). (D,E) Control or MAL KD cells were stained with Laurdan and immunolabeled for galectin-3. Laurdan intensity images were converted into general polarization (GP) images and pseudocolored using the scale on the right to represent low-to-high general polarization values. Scale bar: 10 µm. An enlargement of the boxed region is shown on the right. Scale bar: 3 µm. The general polarization value corresponding to rings enclosing the membrane area delimited by galectin-3 (ciliary base) or to random zones of the same size in the apical membranes (apical) was calculated and represented (E). 15 images were used and 10–20 ciliary bases were evaluated. Data in B, C and E are the mean±s.e.m. from three independent experiments (individual data points are also shown in E). ***P<0.001; ns, not significant.

roles for condensed membranes at the ciliary base (Reiter and Mostov, 2006; Vieira et al., 2006). We concluded that MAL and these specialized membranes are not essential for docking the basal body to the plasma membrane, periciliary ring assembly or fusion of transport vesicles to the base zone. Nor do condensed membranes have general functions in excluding non-ciliary proteins from the ciliary base. Instead, interaction with the cytoskeleton (Francis et al., 2011), or physical barriers based on nucleoporins (Kee et al., 2012), septins (Hu et al., 2010) or on a complex that includes proteins disrupted in ciliopathies (Chih et al., 2011) are involved in regulating the protein composition of the primary cilium. The observation that, despite the presence of protein trafficking machinery at the ciliary base, MAL KD cells were unable to form primary cilia efficiently, and that even those that were formed were shorter than those of control cells, suggest that MAL and condensed membranes are necessary for primary cilium elongation.

Protein trafficking machinery is required for primary cilium assembly and maintenance. On the one hand, the IFT machinery aided by microtubule motors is responsible for protein transport along the cilium. On the other hand, Rab GTPases and the exocyst complex (Heider and Munson, 2012) orchestrate the assembly of the primary cilium through a network of interactions that results in a supply of membranes and ciliary growth (Das and Guo, 2011; Lim et al., 2011; Yoshimura et al., 2007; Zuo et al., 2009). Centrosome distal appendage proteins link the mother centriole with Rab GTPases and the exocyst through the direct interaction of Odf2 with Rab8 (Yoshimura et al., 2007), and the association of Odf2 with Sec15 (also known as EXOC6 in mammals), a subunit of the exocyst, mediated by centriolin (Hehnly et al., 2012). IFT20, which is also present in the Golgi, helps transport vesicular material to the ciliary base (Follit et al., 2006). We examined the presence of Odf2 at the centrosome and the distribution of IFT20, IFT88 and Rab8 and found that all of them were present at the centrosome zone regardless of MAL expression. Therefore, the ciliogenesis defect observed in MAL KD cells was not due to defective recruitment of these components. MAL specifically associates with condensed membrane or raft-enriched fractions and mediates the apical transport of the influenza virus hemagglutinin (Cheong et al.,

Journal of Cell Science (2015) 128, 2261-2270 doi:10.1242/jcs.164970

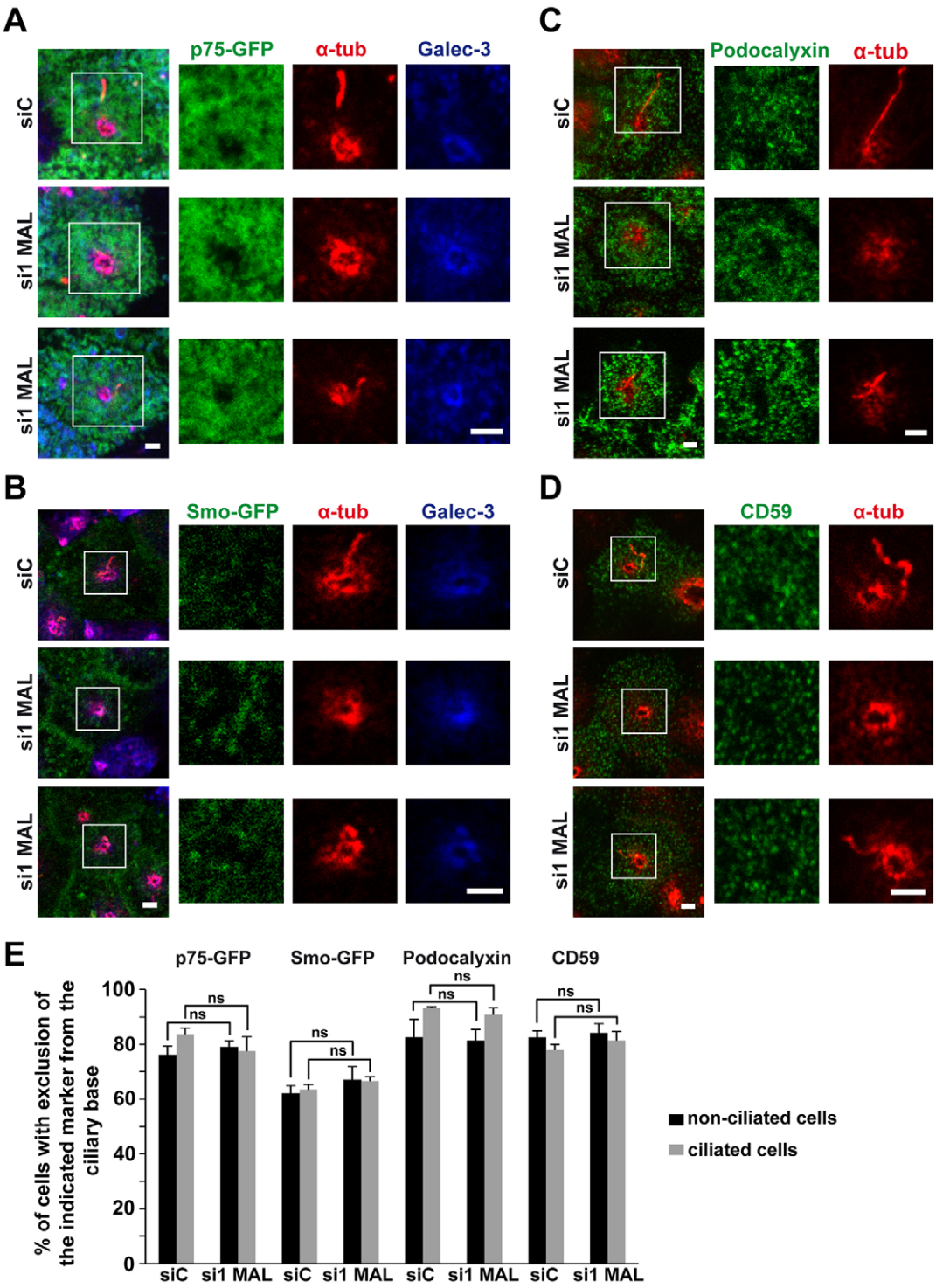

Fig. 6. Exclusion of different apical membrane proteins from the ciliary base. (A–E) Control (top panels) or MAL KD cells (middle and bottom panels) grown on Transwell inserts were labeled for galectin-3 and/or tyrosinated α-tubulin and p75–GFP (A), Smo–GFP in cells without Smo agonist treatment (B), endogenous podocalyxin (C), or exogenous CD59 (D). MAL KD cells without (middle panels) and with (bottom panels) a primary cilium are shown. Note that in A,B both galectin-3 and tyrosinated α-tubulin delimit the periciliary ring. Scale bars: 2 µm. The histogram shows the percentage of cells showing exclusion of the indicated markers from the ciliary base in cells without and with a primary cilium (E). Data are the mean±s.e.m. from three independent experiments. ns, not significant.

1999; Puertollano et al., 1999), a protein cargo associated with raft-enriched membrane fractions. We examined the extent of condensation of the membranes at the ciliary base and found striking differences between control and MAL KD cells. Given that the knockdown of endogenous MAL was quite effective it would be expected that it affects the entire cell population to a greater or lesser extent and, therefore, that the loss of membrane condensation would impair primary cilium formation in the majority of the MAL KD cells. In the case of MAL KD cell population with a primary cilium, the reduction of membrane condensation was probably lower

Journal of Cell Science (2015) 128, 2261-2270 doi:10.1242/jcs.164970

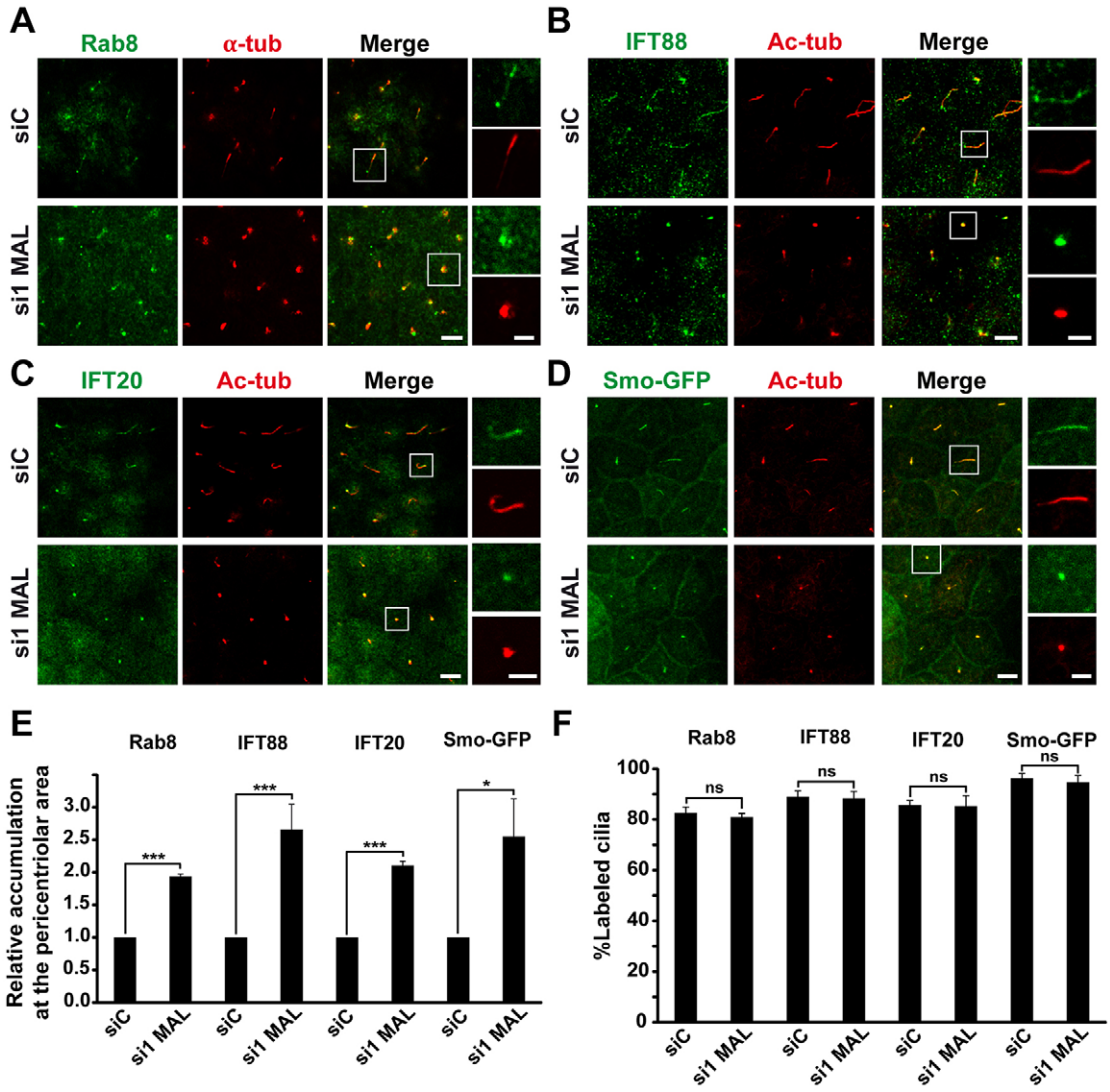

Fig. 7. The impairment of ciliary growth in MAL KD cells is not due to general defects in the recruitment of ciliary extension protein machinery. (A–F) Control or MAL KD cells were labeled for endogenous Rab8 and α-tubulin (A) or acetylated tubulin and IFT88 (B), IFT20 (C) or Smo–GFP in cells treated with 100 nM Smo agonist for 24 h (D). Scale bars: 5 µm (main panels), 2 µm (enlargements). The percentage of MAL KD cells where the indicated markers accumulated at the pericentriolar zone was determined and normalized to that in control cells (E). The percentage of cilia measuring <2 µm that were positive for the indicated markers was measured in control cells and in the remaining cilia of MAL KD cells. Data in E,F are the mean±s.e.m. from three independent experiments (*P<0.05; ***P<0.001; ns, not significant).

allowing the formation of primary cilia with varying sizes. Therefore, we find it is plausible that there is a threshold of membrane condensation at the ciliary base below which the process of ciliogenesis is totally blocked, whereas above which it takes place to a varying extent, depending on the degree of condensation. The treatment of MDCK cells with fumonisin B1, an inhibitor of ceramide biosynthesis, impairs both the percentage of ciliated cells and the length of the remaining cilia (Wang et al., 2009). Given that ceramide is a lipid component of condensed membranes, the effect of fumonisin B1 might be due to a reduction in membrane condensation at the ciliary base. Previous studies have revealed that silencing of FAPP2, another protein involved in apical transport (Vieira et al., 2005), decreases the percentage of ciliated cells in MDCK cells (Vieira et al., 2006). FAPP2 KD cells showed an increase of apical membrane condensation and a 12% reduction in the content of condensed domains of the apical surface (Vieira et al., 2006). Given that the possible effect of FAPP2 KD on the condensation of membranes at the base of the primary cilium was not addressed, we do not know whether FAPP2 is also important for proper membrane condensation at the ciliary base. Given the role of MAL in the transport of raft-associated molecules (Anton et al., 2011; Cheong et al., 1999; Puertollano et al., 1999), it is plausible that MAL affects membrane condensation at the ciliary base through the supply of raft membranes, although a direct role of MAL in the organization of raft lipids is also feasible (Magal et al., 2009). One interesting possibility is that the condensed membranes at the periciliary region are required for efficient assembly of machinery for primary cilium growth. The role of MAL would be reminiscent to that in T cells, in which MAL transports vesicles containing raft-associated Lck and regulates membrane condensation at the immunological synapse (Anton et al., 2011). This similarity offers one additional example of the proposed parallels between the primary cilium and the immunological synapse (Angus and Griffiths, 2013; Finetti and Baldari, 2013).

Journal of Cell Science (2015) 128, 2261-2270 doi:10.1242/jcs.164970

Among the many abnormalities associated with ciliopathies, renal cystic diseases are the most common (Hildebrandt and Otto, 2005; Watnick and Germino, 2003), making research on primary cilium formation in renal epithelial cells, such as MDCK cells, particularly important, especially given that the mechanism of the ciliogenesis process is cell-type- and tissue-dependent (Sorokin, 1962). Our results indicate that MAL, which is expressed in MDCK cells by the time that primary ciliogenesis commences, concentrates at the ciliary base, and is crucial for the proper condensation of membranes at the ciliary base, which is required for efficient primary cilia elongation.

MATERIALS AND METHODS

Reagents

The mouse monoclonal antibody (mAb) 6D9 specific to human MAL and the rat mAb 2E5 specific to canine MAL have been previously described (Millán and Alonso, 1998; Puertollano et al., 1999). The source of commercial antibodies to the indicated proteins used was as follows: γ-tubulin (rabbit polyclonal, T3559; mouse mAb IgG1, clone GTU-88, T6557), total α-tubulin (mouse mAb IgG1, clone DM1A, T9026), acetylated tubulin (mouse mAb IgG2b, clone 6-11B-1, T7451) and IFT20 (rabbit polyclonal, HPA021376) were from Sigma; galectin-3 (rat mAb IgG2a, clone M3/38, 125401) was from Biolegend; polyglutamylation modification (mouse mAb IgG1, clone GT335, AG-20B-0020) was from Adipogen; tyrosinated α-tubulin (rat mAb IgG2a, clone YL1/2, MA1-80017) was from Thermo Scientific; caveolin-1 (rabbit polyclonal, 610059) and Rab8 (mouse mAb IgG2b, 610844) were from BD Transduction Laboratories; ZO-1 (rat mAb IgG1, R26.4C) was from the Developmental Studies Hybridoma Bank; CD59 (mouse mAb IgG2b, ab9183) was from Abcam; podocalyxin (mouse mAb) was a gift from George K. Ojakian (Downstate Medical Center, New York, NY); IFT88 (rabbit polyclonal, 13967-AP) was from Proteintech; β-catenin (rabbit polyclonal, sc-7199), Odf2 (goat polyclonal, sc-23134) and MAL (goat polyclonal antibody, sc-46171) were from Santa Cruz Biotechnology; glyceraldehyde 3-phosphate dehydrogenase (mouse mAb IgG1, clone 6C5, AM4300) was from Life Technologies. Fluorescent phalloidin and secondary antibodies conjugated to Alexa-Fluor-488, -594 or -647 were from Life Technologies. Horseradish peroxidase (HRP)-conjugated secondary antibodies were from Jackson ImmunoResearch. Smo agonist [N-Methyl-N′-(3-pyridinylbenzyl)-N′-(3-chlorobenzo[b]thiophene-2-carbonyl)-1,4-diaminocyclohexane] was from Merck Millipore.

Cell culture, siRNA, DNA constructs and transfection conditions

Epithelial canine MDCK II cells were grown in MEM supplemented with 5% fetal bovine serum (Sigma-Aldrich) at 37°C in a 5% CO_2 atmosphere. 10^6 cells were electroporated with 20 nM of siRNA-negative control Hi GC, si1 MAL (5′-GCUGGGUGAUGUUUGUGUCUGUGUU-3′) or si2 MAL (5′-GGUGUUAUGUUUACUCUCCCAUAUA-3′) stealth-RNAi™ (Life Technologies) using Amaxa equipment run with the L-005 program. Cells were cultured on 35-mm-diameter dishes for 24 h and then grown on 12-mm polycarbonate membranes of 0.2 µm pore size (Transwell, Costar, Inc., Cambridge, MA) for 72 h. Knockdown was verified by immunoblotting 96 h after transfection. The DNA constructs expressing Smo–GFP (Addgene plasmid 25395) (Chen et al., 2002) and GFP–centrin (Addgene plasmid 29559) (Salisbury et al., 2002) were gifts from Philip Beachy (Stanford School of Medicine, Stanford, CA) and Jeffrey Salisbury (Mayo Clinic, Rochester, MN), respectively. The plasmids expressing the p75–GFP and CD59, were generous gifts from Enrique Rodriguez-Boulan (Cornell University, New York, NY) and Václav Horejsi (Institute of Molecular Genetics, Prague, Czech Republic), respectively. The DNA construct expressing intact human MAL was made in the pCDNA3.1 Zeo vector (Life Technologies). MDCK cell clones stably expressing Smo–GFP, GFP–centrin or human MAL were generated by transfection of the appropriate plasmid and selection with 1 mg/ml G-418 (Smo–GFP and GFP–centrin) or 0.75 µg/ml zeocin (MAL) (Life Technologies), respectively. The resulting clones were screened by immunofluorescence and immunoblotting.

Immunofluorescence microscopic analysis

Cells were fixed in formalin for 15 min, rinsed, and treated with 10 mM glycine in PBS for 5 min to quench the aldehyde groups. Cells were then washed, permeabilized or not with 0.1% Triton X-100 in PBS at room temperature for 5 min, rinsed, incubated with 3% (w/v) BSA for 15 min, and incubated with the primary antibody. After 1 h at room temperature, cells were washed and incubated with the appropriate fluorescent secondary antibody. For double-labeling experiments, the same procedure was repeated for the second primary antibody. Cells were mounted in coverslips using ProLong Gold antifade reagent (Invitrogen). Images were obtained using a LSM 710 confocal microscope (Carl Zeiss) with a 63× objective. Brightness and contrast were optimized with Photoshop software (Adobe). Quantifications were performed using Image J software.

Laurdan cell microscopy

Confluent MDCK cells grown on glass coverslips were stained with 50 µM Laurdan (6-dodecanoyl-2-dimethylaminonaphthalene; Life Technologies) for 30 min at 37°C (Gaus et al., 2003), fixed with formalin and immunostained for galectin-3. Laurdan imaging was performed with a TCS SP5 inverted confocal microscope (Leica) equipped with a near infrared laser (Mai Tai Broad Band 710-990 nm) and a HCX PL APO CS lambda blue 63× oil objective (1.4 NA). Confocal A555 signal (excitation 561 nm; emission 570–620 nm) was recorded followed by two-photon Laurdan images acquired at 800 nm excitation and simultaneously collected emission ranges at 400–460 nm and 470–530 nm. Generalized polarization (GP) images were calculated pixel by pixel from the Laurdan intensity images according to the equation: $GP=(I_{(400–460)}-I_{(470–530)})/(I_{(400–460)}+I_{(470–530)})$ (Owen et al., 2011). A total of 10–20 circular areas per condition, corresponding to the ciliary base, were selected on the basis of galectin-3 staining. Generalized polarization values were non-linearly fitted to a Gauss distribution using a custom-built macro in ImageJ (Rentero et al., 2008).

Electron microscopy

For transmission electron microscopy analysis, cells grown on Transwell filters were fixed with 4% paraformaldehyde and 2% glutaraldehyde for 90 min at room temperature. Cell samples were then processed for embedding in Epoxy, TAAB 812 Resin (TAAB Laboratories, Berkshire, UK) according to standard procedures. Orthogonal and parallel (from the bottom to the top of the cell) 80-nm-thick ultrathin sections were stained with saturated uranyl acetate and lead citrate by standard procedures. Samples were examined at 80 kV in a Jeol JEM-1010 (Tokyo, Japan) electron microscope. Pictures were taken with a TemCam-F416 (4 K×4 K) digital camera (TVIPS, Gauting, Germany).

qRT-PCR

Total RNA from MDCK cells was purified using RNeasy (Qiagen). MAL and E-cadherin mRNA levels were quantified by qRT-PCR procedures using the Super Script III First-Strand Synthesis SuperMix kit (Life Technologies, PN 11752250) and the qPCR FAST Sybr Green PCR Master Mix kit (Applied Biosystems, PN 4367659) in an ABI 7900HT equipment. The results were normalized with respect to the expression of β-actin, caveolin-1 and glyceraldehyde 3-phosphate dehydrogenase mRNA in the same samples. Data were analyzed with GenEX software.

Immunoblotting

Samples were subjected to SDS-PAGE and transferred onto Immobilon-P membranes (Millipore). After blocking with 5% non-fat dried milk powder and 0.05% Tween-20 in PBS, blots were incubated with the appropriate antibodies for 1 h. After several washings, blots were incubated for 30 min with secondary antibodies coupled to horseradish peroxidase. The signal was visualized with ECL chemiluminescence detection reagent (Thermo Scientific). Band intensities were quantified using Image J software and results were expressed relative to the control condition.

Statistical analysis

Data are expressed as the mean±s.e.m. of at least three independent experiments. Unless otherwise indicated, statistical significance was determined from a one-sample Student's *t*-test, calculated with GraphPad Prism software.

Acknowledgements

The expert technical advice of the personnel of the Optical and Confocal Microscopy, Electron Microscopy, and Genomics Units of the CBMSO is gratefully acknowledged. We thank Milagros Guerra for her invaluable assistance in the preparation of the EM sections.

Competing interests

The authors declare no competing or financial interests.

Author contributions

E.R and M.B.-R. performed most of the experiments; J.C.-A. analyzed MAL expression and contributed to some of the experiments; J-F.-B. and L.R. participated in some of the experiments; C.E and C.R. performed and analyzed the Laurdan microscopic analysis; I.C. designed and interpreted some of the experiments and participated in the writing of the manuscript; G.A. performed the EM analysis; M.A.A. designed and analyzed the experiments and wrote the manuscript.

Funding

This work was supported by the Ministerio de Economía y Competitividad, Spain [grant numbers BFU2012-32532 and CONSOLIDER COAT CSD2009-00016 to M. A.A.]. G.A. was supported by the Amarouto Program for senior researchers from the Comunidad Autónoma de Madrid.

Supplementary material

Supplementary material available online at
http://jcs.biologists.org/lookup/suppl/doi:10.1242/jcs.164970/-/DC1

References

Angus, K. L. and Griffiths, G. M. (2013). Cell polarisation and the immunological synapse. *Curr. Opin. Cell Biol.* **25**, 85-91.

Anton, O. M., Andrés-Delgado, L., Reglero-Real, N., Batista, A. and Alonso, M. A. (2011). MAL protein controls protein sorting at the supramolecular activation cluster of human T lymphocytes. *J. Immunol.* **186**, 6345-6356.

Bagatolli, L. A., Sanchez, S. A., Hazlett, T. and Gratton, E. (2003). Giant vesicles, Laurdan, and two-photon fluorescence microscopy: evidence of lipid lateral separation in bilayers. *Methods Enzymol.* **360**, 481-500.

Chen, J. K., Taipale, J., Cooper, M. K. and Beachy, P. A. (2002). Inhibition of Hedgehog signaling by direct binding of cyclopamine to Smoothened. *Genes Dev.* **16**, 2743-2748.

Cheong, K. H., Zacchetti, D., Schneeberger, E. E. and Simons, K. (1999). VIP17/MAL, a lipid raft-associated protein, is involved in apical transport in MDCK cells. *Proc. Natl. Acad. Sci. USA* **96**, 6241-6248.

Chih, B., Liu, P., Chinn, Y., Chalouni, C., Komuves, L. G., Hass, P. E., Sandoval, W. and Peterson, A. S. (2011). A ciliopathy complex at the transition zone protects the cilia as a privileged membrane domain. *Nat. Cell Biol.* **14**, 61-72.

Das, A. and Guo, W. (2011). Rabs and the exocyst in ciliogenesis, tubulogenesis and beyond. *Trends Cell Biol.* **21**, 383-386.

Finetti, F. and Baldari, C. T. (2013). Compartmentalization of signaling by vesicular trafficking: a shared building design for the immune synapse and the primary cilium. *Immunol. Rev.* **251**, 97-112.

Follit, J. A., Tuft, R. A., Fogarty, K. E. and Pazour, G. J. (2006). The intraflagellar transport protein IFT20 is associated with the Golgi complex and is required for cilia assembly. *Mol. Biol. Cell* **17**, 3781-3792.

Francis, S. S., Sfakianos, J., Lo, B. and Mellman, I. (2011). A hierarchy of signals regulates entry of membrane proteins into the ciliary membrane domain in epithelial cells. *J. Cell Biol.* **193**, 219-233.

Gaus, K., Gratton, E., Kable, E. P. W., Jones, A. S., Gelissen, I., Kritharides, L. and Jessup, W. (2003). Visualizing lipid structure and raft domains in living cells with two-photon microscopy. *Proc. Nat. Acad. Sci. USA* **100**, 15554-15559.

Gaus, K., Zech, T. and Harder, T. (2006). Visualizing membrane microdomains by Laurdan 2-photon microscopy. *Mol. Membr. Biol.* **23**, 41-48.

Gerdes, J. M., Davis, E. E. and Katsanis, N. (2009). The vertebrate primary cilium in development, homeostasis, and disease. *Cell* **137**, 32-45.

Goetz, S. C. and Anderson, K. V. (2010). The primary cilium: a signalling centre during vertebrate development. *Nat. Rev. Genet.* **11**, 331-344.

Hehnly, H., Chen, C.-T., Powers, C. M., Liu, H.-L. and Doxsey, S. (2012). The centrosome regulates the Rab11- dependent recycling endosome pathway at appendages of the mother centriole. *Curr. Biol.* **22**, 1944-1950.

Heider, M. R. and Munson, M. (2012). Exorcising the exocyst complex. *Traffic* **13**, 898-907.

Hildebrandt, F. and Otto, E. (2005). Cilia and centrosomes: a unifying pathogenic concept for cystic kidney disease? *Nat. Rev. Genet.* **6**, 928-940.

Hildebrandt, F., Benzing, T. and Katsanis, N. (2011). Ciliopathies. *N. Engl. J. Med.* **364**, 1533-1543.

Hu, Q., Milenkovic, L., Jin, H., Scott, M. P., Nachury, M. V., Spiliotis, E. T. and Nelson, W. J. (2010). A septin diffusion barrier at the base of the primary cilium maintains ciliary membrane protein distribution. *Science* **329**, 436-439.

Ishikawa, H. and Marshall, W. F. (2011). Ciliogenesis: building the cell's antenna. *Nat. Rev. Mol. Cell Biol.* **12**, 222-234.

Kee, H. L., Dishinger, J. F., Lynne Blasius, T., Liu, C.-J., Margolis, B. and Verhey, K. J. (2012). A size-exclusion permeability barrier and nucleoporins characterize a ciliary pore complex that regulates transport into cilia. *Nat. Cell Biol.* **14**, 431-437.

Knodler, A., Feng, S., Zhang, J., Zhang, X., Das, A., Peränen, J. and Guo, W. (2010). Coordination of Rab8 and Rab11 in primary ciliogenesis. *Proc. Natl. Acad. Sci. USA* **107**, 6346-6351.

Kreitzer, G., Schmoranzer, J., Low, S. H., Li, X., Gan, Y., Weimbs, T., Simon, S. M. and Rodriguez-Boulan, E. (2003). Three-dimensional analysis of post-Golgi carrier exocytosis in epithelial cells. *Nat. Cell Biol.* **5**, 126-136.

Lim, Y. S., Chua, C. E. L. and Tang, B. L. (2011). Rabs and other small GTPases in ciliary transport. *Biol. Cell* **103**, 209-221.

Lingwood, D. and Simons, K. (2010). Lipid rafts as a membrane-organizing principle. *Science* **327**, 46-50.

Lisanti, M., Le Bivic, A., Saltiel, A. and Rodriguez-Boulan, E. (1990). Preferred apical distribution of glycosyl-phosphatidylinositol (GPI) anchored proteins: a highly conserved feature of the polarized epithelial cell phenotype. *J. Mem. Biol.* **113**, 155-167.

Lisanti, M. and Rodriguez-Boulan, E. (1990). Glycophospholipid membrane anchoring provides clues to the mechanism of protein sorting in polarized epithelial cells. *Trends Biochem. Sci.* **15**, 113-118.

Magal, L. G., Yaffe, Y., Shepshelovich, J., Aranda, J. F., de Marco, M. C., Gaus, K., Alonso, M. A. and Hirschberg, K. (2009). Clustering and lateral concentration of raft lipids by the MAL protein. *Mol. Biol. Cell* **20**, 3751-3762.

Martin-Belmonte, F., Kremer, L., Albar, J., Marazuela, M. and Alonso, M. A. (1998). Expression of the MAL gene in the thyroid: the MAL proteolipid, a component of glycolipid-enriched membranes, is apically distributed in thyroid follicles. *Endocrinology* **139**, 2077-2084.

Meder, D., Shevchenko, A., Simons, K. and Füllekrug, J. (2005). Gp135/podocalyxin and NHERF-2 participate in the formation of a preapical domain during polarization of MDCK cells. *J. Cell Biol.* **168**, 303-313.

Milenkovic, L., Scott, M. P. and Rohatgi, R. (2009). Lateral transport of Smoothened from the plasma membrane to the membrane of the cilium. *J. Cell Biol.* **187**, 365-374.

Millán, J. and Alonso, M. A. (1998). MAL, a novel integral membrane protein of human T lymphocytes, associates with glycosylphosphatidylinositol-anchored proteins and Src-like tyrosine kinases. *Eur. J. Immunol.* **28**, 3675-3684.

Novarino, G., Akizu, N. and Gleeson, J. G. (2011). Modeling human disease in humans: the ciliopathies. *Cell* **147**, 70-79.

Owen, D. M., Rentero, C., Magenau, A., Abu-Siniyeh, A. and Gaus, K. (2011). Quantitative imaging of membrane lipid order in cells and organisms. *Nat. Protoc.* **7**, 24-35.

Pazour, G. J., Dickert, B. L., Vucica, Y., Seeley, E. S., Rosenbaum, J. L., Witman, G. B. and Cole, D. G. (2000). Chlamydomonas IFT88 and Its mouse homologue, polycystic kidney disease gene Tg737, are required for assembly of cilia and flagella. *J. Cell Biol.* **151**, 709-718.

Puertollano, R., Martín-Belmonte, F., Millán, J., de Marco, M. C., Albar, J. P., Kremer, L. and Alonso, M. A. (1999). The MAL proteolipid is necessary for normal apical transport and accurate sorting of the influenza virus hemagglutinin in Madin-Darby canine kidney cells. *J. Cell Biol.* **145**, 141-151.

Reiter, J. F. and Mostov, K. (2006). Vesicle transport, cilium formation, and membrane specialization: the origins of a sensory organelle. *Proc. Natl. Acad. Sci. USA* **103**, 18383-18384.

Rentero, C., Zech, T., Quinn, C. M., Engelhardt, K., Williamson, D., Grewal, T., Jessup, W., Harder, T. and Gaus, K. (2008). Functional implications of plasma membrane condensation for T cell activation. *PLoS ONE* **3**, e2262.

Rosenbaum, J. L. and Witman, G. B. (2002). Intraflagellar transport. *Nat. Rev. Mol. Cell Biol.* **3**, 813-825.

Salisbury, J. L., Suino, K. M., Busby, R. and Springett, M. (2002). Centrin-2 is required for centriole duplication in mammalian cells. *Curr. Biol.* **12**, 1287-1292.

Sorokin, S. (1962). Centrioles and the formation of rudimentary cilia by fibroblasts and smooth muscle cells. *J. Cell Biol.* **15**, 363-377.

Takiar, V., Mistry, K., Carmosino, M., Schaeren-Wiemers, N. and Caplan, M. J. (2012). VIP17/MAL expression modulates epithelial cyst formation and ciliogenesis. *Am. J. Physiol. Cell Physiol.* **303**, C862-C871. .

Torkko, J. M., Manninen, A., Schuck, S. and Simons, K. (2008). Depletion of apical transport proteins perturbs epithelial cyst formation and ciliogenesis. *J. Cell Sci.* **121**, 1193-1203.

Vieira, O. V., Verkade, P., Manninen, A. and Simons, K. (2005). FAPP2 is involved in the transport of apical cargo in polarized MDCK cells. *J. Cell Biol.* **170**, 521-526.

Vieira, O. V., Gaus, K., Verkade, P., Fullekrug, J., Vaz, W. L. C. and Simons, K. (2006). FAPP2, cilium formation, and compartmentalization of the apical

membrane in polarized Madin-Darby canine kidney (MDCK) cells. *Proc. Nat. Acad. Sci. USA* **103**, 18556-18561.

Wang, G., Krishnamurthy, K. and Bieberich, E. (2009). Regulation of primary cilia formation by ceramide. *J. Lipid Res.* **50**, 2103-2110.

Watnick, T. and Germino, G. (2003). From cilia to cyst. *Nat. Genet.* **34**, 355-356.

Westlake, C. J., Baye, L. M., Nachury, M. V., Wright, K. J., Ervin, K. E., Phu, L., Chalouni, C., Beck, J. S., Kirkpatrick, D. S., Slusarski, D. C. et al. (2011). Primary cilia membrane assembly is initiated by Rab11 and transport protein particle II (TRAPPII) complex-dependent trafficking of Rabin8 to the centrosome. *Proc. Natl. Acad. Sci. USA* **108**, 2759-2764.

Yoshimura, S.-i., Egerer, J., Fuchs, E., Haas, A. K. and Barr, F. A. (2007). Functional dissection of Rab GTPases involved in primary cilium formation. *J. Cell Biol.* **178**, 363-369.

Zuo, X., Guo, W. and Lipschutz, J. H. (2009). The exocyst protein sec10 is necessary for primary ciliogenesis and cystogenesis in vitro. *Mol. Biol. Cell* **20**, 2522-2529.

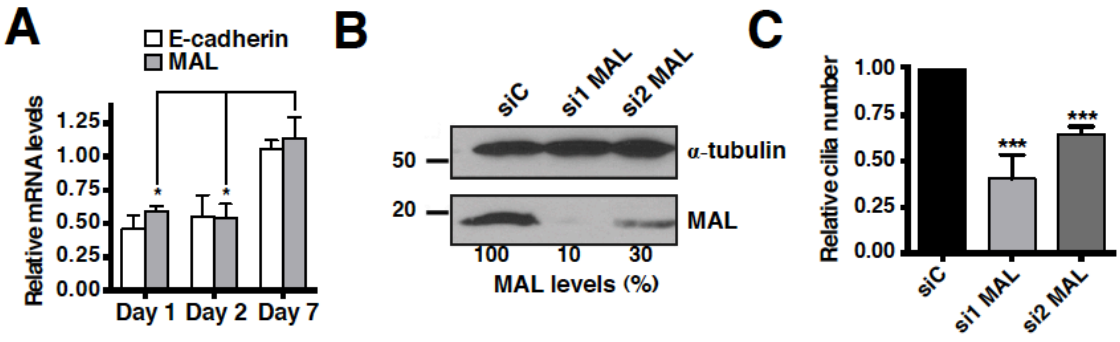

Figure S1. Effect of two siRNA targeting endogenous MAL mRNA on primary cilium formation. **(A)** The mRNA levels of MAL and E-cadherin were determined at different times of cell growth. The histogram shows the levels of mRNA normalized with respect to the value obtained on day 7. (**B, C**) MDCK cells were transfected with a control siRNA (siC) or two siRNAs (si1 MAL and si2 MAL) targeted to MAL. After 4 days, cell extracts were immunoblotted for MAL and α-tubulin. The levels of MAL are indicated at the bottom as the percentage relative to control cells (B). The number of cilia was determined after 4 days and represented relative to that in siC-transfected cells (C). Data in (A, C) are summarized as the mean ± SEM from three independent experiments (***, $p<0.001$).

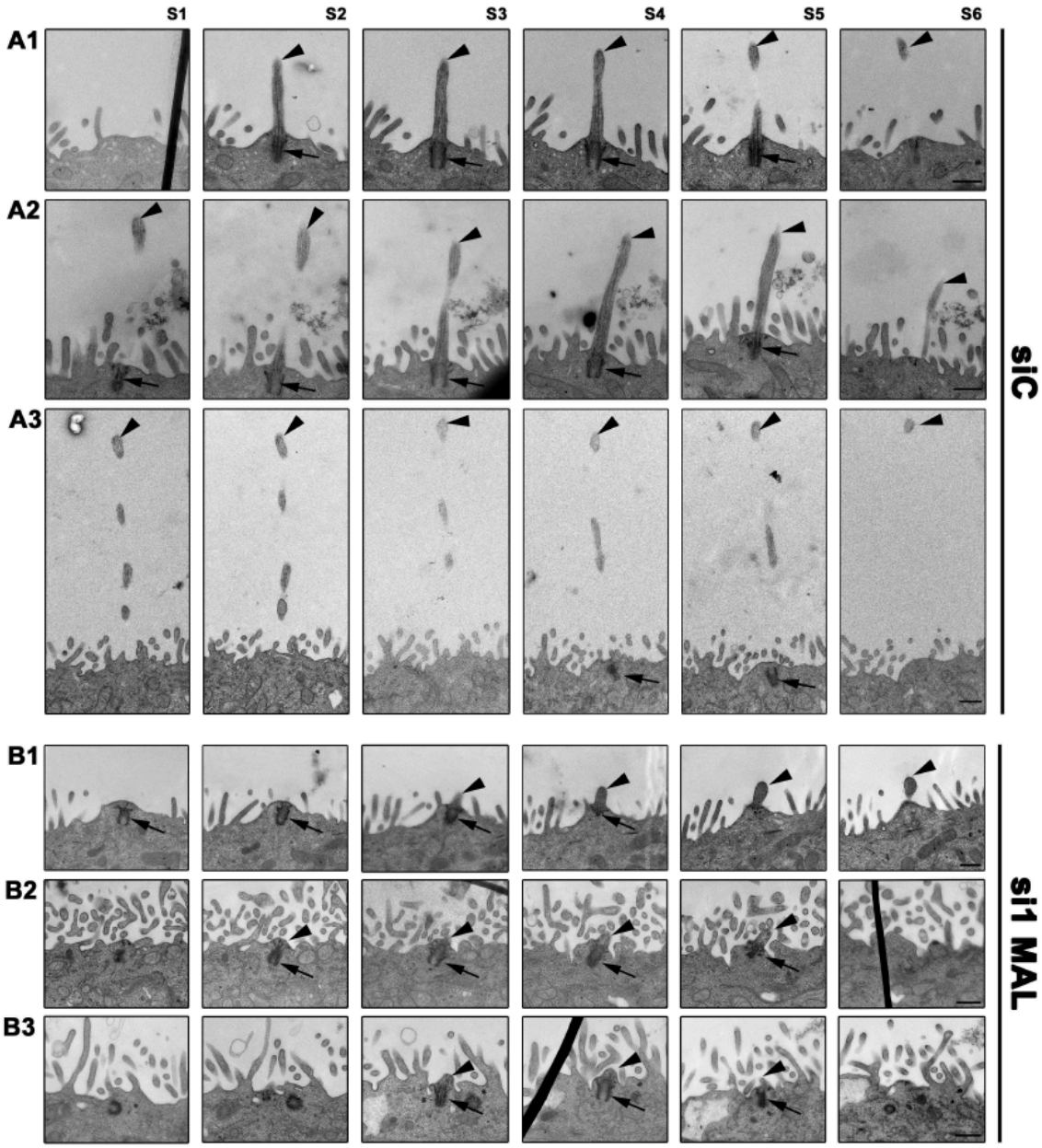

Figure S2. Serial electron microscopy sections of a primary cilium of control and MAL-KD MDCK cells. Longitudinal serial 80-nm thick sections (S1 to S6) of three representative primary cilia of control (A1, A2 and A3) and MAL-KD cells (B1, B2 and B3). Arrowheads indicate the most remote part of the cilium seen in each section. Arrows point to the basal body. Note that primary cilia of MAL-KD cells are shorter than those of control cells. Scale bars, 500 nm.

ANNEX I

The Laurdan molecule (6-lauroyl, 1-2-dimethylaminonaphthalene) is an organic compound consisting of a naphtalene head group and an acyl chain of lauric acid, which has a saturated 12-carbon atom chain (12:0). This acyl chain integrates into biological membranes and, depending on the lipid environment, the Laurdan probe fluoresces at different wavelengths, allowing membrane compaction to be measured (Gaus et al., 2003).

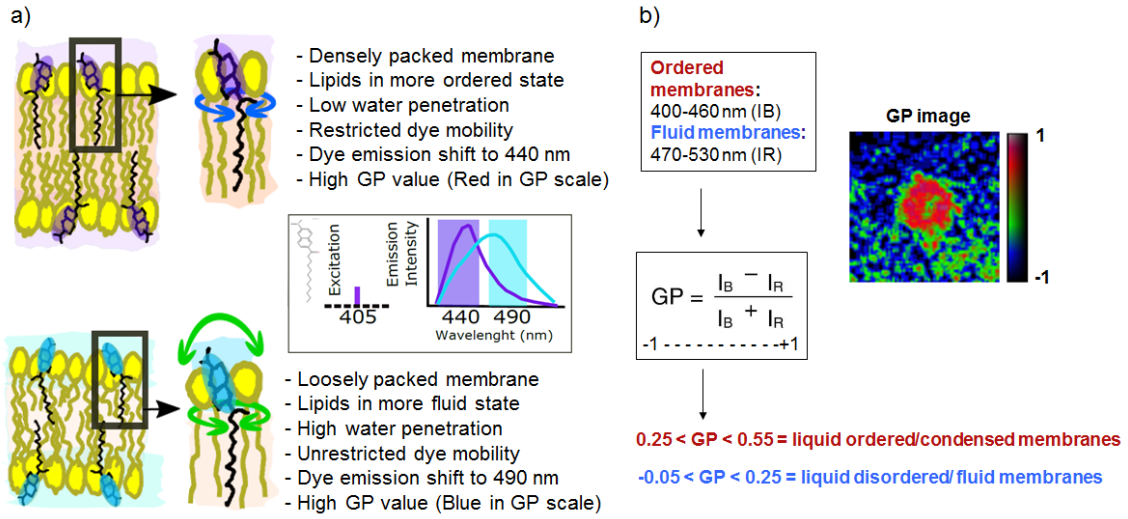

Figure 6. The Laurdan probe. a) The Laurdan dye penetrates the cell and aligns parallel to the phospholipids, undergoing a shift in its peak emission wavelength from 490 nm in fluid membranes to 440 nm in ordered membranes. Diagrams courtesy of Dr. Jorge Bernardino. **b)** A normalized ratio of the two emission regions, given by the general polarization (GP) index, which ranges between -1 and +1, provides a relative measure of membrane order. In model bilayers, GP values greater than 0.25 but smaller than 0.55 correspond to liquid-ordered membranes that are generally assumed to be similar to membrane rafts. The GP values are calculated pixel by pixel in the cell images using the appropriate software and then the values are plotted in a histogram or used to pseudocolor the cells using a color scale to help visualization of the condensation of the membrane at different parts of the cell.

DISCUSSION

1. The alternative pathway of primary ciliogenesis

When renal epithelial cells polarize, the centrosome localizes at the center of their apical membrane. Therefore, according to Sorokin's proposal (Sorokin, 1968), the assembly of the primary cilium in these cells takes place entirely at the plasma membrane. The fact that the primary cilium of renal tubule epithelial cells lacks a ciliary pocket (Latta et al., 1961) is consistent with their function of sensing liquid flow (Praetorius and Spring, 2005) and with the use of the alternative pathway to assemble a primary cilium.

Most of the work on primary cilium biogenesis has focused on cell models that rely on the intracellular pathway, even though the primary cilium is also of pivotal importance in cells that use the alternative pathway. The importance of cilia in renal epithelial cells is exemplified by the ciliary defects that cause kidney cystic diseases, which are the most common of the many abnormalities associated with ciliopathies (Zhang et al., 2004a). Renal epithelial MDCK cells have been used over the last 40 years as a paradigmatic cell model to study polarized membrane trafficking since they are considered to represent *bona fide* distal tubule epithelial cells (Rodriguez-Boulan et al., 2005). Similar to renal tubular epithelial cells, MDCK cells polarize the centrosome to the center of the apical membrane and have no pocket at the base of the primary cilium (Bernabé-Rubio et al., 2016; Reales et al., 2015; Zuo et al., 2009). Consistent with sensing liquid flow, bending of the primary cilium of epithelial MDCK cells results in an increase of intracellular Ca^{2+} (Praetorius and Spring, 2001), whereas removal of the cilium inhibits it (Praetorius and Spring, 2003). Unlike RPE-1 cells, which use the intracellular route, a large ciliary vesicle is not assembled at the distal part of the mother centriole in MDCK cells, although Rab11, Rab8, exocyst subunit Sec8, and BBS1 accumulate in the vicinity of the centrosome at the apical plasma membrane (He et al., 2014). The absence of such a vesicle is consistent with MDCK cells following a route of ciliogenesis different from that of fibroblasts. Given their relevance, MDCK cells have also been adopted to study primary cilia and to identify machinery important for its assembly (Babbey et al., 2010; Corbit et al., 2005; Francis et al., 2011; He et al., 2014; Praetorius et al., 2004; Reales et al., 2015; Sfakianos et al., 2007; Torkko et al., 2008; Vieira et al., 2006; Wang et al., 2009; Zuo et al., 2011; Zuo et al., 2009) and constitute a suitable cell model to study the alternative pathway of primary cilium biogenesis (Bernabé-Rubio et al., 2016).

Several proteins known to have a role in ciliogenesis, such as Sec10, Cep97 and IFT88, are also known to participate in the proper orientation of the mitotic spindle and/or cytokinesis, indicating that primary cilium biogenesis, which takes place in quiescent cells, and mitosis share protein machinery (Delaval et al., 2011; Gromley et al., 2005; Spektor et

al., 2007). In animal cells, cytokinesis begins with the formation of an actomyosin ring at the equator of the two spindle poles (Fededa and Gerlich, 2012; Green et al., 2012). Contraction of the actomyosin ring leads to the ingression of a cleavage furrow that splits the cytoplasm in half. The two halves remain connected by an intercellular bridge containing antiparallel microtubule bundles, which, at least in part, arises from compressed mitotic spindle microtubules covered by plasma membrane (Green et al., 2012; Mullins and Biesele, 1977). The amorphous electron-dense structure situated in the middle of the bridge is referred to as the midbody or Flemming body, which is 1.0-1.5-μm in size. The physical cleavage of the membrane bridge on either side of the midbody by the endosomal sorting complexes required for transport (ESCRT) machinery with the help of transport vesicle fusion, separates the two daughter cells in a process known as abscission (Green et al., 2012; Mierzwa and Gerlich, 2014). Physical separation of the daughter cells requires severing the intercellular bridge at a single site. In this case, one of the daughter cells receives the midbody remnant (Dionne et al., 2015). The inherited remnant can then be conserved on the cell surface as a microtubule-rich membrane protrusion, degraded by autophagy, or released later on if the remnant is cleaved on the other side. The intercellular bridge is often severed on both sides and the remnant is released. Whether the midbody remnant is released, conserved or degraded depends on cell type and status (Kuo et al., 2011; Marzesco et al., 2005; Pohl and Jentsch, 2009; Salzmann et al., 2014). Increasingly, studies are revealing non-cytokinetic implications for the post-mitotic midbody (Chen et al., 2012; Dionne et al., 2015). It is of note that the daughter cell with the older mother centriole tends to inherit the midbody more frequently than its sister cell, implying the existence of communication between the centrosome and the severing machinery (Ettinger et al., 2011; Kuo et al., 2011). Stem cell-like and cancer cells often accumulate more than one remnant. Accumulation of remnants is associated with increased cell reprogramming efficiency and *in vitro* tumorigenicity, respectively, in these cells (Ettinger et al., 2011; Kuo et al., 2011). The midbody remnant also provides polarity cues for the place of the initiation of lumen formation in epithelial MDCK cells and for the formation of the first neurite in *D. melanogaster* neurons and the dorsoventral axis during *C. elegans* development (Li et al., 2014; Pollarolo et al., 2011; Singh and Pohl, 2014).

Proteomic analyses have shown that intercellular bridge midbodies (Skop et al., 2004) and primary cilia (Ishikawa et al., 2012) have a wide spectrum of shared components (Smith et al., 2011). It is of note that Rab11, Rab8, IFT20, IFT88, exocyst complex subunits, acetylated microtubules, BBS6, ESCRT components and septins have been identified in both

structures (Ott, 2016). Some of the shared proteins (e.g., Rab11, Rab8, the exocyst and septins) are known to function in both cytokinesis and primary cilium formation (Fielding et al., 2005; Gromley et al., 2005; Hehnly et al., 2012), whereas the function of others had been traditionally assigned only to one of the two processes. For instance, IFT20 and IFT88 have been found in the intercellular bridge and midbody remnants (Bernabé-Rubio et al., 2016; Wood et al., 2012), although the IFT machinery has long been thought to be exclusive to cilia. Conversely, the ESCRT machinery, which has a role in severing the intercellular bridge, is also present in primary cilia. These observations raise the interesting possibility that a considerable part of the machinery is used for both primary cilium formation and cytokinesis.

The cleavage furrow of MDCK cells and of other polarized epithelial cells initiates coincidently at the apical and basal surfaces but, since the rate of furrow ingression is more rapid from the basal surface, the intercellular bridge becomes located apically (Morais-de-Sá and Sunkel, 2013; Reinsch and Karsenti, 1994) (Fig. 8a). When abscission occurs only on one side, this location of the bridge causes the midbody remnant to become positioned at the periphery of the apical surface of the cell, close to the tight junction (Fig. 8b). The remnant remains physically tethered to the surface of the cell that inherits it by a thin plasma membrane stalk that originates from the unresolved side of the bridge.

After abscission, the midbody remnant can remain tethered to the cell for a long period, moving across the cell surface (Bernabé-Rubio et al., 2016; Crowell et al., 2014; Gromley et al., 2005). In polarized MDCK cells, the remnant, which carries Rab8, IFT20, IFT88, exocyst subunits and, probably, other ciliary machinery, traffics to the central part of the apical surface to meet the centrosome (Fig. 8c). Although it is not clear how the remnant reaches the center of the apical surface, it is known that its journey is dependent on Rab8 expression. The encounter between the midbody remnant and the centrosome is essential for primary cilium formation since ciliogenesis is severely impaired in cells whose remnant has been removed (Bernabé-Rubio et al., 2016). Ultrastructural analysis of serial sections shows that the membrane of the midbody remnant is still connected to the adjacent plasma membrane by a membranous stalk. The establishment of a short microtubular connection between the midbody remnant and the centrosome has been detected before primary cilium starts forming, but the function of such a connection is currently unknown. The physical continuity of the remnant membrane and the plasma membrane raises the possibility that the remnant could transfer to the centrosome materials required for ciliogenesis (Bernabé-Rubio et al., 2016). A second possibility for the role of the remnant in ciliogenesis is that, because the primary cilium has compact membranes at its base (Vieira et al., 2006) and these specialized

membranes are required for cilium formation (Reales et al., 2015), the stalk zone constitutes a compact membrane domain used to form the ciliary base. Another possibility is that the remnant signals to the basal body to start primary cilium assembly. Further studies are required to understand the mechanism by which the midbody remnant licenses the centrosome for primary ciliogenesis (Fig. 8d).

Primary ciliogenesis is regulated by cell confinement in non-polarized cells, as shown by RPE-1 cells cultured on adhesive micropatterns, in which high spatial confinement results in a greater percentage of ciliated cells (Pitaval et al., 2010). This is also true in epithelial MDCK cells, since cell-cell contacts are crucial to ciliogenesis (Bernabé-Rubio et al., 2016). It is of note that the area of these cells governs the conservation of the midbody remnant, its movement to the center of the apical membrane and the beginning of primary cilium assembly. When cells proliferate, the availability of space becomes limited and cells are progressively constrained by their neighbors. Under these conditions, cells grow in height and reduce their area of attachment to the substrate, and the midbody remnant is conserved. Successive cycles of cell division increase the number of cells with a midbody remnant and, subsequently, the percentage of ciliated cells (Bernabé-Rubio et al., 2016). As this process progresses, compressive stress replaces tensile stress (Bazellières et al., 2015; Trepat et al., 2009). These gradual changes in stress forces probably trigger the conservation of the remnant, its transition to the center of the apical surface to meet the centrosome and the beginning of ciliogenesis in polarized epithelial cells.

Therefore, establishment of cell polarization is required for midbody conservation, and subsequent midbody translocation and cilium formation. It would be very interesting to address the question of whether the midbody remnant is reciprocally involved in the acquisition of cell polarity, although the subcellular distribution of podocalyxin, ZO-1 and β-catenin is not affected by remnant removal (Bernabé-Rubio et al., 2016). Intriguingly, the midbody colocalizes with apical determinants such as Par3, aPKC and Crb3a, and trafficking of Crb3a in Rab11 positive vesicles to the proximities of the midbody is required for initial formation of the apical membrane and subsequent lumen formation. Besides, the exocyst regulates the tethering of Rab11 positive vesicles to the cleavage furrow in Hela cells (Fielding et al., 2005). Whether polarity components localized to the midbody are transported by the midbody remnant to be recycled as precursors for cilium formation is a question that will need further research.

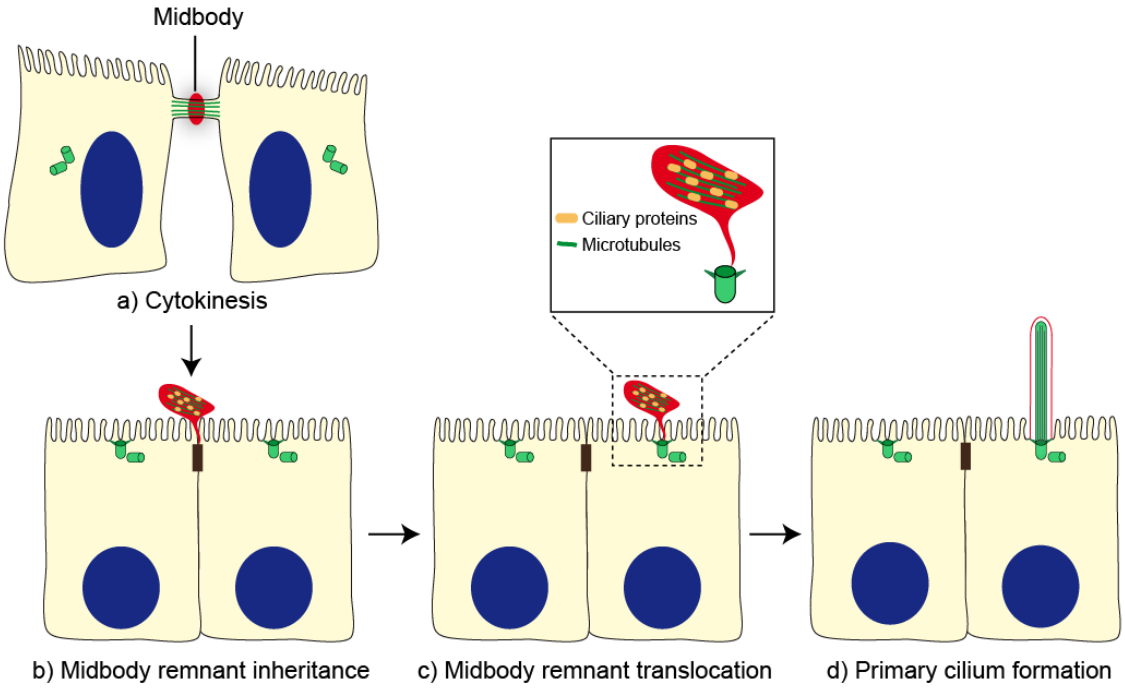

Figure 8. **The alternative route**. **a**) In polarized epithelial cells, the intercellular bridge containing ciliary proteins forms at the apical cell surface during cytokinesis. **b**) When abscission occurs, one of the two daughter cells inherits the midbody remnant, which localizes apically at the cell periphery, near the tight junctions. **c**) The remnant subsequently moves over the apical surface towards the centrosome, which is docked at the center of the apical membrane. **d**) When the midbody meets the centrosome the initiation of primary cilium assembly is facilitated. The entire process of primary cilium formation takes place in the plasma membrane.

2. Ciliary lipids and their role in primary cilium formation

Organelle identity and function depend not only on a unique protein content, but also on a unique lipid composition. In particular, phosphoinositide (PIP) content is crucial for dictating organelle identity. PIPs are a type of membrane phospholipid that regulate a wide spectrum of physiological processes in various cellular compartments (Balla, 2013), and cilia are not exception. Recent studies have demonstrated that PIPs modulate ciliary trafficking involved in Hh signaling at the primary cilium (Chávez et al., 2015; Garcia-Gonzalo et al., 2015). PIPs are produced by phosphorylation of phosphatidylinositol (PtdIns) at the 3, 4, and/or 5 positions of the inositol ring. It is of note that whereas PI(4)P distributes along the entire ciliary membrane, $PI(4,5)P_2$ localization is restricted to the proximal part of the ciliary membrane of renal IMCD3, NIH-3T3 and neural stem cells and MEFs. Inositol polyphosphate-5-phosphatase E (Inpp5e) converts ciliary $PI(4,5)P_2$ into PI(4)P. In mammalian cells, Inpp5e localizes to the primary cilium. $PI(4,5)P_2$ accumulates on the entire ciliary membrane in the absence of Inpp5e and produces retention in the ciliary compartment of Tulp3 and Gpr161, which are negative regulators of Hh signaling (Mukhopadhyay et al.,

2013). Thus, proper Hh signaling requires phosphoinositide homeostasis at the primary cilium.

Additionally, coordination of Iγ (PtdIns(4)P) 5-kinase (PIPKIγ), a PI(4)P kinase, with its opposing phosphatase Inpp5e, regulates initiation of ciliogenesis (Xu et al., 2016). PIPKIγ localizes to the mother centriole of a wide range of cell lines, such as polarized IMCD3 and human renal cortical tubular epithelial cells, as well as in NIH-3T3 fibroblasts and RPE-1 cells. In non-ciliated cells, Innp5e and its product, PI(4)P, which is the substrate of PIPKIγ, distributes at the mother centriole. When PI(4)P accumulates, it inhibits Ttbk2 recruitment to the mother centriole and impairs ciliogenesis, since Cp110 remains at the basal body. For primary cilium initiation, Inpp5e relocalizes from the mother centriole to the ciliary compartment, enabling PIPKIγ-mediated elimination of its substrate PI(4)P from the basal body (Xu et al., 2016). Therefore, regulation of lipid content is necessary for proper ciliary function.

Accumulation of $PI(4,5)P_2$ produced by displacement of Inpp5e from cilia induces excision of cilia tips and their release as ectosomes. This process, known as cilia decapitation, regulates cilia size, removes unwanted membrane receptors, and precedes cilia reabsorption. It has been proposed to constitute a link between the life of cilia and cell-division cycle (Phua et al., 2017) (Nager et al., 2017). The importance of Inpp5e in primary cilia is supported by the fact that mutations in the human *INNP5E* gene lead to JBTS ciliopathy (Bielas et al., 2009; Jacoby et al., 2009).

The ciliary base also contains a zone of highly condensed membranes whose relevance is not known. The sphingolipid ceramide, which is a component of condensed membranes, localizes at the ciliary base in a compartment known as the apical ceramide-enriched compartment, where it regulates a lipid-protein molecular network that sustains the primary cilium (He et al., 2012; Wang et al., 2009). Ceramide binds and activates aPKC, which, in turn, colocalizes with Rab11 in the apical ceramide-enriched compartment.

Disruption of the ceramide-aPKC interaction results in impaired primary cilium formation and loss of the association of Rab11 vesicles with Cdc42, exocyst subunit Sec8 and Rab8 (He et al., 2012). Supporting the important role of ceramide, inhibition of ceramide biosynthesis by fumonisin B1 severely impairs primary ciliogenesis in MDCK cells (Wang et al., 2009).

Accordingly, we observed that the MAL protein, which is a component of the machinery of apical transport of MDCK cells (Cheong et al., 1999; Puertollano et al., 1999), specifically

regulates the condensation of membranes at the ciliary base (Fig. 9) (Reales et al., 2015). In the absence of MAL, membrane condensation at the ciliary base decreased, the number of primary cilia was greatly diminished, and the remaining cilia were stunted. The alteration of membrane condensation at the ciliary base did not disrupt the docking of the centrosome to the plasma membrane or the recruitment of ciliary machinery, such as IFT20, IFT88 and Rab8, to the ciliary base, or produced missorting of apical membrane proteins to the membrane of atrophied remaining cilia. These findings indicate that the unique lipid composition at the ciliary base is required for cilium elongation, and that the condensed zone of the ciliary base does not appear to function as a general physical barrier to entry of membrane proteins into the cilium.

The observation that apical membrane proteins such as podocalyxin are excluded from the patch of compact membranes present at the ciliary base led to the proposal that these specialized membranes could function as a fence for diffusion and could thereby contribute to the regulation of the protein and lipid composition of the ciliary membrane (Vieira et al., 2006). However, this proposal has been challenged by the observations that disruption of the compact membranes does not allow the entry of podocalyxin into the cilia (Reales et al., 2015) and that podocalyxin exclusion can be explained only on the basis of its interaction with the actin network (Francis et al., 2011). Instead, interaction with the cytoskeleton (Francis et al., 2011), or physical barriers based on nucleoporins (Kee et al., 2012), septins (Hu et al., 2010) or on a complex that includes proteins disrupted in ciliopathies (Chih et al., 2011) are involved in regulating the protein composition of the primary cilium, whereas the region of condensed membranes may contribute to establishing and/or maintaining unique lipid environments for the ciliary and plasma membranes.

Despite the KD of endogenous MAL was quite effective, there was a great percentage of the cell population with a short primary cilium. In this case, the reduction of membrane condensation caused by MAL KD was probably lower allowing the formation of primary cilia with varying sizes. Therefore, we find it is feasible that there is a threshold of membrane condensation at the ciliary base below which the process of ciliogenesis is totally blocked, whereas above which it takes place to a varying extent, depending on the degree of condensation. This finding together with the fact that the ciliary machinery is properly recruited to the cilium in MAL KD cells, indicates that MAL participates in late stages of ciliogenesis. In according to this, preliminary data from our laboratory indicate that the KD of MAL does not affect the translocation of the midbody remnant from peripheral to central positions, which is an early step in the initiation of primary ciliogenesis in MDCK cells

(Bernabé-Rubio et al., 2016). Therefore, membrane condensation at the ciliary base would not be necessary for the encounter between the midbody remnant and the centrosome to occur, although it is required for ciliogenesis (Reales et al., 2015). An important question raises with regard to the exact step of ciliogenesis in which MAL is involved, which is connected to the formation of such a membrane patch. In which precise moment does MAL organize membrane condensation at the ciliary base during ciliogenesis process? Is this process connected to the midbody-mediated pathway? Interestingly, lipidomic analysis showed that the midbody has a lipid composition different from that of the bulk of cellular membranes (Arai et al., 2015), so one intriguing possibility would be that the midbody organizes the membrane rafts present at the ciliary base in coordination with MAL.

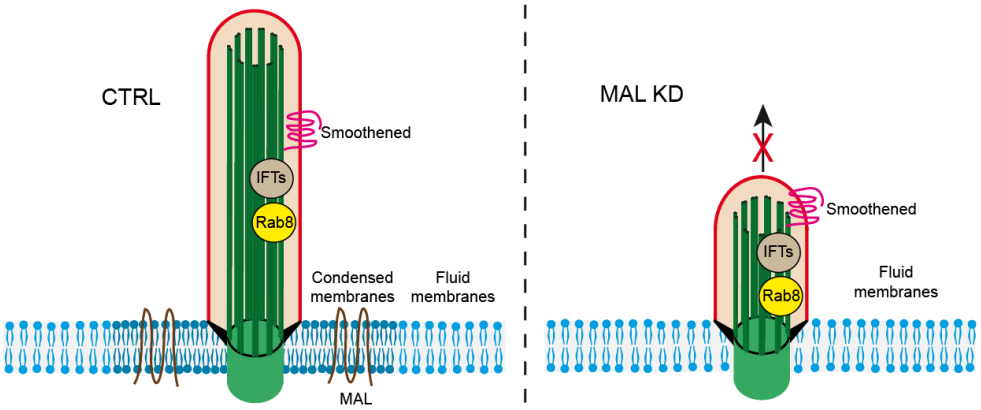

Figure 9. Membrane condensation at the ciliary base is required for cilium elongation. MAL accumulates at the ciliary base, where it regulates primary cilium assembly by packing the lipids situated at the base of the cilium. In the absence of MAL, membrane condensation at the ciliary base decreases, the number of primary cilia is reduced, and the remaining cilia are shorter. The perturbation of membrane condensation at the ciliary base does not affect the docking of the centrosome to the plasma membrane or the recruitment of ciliary machinery, such as IFTs, Smo, or Rab8, to the ciliary base.

3. Conclusions and future directions

Despite Sorokin's proposal nearly 50 years ago of the existence of two distinct pathways for ciliogenesis, most of the work on primary ciliogenesis has focused on cell models that rely on the intracellular pathway, even though the primary cilium is also of crucial importance in cells that were postulated to use an alternative pathway, as is the case of renal epithelial cells. The great efforts made to investigate the intracellular route has driven advances in the field, revealing many molecular details of the cellular events and the machinery involved. However, there is still a long way to go before the process is fully understood. In polarized epithelial cells, primary cilium biogenesis seems to be a sequential process by which the establishment of tight cell junctions and subsequent cell polarization modulates the

conservation of the midbody remnant, its movement to meet the centrosome, and the beginning of primary cilium assembly at the middle of the apical surface. Cell polarization and midbody function should be in concert with the formation of the condensed membrane patch present at the ciliary base, which is required for cilium assembly, although the spatiotemporal coordination of these key events of ciliogenesis are still far from being understood.

The route of primary ciliogenesis regulated by the midbody establishes a new biological mechanism that links the three major microtubule-based organelles—the centrosome, the cilium and the midbody— in the same process. Since this mechanism is entirely new, it raises many interesting questions that, it is to be hoped, will stimulate research on this pathway and help us understand the function of the midbody remnant, whose relevance to cellular processes other than cytokinesis has only recently begun to be considered.

One of the most important questions that arises is whether there is a transfer of materials from the midbody remnant to the centrosome to feed primary ciliogenesis. If this is the case, this material will need to be characterized in order to appreciate how it potentiates the centrosome for cilium formation. A very intriguing question that will also require further research is whether the midbody participates in the packing of the membrane lipids at the ciliary base. A second point is to understand how the midbody remnant moves towards the center of the apical surface until it meets the centrosome. How is the remnant propelled? How does the remnant "know" where to go and how is it able to arrive at the cell center despite the conspicuous presence of microvilli at the apical surface? What causes it to stop? Another important matter concerns the possible involvement of the midbody in the intracellular pathway. Is the participation of the midbody remnant exclusive to polarized epithelial cells or does it also intervene in cells using the intracellular route? In this regard, the midbody might also participate, for instance, by providing materials for the formation of the ciliary vesicles that surround the intracellular, nascent cilium. The mother centriole approaches the intercellular bridge of dividing mouse L929 fibroblasts and HeLa cells (Gromley et al., 2005; Jonsdottir et al., 2010; Piel et al., 2001), so it is possible that this contact could serve the centriole to obtain materials used subsequently for primary cilium formation. Activation of autophagy and initiation of ciliogenesis are simultaneous events in which some proteins participate direct or indirectly in both processes (Pampliega et al., 2013; Tang et al., 2013). For instance, Ofd1, which is a repressor of ciliogenesis, is removed from the centriolar satellites by autophagy, enabling primary cilium biogenesis (Tang et al., 2013). It would also be fascinating to examine whether there is a transfer of ciliary material to the centrosome

during autophagy of the midbody remnant in cells relying on the intracellular pathway and in which the remnant is internalized. Finally, it will be interesting to identify the protein machinery specific to each of the two pathways of ciliogenesis. Therefore, further research is needed to elucidate the cellular and molecular basis that controls the process of primary cilium biogenesis in different cell types.

CONCLUSIONES/CONCLUSIONS

1. El remanente del cuerpo medio de las células polarizadas epiteliales MDCK es heredado por una de las células hijas posicionándose en la superficie apical próximo a las uniones estrechas intercelulares.

2. La maquinaria ciliar, como los complejos IFTs, Rab8, y el complejo exocisto, se concentra en el remanente del cuerpo medio.

3. El remanente del cuerpo medio viaja sobre la superficie apical desde una posición periférica hasta una posición central reuniéndose con el centrosoma en un proceso dependiente de Rab8.

4. El encuentro entre el remanente del cuerpo medio y el centrosoma facilita la formación del cilio primario.

5. El área celular regula el movimiento del cuerpo medio y la ciliogénesis primaria a nivel de una sola célula.

6. MAL se induce con la confluencia celular, se acumula en la base del cilio primario y es necesaria para la correcta elongación del mismo en células MDCK.

7. MAL regula específicamente la condensación de membranas en la base ciliar.

8. La ausencia de condensación de membranas en la base del cilio no afecta al anclaje del centriolo materno a la membrana plasmática, a la barrera de difusión, o al reclutamiento de maquinaria ciliar como los complejos IFTs, Rab8, o Smoothened.

9. La elongación eficiente del cilio primario requiere una condensación correcta de las membranas situadas en la base ciliar.

CONCLUSIONS

1. The midbody remnant of polarized renal epithelial MDCK cells is inherited by one of the daughter cells and becomes located at the apical surface close to the tight junctions between cells.

2. Ciliary machinery, such as IFTs, Rab8, and the exocyst complex, concentrates at the midbody remnant.

3. The midbody remnant traffics along the apical cell surface from a peripheral to a central position in a Rab8-dependent manner to meet the centrosome.

4. The encounter between the midbody remnant and the centrosome enables the centrosome for primary cilium formation.

5. Midbody remnant movement and primary ciliogenesis are modulated by cell area constraints at the single-cell level.

6. MAL is induced by cell confluence, accumulates at the base of the cilium, and is necessary for proper cilium elongation in MDCK cells.

7. MAL specifically regulates the membrane condensation at the ciliary base.

8. The loss of membrane condensation at the ciliary base does not affect the docking of the mother centriole to the plasma membrane, ciliary barrier function, or the recruitment of ciliary machinery such as IFTs, Rab8, or Smoothened.

9. Efficient primary cilium elongation requires proper condensation of membranes at the ciliary base.

REFERENCES

Aguilar, A., Becker, L., Tedeschi, T., Heller, S., Iomini, C., and Nachury, M.V. (2014). α-Tubulin K40 acetylation is required for contact inhibition of proliferation and cell-substrate adhesion. Mol Biol Cell *25*, 1854-1866.

Alonso, M.A., and Millán, J. (2001). The role of lipid rafts in signalling and membrane trafficking in T lymphocytes. J Cell Sci *114*, 3957-3965.

Alonso, M.A., and Weissman, S.M. (1987). cDNA cloning and sequence of MAL, a hydrophobic protein associated with human T-cell differentiation. Proc Natl Acad Sci USA *84*, 1997-2001.

Antón, O., Batista, A., Millan, J., Andres-Delgado, L., Puertollano, R., Correas, I., and Alonso, M.A. (2008). An essential role for the MAL protein in targeting Lck to the plasma membrane of human T lymphocytes. J Exp Med *205*, 3201-3213.

Antón, O.M., Andrés-Delgado, L., Reglero-Real, N., Batista, A., and Alonso, M.A. (2011). MAL protein controls protein sorting at the supramolecular activation cluster of human T lymphocytes. J Immunol *186*, 6345-6356.

Babbey, C.M., Bacallao, R.L., and Dunn, K.W. (2010). Rab10 associates with primary cilia and the exocyst complex in renal epithelial cells. Am J Physiol -Renal Physiol *299*, F495-F506.

Balla, T. (2013). Phosphoinositides: tiny lipids with giant impact on cell regulation. Physiol Rev *93*, 1019-1137.

Baron Gaillard, C.L., Pallesi-Pocachard, E., Massey-Harroche, D., Richard, F., Arsanto, J.-P., Chauvin, J.-P., Lecine, P., Krämer, H., Borg, J.-P., and Le Bivic, A. (2011). Hook2 is involved in the morphogenesis of the primary cilium. Mol Biol Cell *22*, 4549-4562.

Battle, C., Ott, C.M., Burnette, D.T., Lippincott-Schwartz, J., and Schmidt, C.F. (2015). Intracellular and extracellular forces drive primary cilia movement. Proc Natl Acad Sci USA *112*, 1410-1415.

Bazellières, E., Conte, V., Elosegui-Artola, A., Serra-Picamal, X., Bintanel-Morcillo, M., Roca-Cusachs, P., Muñoz, J.J., Sales-Pardo, M., Guimerá, R., and Trepat, X. (2015). Control of cell-cell forces and collective cell dynamics by the intercellular adhesome. Nat Cell Biol *17*, 409-420.

Benmerah, A. (2013). The ciliary pocket. Curr Opin Cell Biol *25*, 78-84.

Benzing, T., and Schermer, B. (2011). Transition zone proteins and cilia dynamics. Nat Genet *43*, 723-724.

Berbari, N.F., Lewis, J.S., Bishop, G.A., Askwith, C.C., and Mykytyn, K. (2008). Bardet-Biedl syndrome proteins are required for the localization of G protein-coupled receptors to primary cilia. Prooc Natl Acad Sci USA *105*, 4242-4246.

Bernabé-Rubio, M., Andrés, G., Casares-Arias, J., Fernández-Barrera, J., Rangel, L., Reglero-Real, N., Gershlick, D.C., Fernández, J.J., Millán, J., Correas, I.*, et al.* (2016). Novel role for the midbody in primary ciliogenesis by polarized epithelial cells. J Cell Biol *214*, 259-273.

Bhogaraju, S., Engel, B.D., and Lorentzen, E. (2013). Intraflagellar transport complex structure and cargo interactions. Cilia *2*, 10-10.

Bielas, S.L., Silhavy, J.L., Brancati, F., Kisseleva, M.V., Al-Gazali, L., Sztriha, L., Bayoumi, R.A., Zaki, M.S., Abdel-Aleem, A., Rosti, R.O.*, et al.* (2009). Mutations in INPP5E, encoding inositol polyphosphate-5-phosphatase E, link phosphatidyl inositol signaling to the ciliopathies. Nat Genet *41*, 1032-1036.

Bornens, M. (2002). Centrosome composition and microtubule anchoring mechanisms. Curr Opin Cell Biol *14*, 25-34.

Braun, D.A., and Hildebrandt, F. (2017). Ciliopathies. Cold Spring Harb Perspect Biol *9*.

Briscoe, J., and Therond, P.P. (2013). The mechanisms of Hedgehog signalling and its roles in development and disease. Nat Rev Mol Cell Biol *14*, 416-429.

Brooks, E.R., and Wallingford, J.B. (2014). Multiciliated cells: a review. Curr Biol *24*, R973-R982.

Cajanek, L., and Nigg, E.A. (2014). Cep164 triggers ciliogenesis by recruiting Tau tubulin kinase 2 to the mother centriole. Proc Natl Acad Sci USA *111*, E2841-E2850.

Cao, M., Ning, J., Hernandez-Lara, C.I., Belzile, O., Wang, Q., Dutcher, S.K., Liu, Y., and Snell, W.J. (2015). Uni-directional ciliary membrane protein trafficking by a cytoplasmic retrograde IFT motor and ciliary ectosome shedding. eLife *4*, e05242.

Clement, C.A., Ajbro, K.D., Koefoed, K., Vestergaard, M.L., Veland, I.R., Henriques de Jesus, M.P., Pedersen, L.B., Benmerah, A., Andersen, C.Y., Larsen, L.A.*, et al.* (2013). TGF-β signaling is associated with endocytosis at the pocket region of the primary cilium. Cell Rep *3*, 1806-1814.

Corbit, K.C., Aanstad, P., Singla, V., Norman, A.R., Stainier, D.Y.R., and Reiter, J.F. (2005). Vertebrate Smoothened functions at the primary cilium. Nature *437*, 1018-1021.

Crowell, E.F., Gaffuri, A.-L., Gayraud-Morel, B., Tajbakhsh, S., and Echard, A. (2014). Engulfment of the midbody remnant after cytokinesis in mammalian cells. J Cell Sci *127*, 3840-3851.

Chávez, M., Ena, S., Van Sande, J., de Kerchove d'Exaerde, A., Schurmans, S., and Schiffmann, S.N. (2015). Modulation of ciliary phosphoinositide content regulates trafficking and sonic Hedgehog signaling output. Dev Cell *34*, 338-350.

Chen, C.-T., Ettinger, A.W., Huttner, W.B., and Doxsey, S.J. (2012). Resurrecting remnants: the lives of post-mitotic midbodies. Trends Cell Biol *23*, 118-128.

Cheong, K.H., Zacchetti, D., Schneeberger, E.E., and Simons, K. (1999). VIP17/MAL, a lipid raft-associated protein, is involved in apical transport in MDCK cells. Proc Natl Acad Sci USA *96*, 6241-6248.

Chih, B., Liu, P., Chinn, Y., Chalouni, C., Komuves, L.G., Hass, P.E., Sandoval, W., and Peterson, A.S. (2011). A ciliopathy complex at the transition zone protects the cilia as a privileged membrane domain. Nat Cell Biol *14*, 61-72.

DeCaen, P.G., Delling, M., Vien, T.N., and Clapham, D.E. (2013). Direct recording and molecular identification of the calcium channel of primary cilia. Nature *504*, 315-318.

Delaval, B., Bright, A., Lawson, N.D., and Doxsey, S. (2011). The cilia protein IFT88 is required for spindle orientation in mitosis. Nat Cell Biol *13*, 461-468.

Delling, M., DeCaen, P.G., Doerner, J.F., Febvay, S., and Clapham, D.E. (2013). Primary cilia are specialized calcium signalling organelles. Nature *504*, 311-314.

Delling, M., Indzhykulian, A.A., Liu, X., Liu, Y., Xie, T., Corey, D.P., and Clapham, D.E. (2016). Primary cilia are not calcium-responsive mechanosensors. Nature *531*, 656-660.

Dentler, W.L. (1980). Structures linking the tips of ciliary and flagellar microtubules to the membrane. J Cell Sci *42*, 207.

Dentler, W.L., and Rosenbaum, J.L. (1977). Flagellar elongation and shortening in Chlamydomonas. III. structures attached to the tips of flagellar microtubules and their relationship to the directionality of flagellar microtubule assembly. J Cell Biol *74*, 747-759.

Dionne, L.K., Wang, X.-J., and Prekeris, R. (2015). Midbody: from cellular junk to regulator of cell polarity and cell fate. Curr Opin Cell Biol *35*, 51-58.

Doerner, J.F., Delling, M., and Clapham, D.E. (2015). Ion channels and calcium signaling in motile cilia. eLife *4*, e11066.

Domire, J.S., Green, J.A., Lee, K.G., Johnson, A.D., Askwith, C.C., and Mykytyn, K. (2011). Dopamine receptor 1 localizes to neuronal cilia in a dynamic process that requires the Bardet-Biedl syndrome proteins. Cell Mol Life Sci *68*, 2951-2960.

Eguether, T., San Agustin, J.T., Keady, B.T., Jonassen, J.A., Liang, Y., Francis, R., Tobita, K., Johnson, C.A., Abdelhamed, Z.A., Lo, C.W.*, et al.* (2014). IFT27 links the BBSome to IFT for maintenance of the ciliary signaling compartment. DevCell *31*, 279-290.

Ettinger, A.W., Wilsch-Brauninger, M., Marzesco, A.-M., Bickle, M., Lohmann, A., Maliga, Z., Karbanova, J., Corbeil, D., Hyman, A.A., and Huttner, W.B. (2011). Proliferating versus differentiating stem and cancer cells exhibit distinct midbody-release behaviour. Nat Commun *2*, 503.

Falk, N., Lösl, M., Schöeder, N., and Giebl, A. (2015). Specialized cilia in mammalian sensory systems. Cells *4*, 500-519.

Fan, S., Hurd, T.W., Liu, C.-J., Straight, S.W., Weimbs, T., Hurd, E.A., Domino, S.E., and Margolis, B. (2004). Polarity proteins control ciliogenesis via kinesin motor interactions. Curr Biol *14*, 1451-1461.

Fededa, J.P., and Gerlich, D.W. (2012). Molecular control of animal cell cytokinesis. Nat Cell Biol *14*, 440-447.

Fielding, A.B., Schonteich, E., Matheson, J., Wilson, G., Yu, X., Hickson, G.R.X., Srivastava, S., Baldwin, S.A., Prekeris, R., and Gould, G.W. (2005). Rab11-FIP3 and FIP4 interact with Arf6 and the exocyst to control membrane traffic in cytokinesis. EMBO J *24*, 3389-3399.

Fliegauf, M., Benzing, T., and Omran, H. (2007). When cilia go bad: cilia defects and ciliopathies. Nat Rev Mol Cell Biol *8*, 880-893.

Francis, S.S., Sfakianos, J., Lo, B., and Mellman, I. (2011). A hierarchy of signals regulates entry of membrane proteins into the ciliary membrane domain in epithelial cells. J Cell Biol *193*, 219-233.

Galati, D.F., Mitchell, B.J., and Pearson, C.G. (2016). Subdistal appendages stabilize the ups and downs of ciliary life. Dev Cell *39*, 387-389.

Garcia-Gonzalo, F.R., Corbit, K.C., Sirerol-Piquer, M.S., Ramaswami, G., Otto, E.A., Noriega, T.R., Seol, A.D., Robinson, J.F., Bennett, C.L., Josifova, D.J.*, et al.* (2011). A transition zone complex regulates mammalian ciliogenesis and ciliary membrane composition. Nat Genet *43*, 776-784.

Garcia-Gonzalo, F.R., Phua, S.C., Roberson, E.C., Garcia, G., Abedin, M., Schurmans, S.p., Inoue, T., and Reiter, J.F. (2015). Phosphoinositides regulate ciliary protein trafficking to modulate hedgehog signaling. Dev Cell *34*, 400-409.

Garcia-Gonzalo, F.R., and Reiter, J.F. (2012). Scoring a backstage pass: mechanisms of ciliogenesis and ciliary access. J Cell Biol *197*, 697-709.

Garcia-Gonzalo, F.R., and Reiter, J.F. (2017). Open sesame: how transition fibers and the transition zone control ciliary composition. Cold Spring Harb Perspect Biol *9*.

Garcia, G., and Reiter, J.F. (2016). A primer on the mouse basal body. Cilia *5*, 17.

Gaus, K., Gratton, E., Kable, E.P.W., Jones, A.S., Gelissen, I., Kritharides, L., and Jessup, W. (2003). Visualizing lipid structure and raft domains in living cells with two-photon microscopy. Proc Nat Acad Sci USA *100*, 15554-15559.

Ghossoub, R., Molla-Herman, A., Bastin, P., and Benmerah, A. (2011). The ciliary pocket: a once-forgotten membrane domain at the base of cilia. Biol Cell *103*, 131-144.

Goetz, S.C., and Anderson, K.V. (2010). The primary cilium: a signalling centre during vertebrate development. Nat Rev Genet *11*, 331-344.

Goetz, S.C., Liem, K.F., and Anderson, K.V. (2012). The spinocerebellar ataxia-associated gene Tau tubulin kinase 2 (TTBK2) controls the initiation of ciliogenesis. Cell *151*, 847-858.

Gorojankina, T. (2016). Hedgehog signaling pathway: a novel model and molecular mechanisms of signal transduction. Cell Mol Life Sci *73*, 1317-1332.

Green, R.A., Paluch, E., and Oegema, K. (2012). Cytokinesis in animal cells. Annu Rev Cell Dev Biol *28*, 29-58.

Gromley, A., Yeaman, C., Rosa, J., Redick, S., Chen, C.-T., Mirabelle, S., Guha, M., Sillibourne, J., and Doxsey, S.J. (2005). Centriolin anchoring of exocyst and SNARE complexes at the midbody is required for secretory-vesicle-mediated abscission. Cell *123*, 75-87.

Habbig, S., Bartram, M.P., Müller, R.U., Schwarz, R., Andriopoulos, N., Chen, S., Sägmüller, J.G., Hoehne, M., Burst, V., Liebau, M.C.*, et al.* (2011). NPHP4, a cilia-associated protein, negatively regulates the Hippo pathway. J Cell Biol *193*, 633-642.

He, M., Subramanian, R., Bangs, F., Omelchenko, T., Liem, K.F., Kapoor, T.M., and Anderson, K.V. (2014). The kinesin-4 protein KIF7 regulates mammalian hedgehog signaling by organizing the cilia tip compartment. Nat Cell Biol *16*, 663-672.

He, Q., Wang, G., Dasgupta, S., Dinkins, M., Zhu, G., and Bieberich, E. (2012). Characterization of an apical ceramide-enriched compartment regulating ciliogenesis. Mol Biol Cell *23*, 3156-3166.

Hehnly, H., Chen, C.-T., Powers, C.M., Liu, H.-L., and Doxsey, S. (2012). The centrosome regulates the Rab11- dependent recycling endosome pathway at appendages of the mother centriole. Curr Biol *22*, 1944-1950.

Heider, M.R., and Munson, M. (2012). Exorcising the exocyst complex. Traffic *13*, 898-907.

Hernandez-Hernandez, V., and Henkins, D. (2015). Advances in the understanding of the BBSome complex structure and function. Res Rep Biol *6*, 191-201.

Hertzog, M., and Chavrier, P. (2011). Cell polarity during motile processes: keeping on track with the exocyst complex. Biochem J *433*, 403.

Hildebrandt, F., Benzing, T., and Katsanis, N. (2011). Ciliopathies. N Engl J Med *364*, 1533-1543.

Hilgendorf, K.I., Johnson, C.T., and Jackson, P.K. (2016). The primary cilium as a cellular receiver: organizing ciliary GPCR signaling. Curr Opin Cell Biol *39*, 84-92.

Hofherr, A., and Kottgen, M. (2016). Polycystic kidney disease: cilia and mechanosensation revisited. Nat Rev Nephrol *12*, 318-319.

Hu, Q., Milenkovic, L., Jin, H., Scott, M.P., Nachury, M.V., Spiliotis, E.T., and Nelson, W.J. (2010). A septin diffusion barrier at the base of the primary cilium maintains ciliary membrane protein distribution. Science *329*, 436-439.

Hu, Q., and Nelson, W.J. (2011). The ciliary diffusion barrier: the gatekeeper for the primary cilium compartment. Cytoskeleton (Hoboken, NJ) *68*, 313-324.

Hurd, T.W., Fan, S., Liu, C.-J., Kweon, H.K., Hakansson, K., and Margolis, B. (2003). Phosphorylation-dependent binding of 14-3-3 to the polarity protein Par3 regulates cell polarity in mammalian epithelia. Curr Biol *13*, 2082-2090.

Ishikawa, H., and Marshall, W.F. (2011). Ciliogenesis: building the cell's antenna. Nat Rev Mol Cell Biol *12*, 222-234.

Ishikawa, H., and Marshall, W.F. (2014). Mechanobiology of ciliogenesis. Bioscience *64*, 1084-1091.

Ishikawa, H., Thompson, J., Yates, J.R., and Marshall, W.F. (2012). Proteomic analysis of mammalian primary cilia. Curr Biol *22*, 414-419.

Jacoby, M., Cox, J.J., Gayral, S., Hampshire, D.J., Ayub, M., Blockmans, M., Pernot, E., Kisseleva, M.V., Compere, P., Schiffmann, S.N.*, et al.* (2009). INPP5E mutations cause primary cilium signaling defects, ciliary instability and ciliopathies in human and mouse. Nat Genet *41*, 1027-1031.

Jana, S.C., Marteil, G.l., and Bettencourt-Dias, M.n. (2014). Mapping molecules to structure: unveiling secrets of centriole and cilia assembly with near-atomic resolution. Curr Opin Cell Biol *26*, 96-106.

Jenkins, P.M., McEwen, D.P., and Martens, J.R. (2009). Olfactory cilia: linking sensory cilia function and human disease. Chem Senses *34*, 451-464.

Jin, H., and Nachury, M.V. (2009). The BBSome. Curr Biol *19*, R472-R473.

Jin, H., White, S.R., Shida, T., Schulz, S., Aguiar, M., Gygi, S.P., Bazan, J.F., and Nachury, M.V. (2010). The conserved Bardet-Biedl Syndrome proteins assemble a coat that traffics membrane proteins to cilia. Cell *141*, 1208-1219.

Joberty, G., Petersen, C., Gao, L., and Macara, I.G. (2000). The cell-polarity protein Par6 links Par3 and atypical protein kinase C to Cdc42. Nat Cell Biol *2*, 531-539.

Jonsdottir, A.B., Dirks, R.W., Vrolijk, J., Ögmundsdottir, H.M., Tanke, H.J., Eyfjörd, J.E., and Szuhai, K. (2010). Centriole movements in mammalian epithelial cells during cytokinesis. BMC Cell Biol *11*, 1-9.

Kee, H.L., Dishinger, J.F., Lynne Blasius, T., Liu, C.-J., Margolis, B., and Verhey, K.J. (2012). A size-exclusion permeability barrier and nucleoporins characterize a ciliary pore complex that regulates transport into cilia. Nat Cell Biol *14*, 431-437.

Kim, S., and Tsiokas, L. (2011). Cilia and cell cycle re-entry: More than a coincidence. Cell Cycle *10*, 2683-2690.

Kim, T., Fiedler, K., Madison, D.L., Krueger, W.H., and Pfeiffer, S.E. (1995). Cloning and characterization of MVP17: A developmentally regulated myelin protein in oligodendrocytes. J Neurosci Res *42*, 413-422.

Knodler, A., Feng, S., Zhang, J., Zhang, X., Das, A., Peränen, J., and Guo, W. (2010). Coordination of Rab8 and Rab11 in primary ciliogenesis. Proc Natl Acad Sci USA *107*, 6346-6351.

Kobayashi, T., and Dynlacht, B.D. (2011). Regulating the transition from centriole to basal body. J Cell Biol *193*, 435-444.

Kuhns, S., Schmidt, K.N., Reymann, J.r., Gilbert, D.F., Neuner, A., Hub, B., Carvalho, R., Wiedemann, P., Zentgraf, H., Erfle, H.*, et al.* (2013). The microtubule affinity regulating kinase MARK4 promotes axoneme extension during early ciliogenesis. J Cell Biol *200*, 505-522.

Kuo, T.-C., Chen, C.-T., Baron, D., Onder, T.T., Loewer, S., Almeida, S., Weismann, C., Xu, P., Houghton, J.-M., Gao, F.-B.*, et al.* (2011). Midbody accumulation through evasion of autophagy contributes to cellular reprogramming and tumorigenicity. Nat Cell Biol *13*, 1214-1223.

Latta, H., Maunsbach, A.B., and Madden, S.C. (1961). Cilia in different segments of the rat nephron. J Biophys Biochem Cytol *11*, 248-252.

Lechtreck, K.-F., Johnson, E.C., Sakai, T., Cochran, D., Ballif, B.A., Rush, J., Pazour, G.J., Ikebe, M., and Witman, G.B. (2009). The Chlamydomonas reinhardtii BBSome is an IFT cargo required for export of specific signaling proteins from flagella. J Cell Biol *187*, 1117-1132.

Lechtreck, K.F., Brown, J.M., Sampaio, J.L., Craft, J.M., Shevchenko, A., Evans, J.E., and Witman, G.B. (2013). Cycling of the signaling protein phospholipase D through cilia requires the BBSome only for the export phase. J Cell Biol *201*, 249-261.

Lemmers, C., Michel, D., Lane-Guermonprez, L., Delgrossi, M.-H., Médina, E., Arsanto, J.-P., and Le Bivic, A. (2004). CRB3 binds directly to Par6 and regulates the morphogenesis of the tight junctions in mammalian epithelial cells. Mol Biol Cell *15*, 1324-1333.

Li, C., Jensen, V.L., Park, K., Kennedy, J., Garcia-Gonzalo, F.R., Romani, M., De Mori, R., Bruel, A.-L., Gaillard, D., Doray, B.r.n.*, et al.* (2016). MKS5 and CEP290 dependent assembly pathway of the ciliary transition zone. PLoS Biology *14*, e1002416.

Li, D., Mangan, A., Cicchini, L., Margolis, B., and Prekeris, R. (2014). FIP5 phosphorylation during mitosis regulates apical trafficking and lumenogenesis. EMBO Rep *15*, 428-437.

Li, S., Fernandez, J.-J., Marshall, W.F., and Agard, D.A. (2012). Three-dimensional structure of basal body triplet revealed by electron cryo-tomography. EMBO J *31*, 552-562.

Liang, Y., Meng, D., Zhu, B., and Pan, J. (2016). Mechanism of ciliary disassembly. Cell Mol Life Sci *73*, 1787-1802.

Liew, G.M., Ye, F., Nager, A.R., Murphy, J.P., Lee, J.S., Aguiar, M., Breslow, D.K., Gygi, S.P., and Nachury, M.V. (2014). The intraflagellar transport protein IFT27 promotes BBSome exit from cilia through the GTPase ARL6/BBS3. Dev Cell *31*, 265-278.

Lindemann, C.B., and Lesich, K.A. (2016). Functional anatomy of the mammalian sperm flagellum. Cytoskeleton *73*, 652-669.

Loktev, A.V., and Jackson, P.K. (2013). Neuropeptide Y family receptors traffic via the Bardet-Biedl syndrome pathway to signal in neuronal primary cilia. Cell Rep *5*, 1316-1329.

Lu, Q., Insinna, C., Ott, C., Stauffer, J., Pintado, P.A., Rahajeng, J., Baxa, U., Walia, V., Cuenca, A., Hwang, Y.-S.*, et al.* (2015). Early steps in primary cilium assembly require EHD1- and EHD3-dependent ciliary vesicle formation. Nat Cell Biol *17*, 228-240.

Magal, L.G., Yaffe, Y., Shepshelovich, J., Aranda, J.F., de Marco, M.d.C., Gaus, K., Alonso, M.A., and Hirschberg, K. (2009). Clustering and lateral concentration of raft lipids by the MAL protein. Mol Biol Cell *20*, 3751-3762.

Malicki, J.J., and Johnson, C.A. (2017). The cilium: cellular antenna and central processing unit. Trends Cell Biol *27*, 126-140.

Martin-Belmonte, F., Arvan, P., and Alonso, M.A. (2001). MAL mediates apical transport of secretory proteins in polarized epithelial Madin-Darby canine kidney cells. J Biol Chem *276*, 49337-49342.

Martin-Belmonte, F., Puertollano, R., Millan, J., and Alonso, M.A. (2000). The MAL proteolipid is necessary for the overall apical delivery of membrane proteins in the polarized epithelial Madin-Darby canine kidney and Fischer rat thyroid cell lines. Mol Biol Cell *11*, 2033-2045.

Marzesco, A.-M., Janich, P., Wilsch-Bräuninger, M., Dubreuil, V., Langenfeld, K., Corbeil, D., and Huttner, W.B. (2005). Release of extracellular membrane particles carrying the stem cell marker prominin-1 (CD133) from neural progenitors and other epithelial cells. J Cell Sci *118*, 2849-2858.

May-Simera, H.L., and Kelley, M.W. (2012). Cilia, Wnt signaling, and the cytoskeleton. Cilia *1*, 7-7.

Mazo, G., Soplop, N., Wang, W.-J., Uryu, K., and Tsou, M.-F.B. (2016). Spatial control of primary ciliogenesis by subdistal appendages alters sensation-associated properties of cilia. Dev Cell *39*, 424-437.

Mierzwa, B., and Gerlich, D.W. (2014). Cytokinetic abscission: molecular mechanisms and temporal control. Dev Cell *31*, 525-538.

Millán, J., Puertollano, R., Fan, L., Rancaño, C., and Alonso, M.A. (1997). The MAL proteolipid is a component of the detergent-insoluble membrane subdomains of human T-lymphocytes. Biochem J *321*, 247.

Mitchell, D.R. (2017). Evolution of Cilia. Cold Spring Harb Perspect Biol *9*.

Mizuno, N., Taschner, M., Engel, B.D., and Lorentzen, E. (2012). Structural studies of ciliary components. J Mol Biol *422*, 163-180.

Molla-Herman, A., Ghossoub, R., Blisnick, T., Meunier, A., Serres, C., Silbermann, F., Emmerson, C., Romeo, K., Bourdoncle, P., Schmitt, A.*, et al.* (2010). The ciliary pocket: an endocytic membrane domain at the base of primary and motile cilia. J Cell Sci *123*, 1785-1795.

Morais-de-Sá, E., and Sunkel, C. (2013). Adherens junctions determine the apical position of the midbody during follicular epithelial cell division. EMBO Rep *14*, 696-703.

Mukhopadhyay, S., Badgandi, H.B., Hwang, S.-h., Somatilaka, B., Shimada, I.S., and Pal, K. (2017). Trafficking to the primary cilium membrane. Mol Biol Cell *28*, 233-239.

Mukhopadhyay, S., Wen, X., Ratti, N., Loktev, A., Rangell, L., Scales, S.J., and Jackson, P.K. (2013). The ciliary G-protein-coupled receptor Gpr161 negatively regulates the sonic hedgehog pathway via cAMP signaling. Cell *152*, 210-223.

Mullins, J., and Biesele, J.J. (1977). Terminal phase of cytokinesis in D-98S cells. J Cell Biol *73*, 672.

Munson, M., and Novick, P. (2006). The exocyst defrocked, a framework of rods revealed. Nat Struct Mol Biol *13*, 577-581.

Nachury, M.V., Loktev, A.V., Zhang, Q., Westlake, C.J., Peränen, J., Merdes, A., Slusarski, D.C., Scheller, R.H., Bazan, J.F., Sheffield, V.C.*, et al.* (2007). A core complex of BBS proteins cooperates with the GTPase Rab8 to promote ciliary membrane biogenesis. Cell *129*, 1201-1213.

Nachury, M.V., Seeley, E.S., and Jin, H. (2010). Trafficking to the ciliary membrane: how to get across the periciliary diffusion barrier? Annu Rev Cell Dev Biol *26*, 59-87.

Nager, A.R., Goldstein, J.S., Herranz-Pérez, V., Portran, D., Ye, F., Garcia-Verdugo, J.M., and Nachury, M.V. (2017). An actin network dispatches ciliary GPCRs into extracellular vesicles to modulate signaling. Cell *168*, 1-12.

Novarino, G., Akizu, N., and Gleeson, J.G. (2011). Modeling human disease in humans: the ciliopathies. Cell *147*, 70-79.

Oberholzer, M., Bregy, P., Marti, G., Minca, M., Peier, M., and Seebeck, T. (2007). Trypanosomes and mammalian sperm: one of a kind? Trends Parasitol *23*, 71-77.

Ott, C.M. (2016). Midbody remnant licenses primary cilia formation in epithelial cells. J Cell Biol *214*, 237-239.

Pampliega, O., Orhon, I., Patel, B., Sridhar, S., Diaz-Carretero, A., Beau, I., Codogno, P., Satir, B.H., Satir, P., and Cuervo, A.M. (2013). Functional interaction between autophagy and ciliogenesis. Nature *502*, 194-200.

Paridaen, J.T.M.L., Wilsch-Bräuninger, M., and Huttner, W.B. (2013). Asymmetric inheritance of centrosome-associated primary cilium membrane directs ciliogenesis after cell division. Cell *155*, 333-344.

Pazour, G.J., and Bloodgood, R.A. (2008). Targeting proteins to the ciliary membrane. CurrTop Dev Biol *Volume 85*, 115-149.

Pearring, J.N., Salinas, R.Y., Baker, S.A., and Arshavsky, V.Y. (2013). Protein sorting, targeting and trafficking in photoreceptor cells. Prog Retin Eye Res *0*, 24-51.

Pedersen, L.B., Veland, I.R., Schrøder, J.M., and Christensen, S.T. (2008). Assembly of primary cilia. Dev Dyn *237*, 1993-2006.

Phua, S.C., Chiba, S., Suzuki, M., Su, E., Roberson, E.C., Pusapati, G.V., Setou, M., Rohatgi, R., Reiter, J.F., Ikegami, K.*, et al.* (2017). Dynamic remodeling of membrane composition drives cell cycle through primary cilia excision. Cell *168*, 264-279.e215.

Piel, M., Nordberg, J., Euteneuer, U., and Bornens, M. (2001). Centrosome-dependent exit of cytokinesis in animal cells. Science *291*, 1550-1553.

Pitaval, A., Tseng, Q., Bornens, M., and Thery, M. (2010). Cell shape and contractility regulate ciliogenesis in cell cycle-arrested cells. J Cell Biol *191*, 303-312.

Pohl, C., and Jentsch, S. (2009). Midbody ring disposal by autophagy is a post-abscission event of cytokinesis. Nat Cell Biol *11*, 65-70.

Polgar, N., Lee, A.J., Lui, V.H., Napoli, J.A., and Fogelgren, B. (2015). The exocyst gene Sec10 regulates renal epithelial monolayer homeostasis and apoptotic sensitivity. Am J Physiol - Cell Physiol *309*, C190-C201.

Pollarolo, G., Schulz, J.G., Munck, S., and Dotti, C.G. (2011). Cytokinesis remnants define first neuronal asymmetry in vivo. Nat Neurosci *14*, 1525-1533.

Portman, R.W., LeCluyse, E.L., and Dentler, W.L. (1987). Development of microtubule capping structures in ciliated epithelial cells. J Cell Sci *87*, 85.

Portran, D., Schaedel, L., Xu, Z., Thery, M., and Nachury, M.V. (2017). Tubulin acetylation protects long-lived microtubules against mechanical ageing. Nat Cell Biol *advance online publication*.

Praetorius, H.A. (2015). The primary cilium as sensor of fluid flow: new building blocks to the model. Am J Physiol - Cell Physiol *308*, C198.

Praetorius, H.A., Frokiaer, J., Nielsen, S., and Spring, K.R. (2003). Bending the primary cilium opens Ca2+-sensitive intermediate-conductance K+ channels in MDCK cells. J Memb Biol *191*, 193-200.

Praetorius, H.A., Praetorius, J., Nielsen, S., Frokiaer, J., and Spring, K.R. (2004). β-Integrins in the primary cilium of MDCK cells potentiate fibronectin-induced Ca^{2+} signaling. Am J Physiol- Renal Physiol *287*, F969.

Praetorius, H.A., and Spring, K.R. (2001). Bending the MDCK cell primary cilium increases intracellular calcium. J Memb Biol *184*, 71-79.

Praetorius, H.A., and Spring, K.R. (2003). Removal of the MDCK cell primary cilium abolishes flow sensing. J Memb Biol *191*, 69-76.

Praetorius, H.A., and Spring, K.R. (2005). A physiological view of the primary cilium. Annu Rev Physiol *67*, 515-529.

Prosser, S.L., and Morrison, C.G. (2015). Centrin2 regulates CP110 removal in primary cilium formation. J Cell Biol *208*, 693-701.

Puertollano, R., Li, S., Lisanti, M.P., and Alonso, M.A. (1997). Recombinant expression of the MAL proteolipid, a component of glycolipid-enriched membrane microdomains, induces the formation of vesicular structures in insect cells. J Biol Chem *272*, 18311-18315.

Puertollano, R., Martin-Belmonte, F., Millan, J., de Marco, M.C., Albar, J.P., Kremer, L., and Alonso, M.A. (1999). The MAL proteolipid is necessary for normal apical transport and accurate sorting of the influenza virus hemagglutinin in Madin-Darby canine kidney cells. J Cell Biol *145*, 141-151.

Pusapati, G.V., and Rohatgi, R. (2014). Location, location, and location: compartmentalization of Hedgehog signaling at primary cilia. EMBO J *33*, 1852-1854.

Rancaño, C., Rubio, T., Correas, I., and Alonso, M.A. (1994). Genomic structure and subcellular localization of MAL, a human T-cell-specific proteolipid protein. J Biol Chem *269*, 8159-8164.

Rattner, J.B., P., S., Y., O., van der Hoorn, F.A., ., and Lo, I.K. (2010). Primary cilia in fibroblast-like type B synoviocytes lie within a cilium pit: a site of endocytosis. Histol Histopathol *25*, 865-875.

Reales, E., Bernabé-Rubio, M., Casares-Arias, J., Rentero, C., Fernández-Barrera, J., Rangel, L., Correas, I., Enrich, C., Andrés, G., and Alonso, M.A. (2015). The MAL protein is crucial for proper membrane condensation at the ciliary base, which is required for primary cilium elongation. J Cell Sci *128*, 2261-2270.

Reinsch, S., and Karsenti, E. (1994). Orientation of spindle axis and distribution of plasma membrane proteins during cell division in polarized MDCKII cells. J Cell Biol *126*, 1509-1526.

Reiter, J.F., Blacque, O.E., and Leroux, M.R. (2012). The base of the cilium: roles for transition fibres and the transition zone in ciliary formation, maintenance and compartmentalization. EMBO Rep *13*, 608-618.

Reiter, J.F., and Mostov, K. (2006). Vesicle transport, cilium formation, and membrane specialization: The origins of a sensory organelle. Proc Natl Acad Sci USA *103*, 18383-18384.

Rink, J., Ghigo, E., Kalaidzidis, Y., and Zerial, M. (2005). Rab conversion as a mechanism of progression from early to late endosomes. Cell *122*, 735-749.

Robbins, D.J., Fei, D.L., and Riobo, N.A. (2012). The Hedgehog signal transduction tetwork. Sci Signal *5*, re6-re6.

Rodriguez-Boulan, E., Kreitzer, G., and Musch, A. (2005). Organization of vesicular trafficking in epithelia. Nat Rev Mol Cell Biol *6*, 233-247.

Rohatgi, R., and Snell, W.J. (2010). The ciliary membrane. Curr Opin Cell Biol *22*, 541-546.

Rosenbaum, J.L., and Witman, G.B. (2002). Intraflagellar transport. Nat Rev Mol Cell Biol *3*, 813-825.

Salzmann, V., Chen, C., Chiang, C.Y.A., Tiyaboonchai, A., Mayer, M., and Yamashita, Y.M. (2014). Centrosome-dependent asymmetric inheritance of the midbody ring in Drosophila germline stem cell division. Mol Biol Cell *25*, 267-275.

Sánchez, I., and Dynlacht, B.D. (2016). Cilium assembly and disassembly. Nat Cell Biol *18*, 711-717.

Satir, P. (1968). Studies on cilia: III. Further studies on the cilium tip and a "sliding filament" model of ciliary motility. J Cell Biol *39*, 77-94.

Satir, P., and Christensen, S.r.T. (2007). Overview of structure and function of mammalian cilia. Annu Rev Physiol *69*, 377-400.

Sato, T., Iwano, T., Kunii, M., Matsuda, S., Mizuguchi, R., Jung, Y., Hagiwara, H., Yoshihara, Y., Yuzaki, M., Harada, R*., et al.* (2014). Rab8a and Rab8b are essential for several apical transport pathways but insufficient for ciliogenesis. J Cell Sci *127*, 422-431.

Schaeren-Wiemers, N., Bonnet, A., Erb, M., Erne, B., Bartsch, U., Kern, F., Mantei, N., Sherman, D., and Suter, U. (2004). The raft-associated protein MAL is required for maintenance of proper axon,Äìglia interactions in the central nervous system. J Cell Biol *166*, 731-742.

Schmidt, K.N., Kuhns, S., Neuner, A., Hub, B., Zentgraf, H., and Pereira, G. (2012). Cep164 mediates vesicular docking to the mother centriole during early steps of ciliogenesis. J Cell Biol *199*, 1083-1101.

Schneider, L., Clement, C.A., Teilmann, S.C., Pazour, G.J., Hoffmann, E.K., Satir, P., and Christensen, S.r.T. (2005). PDGFRalpha signaling is regulated through the primary cilium in fibroblasts. Curr Biol *15*, 1861-1866.

Schou, K.B.d., Pedersen, L.B., and Christensen, S.r.T. (2015). Ins and outs of GPCR signaling in primary cilia. EMBO Rep *16*, 1099-1113.

Sfakianos, J., Togawa, A., Maday, S., Hull, M., Pypaert, M., Cantley, L., Toomre, D., and Mellman, I. (2007). Par3 functions in the biogenesis of the primary cilium in polarized epithelial cells. J Cell Biol *179*, 1133-1140.

Sheffield, V.C. (2010). The blind leading the obese: the molecular pathophysiology of a human obesity syndrome. Trans Am Clin Climatol Assoc *121*, 172-182.

Shinohara, K., Chen, D., Nishida, T., Misaki, K., Yonemura, S., and Hamada, H. (2015). Absence of radial spokes in mouse node cilia is required for rotational movement but confers ultrastructural instability as a trade-off. Dev Cell *35*, 236-246.

Simons, K., and Ikonen, E. (1997). Functional rafts in cell membranes. Nature *387*, 569-572.

Simons, K., and Toomre, D. (2000). Lipid rafts and signal transduction. Nat Rev Mol Cell Biol *1*, 31-39.

Simons, K., and Wandinger-Ness, A. (1990). Polarized sorting in epithelia. Cell *62*, 207-210.

Singh, D., and Pohl, C. (2014). Coupling of rotational cortical flow, asymmetric midbody positioning, and spindle rotation mediates dorsoventral axis formation in C. elegans. Dev Cell *28*, 253-267.

Skop, A.R., Liu, H., Yates, J., Meyer, B.J., and Heald, R. (2004). Dissection of the mammalian midbody proteome reveals conserved cytokinesis mechanisms. Science *305*, 61-66.

Sloboda, R.D. (2005). Intraflagellar transport and the flagellar tip complex. J Cell Biochem *94*, 266-272.

Smith, K.R., Kieserman, E.K., Wang, P.I., Basten, S.G., Giles, R.H., Marcotte, E.M., and Wallingford, J.B. (2011). A role for central spindle proteins in cilia structure and function. Cytoskeleton (Hoboken, NJ) *68*, 112-124.

Sorokin, S. (1962). Centrioles and the formation of rudimentary cilia by fibroblasts and smooth muscle cells. J Cell Biol *15*, 363-377.

Sorokin, S.P. (1968). Reconstructions of centriole formation and ciliogenesis in mammalian lungs. J Cell Sci *3*, 207-230.

Spektor, A., Tsang, W.Y., Khoo, D., and Dynlacht, B.D. (2007). Cep97 and CP110 suppress a cilia assembly program. Cell *130*, 678-690.

Stepanek, L., and Pigino, G. (2016). Microtubule doublets are double-track railways for intraflagellar transport trains. Science *352*, 721.

Sung, C.-H., and Leroux, M.R. (2013). The roles of evolutionarily conserved functional modules in cilia-related trafficking. Nat Cell Biol *15*, 1387-1397.

Szymanska, K., and Johnson, C.A. (2012). The transition zone: an essential functional compartment of cilia. Cilia *1*, 10-10.

Takao, D., Nemoto, T., Abe, T., Kiyonari, H., Kajiura-Kobayashi, H., Shiratori, H., and Nonaka, S. (2013). Asymmetric distribution of dynamic calcium signals in the node of mouse embryo during left-right axis formation. Dev Biol *376*, 23-30.

Takao, D., and Verhey, K.J. (2016). Gated entry into the ciliary compartment. Cell Mol Life Sci *73*, 119-127.

Takiar, V., Mistry, K., Carmosino, M., Schaeren-Wiemers, N., and Caplan, M.J. (2012). VIP17/MAL expression modulates epithelial cyst formation and ciliogenesis. Am J Physiol - Cell Physiol *303*, C862-C871.

Tang, Z., Lin, M.G., Stowe, T.R., Chen, S., Zhu, M., Stearns, T., Franco, B., and Zhong, Q. (2013). Autophagy promotes primary ciliogenesis by removing OFD1 from centriolar satellites. Nature *502*, 254-257.

Taschner, M., and Lorentzen, E. (2016). The intraflagellar transport machinery. Cold Spring Harbor Perspect Biol *8*.

Tateishi, K., Yamazaki, Y., Nishida, T., Watanabe, S., Kunimoto, K., Ishikawa, H., and Tsukita, S. (2013). Two appendages homologous between basal bodies and centrioles are formed using distinct Odf2 domains. J Cell Biol *203*, 417-425.

Thomas, L.L., and Fromme, J.C. (2016). GTPase cross talk regulates TRAPPII activation of Rab11 homologues during vesicle biogenesis. J Cell Biol *215*, 499.

Tobin, J.L., and Beales, P.L. (2009). The nonmotile ciliopathies. Genet Med *11*, 386-402.

Torkko, J.M., Manninen, A., Schuck, S., and Simons, K. (2008). Depletion of apical transport proteins perturbs epithelial cyst formation and ciliogenesis. J Cell Sci *121*, 1193-1203.

Trepat, X., Wasserman, M.R., Angelini, T.E., Millet, E., Weitz, D.A., Butler, J.P., and Fredberg, J.J. (2009). Physical forces during collective cell migration. Nat Phys *5*, 426-430.

Tsang, W.Y., Bossard, C., Khanna, H., Peranen, J., Swaroop, A., Malhotra, V., and Dynlacht, B.D. (2008). CP110 suppresses primary cilia formation through its interaction with CEP290, a protein deficient in human ciliary disease. Dev Cell *15*, 187-197.

Tsang, W.Y., and Dynlacht, B.D. (2013). CP110 and its network of partners coordinately regulate cilia assembly. Cilia *2*, 9-9.

Tucker, R.W., Pardee, A.B., and Fujiwara, K. (1979). Centriole ciliation is related to quiescence and DNA synthesis in 3T3 cells. Cell *17*, 527-535.

Verhey, K.J., and Yang, W. (2016). Permeability barriers for generating a unique ciliary protein and lipid composition. Curr Opin Cell Biol *41*, 109-116.

Vertii, A., Hehnly, H., and Doxsey, S. (2016a). The centrosome, a multitalented renaissance organelle. Cold Spring Harb Perspect Biol *8*.

Vertii, A., Hung, H.-F., Hehnly, H., and Doxsey, S. (2016b). Human basal body basics. Cilia *5*, 13.

Vieira, O.V., Gaus, K., Verkade, P., Fullekrug, J., Vaz, W.L.C., and Simons, K. (2006). FAPP2, cilium formation, and compartmentalization of the apical membrane in polarized Madin-Darby canine kidney (MDCK) cells. Proc Nat Acad Sci USA *103*, 18556-18561.

Wallingford, J.B., and Mitchell, B. (2011). Strange as it may seem: the many links between Wnt signaling, planar cell polarity, and cilia. Genes Dev *25*, 201-213.

Wang, G., Krishnamurthy, K., and Bieberich, E. (2009). Regulation of primary cilia formation by ceramide. J Lipid Res *50*, 2103-2110.

Wang, J., Silva, M., Haas, L., Morsci, N., Nguyen, K.C.Q., Hall, D.H., and Barr, M.M. (2014). C. elegans ciliated sensory neurons release extracellular vesicles that function in animal communication. Curr Biol *24*, 519-525.

Wei, Q., Ling, K., and Hu, J. (2015). The essential roles of transition fibers in the context of cilia. Curr Opin Cell Biol *35*, 98-105.

Westlake, C.J., Baye, L.M., Nachury, M.V., Wright, K.J., Ervin, K.E., Phu, L., Chalouni, C., Beck, J.S., Kirkpatrick, D.S., Slusarski, D.C*., et al.* (2011). Primary cilia membrane assembly is initiated by Rab11 and transport protein particle II (TRAPPII) complex-dependent trafficking of Rabin8 to the centrosome. Proc Nat Acad Sci USA *108*, 2759-2764.

Wheatley, D.N., Wang, A.M., and Strugnell, G.E. (1996). Expression of primary cilia in mammalian cells. Cell Biol Int *20*, 73-81.

Wilcockson, S.G., Sutcliffe, C., and Ashe, H.L. (2016). Control of signaling molecule range during developmental patterning. Cell Mol Life Sci, 1-20.

Wloga, D., Joachimiak, E., Louka, P., and Gaertig, J. (2016). Posttranslational modifications of tubulin and cilia. Cold Spring Harb Perspect Biol.

Wood, C.R., Huang, K., Diener, D.R., and Rosenbaum, J.L. (2013). The cilium secretes bioactive ectosomes. Curr Biol *23*, 906-911.

Wood, C.R., and Rosenbaum, J.L. (2015). Ciliary ectosomes: transmissions from the cell's antenna. Trends Cell Biol *25*, 276-285.

Wood, C.R., Wang, Z., Diener, D., Zones, J.M., Rosenbaum, J., and Umen, J.G. (2012). IFT proteins accumulate during cell division and localize to the cleavage furrow in Chlamydomonas. PLoS ONE *7*, e30729.

Wu, S., Mehta, S.Q., Pichaud, F., Bellen, H.J., and Quiocho, F.A. (2005). Sec15 interacts with Rab11 via a novel domain and affects Rab11 localization in vivo. Nat Struct Mol Biol *12*, 879-885.

Xu, Q., Zhang, Y., Wei, Q., Huang, Y., Hu, J., and Ling, K. (2016). Phosphatidylinositol phosphate kinase PIPKIgamma and phosphatase INPP5E coordinate initiation of ciliogenesis. Nat Commun *7*, 10777.

Xu, Q., Zhang, Y., Wei, Q., Huang, Y., Li, Y., Ling, K., and Hu, J. (2015). BBS4 and BBS5 show functional redundancy in the BBSome to regulate the degradative sorting of ciliary sensory receptors. Sci Rep *5*, 11855.

Yang, J., Liu, X., Yue, G., Adamian, M., Bulgakov, O., and Li, T. (2002). Rootletin, a novel coiled-coil protein, is a structural component of the ciliary rootlet. J Cell Biol *159*, 431-440.

Yee, L.E., Garcia-Gonzalo, F.R., Bowie, R.V., Li, C., Kennedy, J.K., Ashrafi, K., Blacque, O.E., Leroux, M.R., and Reiter, J.F. (2015). Conserved genetic interactions between ciliopathy complexes cooperatively support ciliogenesis and ciliary signaling. PLoS Genet *11*, e1005627.

Yee, L.E., and Reiter, J.F. (2015). Ciliary vesicle formation: a prelude to ciliogenesis. Dev Cell *32*, 665-666.

Yoshiba, S., and Hamada, H. (2014). Roles of cilia, fluid flow, and Ca2+ signaling in breaking of left-right symmetry. Trends Genet *30*, 10-17.

Yoshimura, S.-i., Egerer, J., Fuchs, E., Haas, A.K., and Barr, F.A. (2007). Functional dissection of Rab GTPases involved in primary cilium formation. J Cell Biol *178*, 363-369.

Yu, I.M., and Hughson, F.M. (2010). Tethering factors as organizers of intracellular vesicular traffic. Annu Rev Cell Dev Biol *26*, 137-156.

Zacchetti, D., Peranen, J., Murata, M., Fiedler, K., and Simons, K. (1995). VIP17/MAL, a proteolipid in apical transport vesicles. FEBS Lett *377*, 465-469.

Zariwala, M.A., Knowles, M.R., and Omran, H. (2007). Genetic defects in ciliary structure and function. Annu Rev Physiol *69*, 423-450.

Zhang, Q., Taulman, P.D., and Yoder, B.K. (2004a). Cystic kidney diseases: all roads lead to the cilium. Physiology *19*, 225.

Zhang, X.-M., Ellis, S., Sriratana, A., Mitchell, C.A., and Rowe, T. (2004b). Sec15 is an effector for the Rab11 GTPase in mammalian cells. J Biol Chem *279*, 43027-43034.

Zhao, B., Li, L., Lei, Q., and Guan, K.-L. (2010). The Hippo-YAP pathway in organ size control and tumorigenesis: an updated version. Genes Dev *24*, 862-874.

Zhou, J. (2009). Polycystins and primary cilia: primers for cell cycle progression. Annu Rev Physiol *71*.
Zimmerman, K., and Yoder, B.K. (2015). Snapshot: sensing and signaling by cilia. Cell *161*, 692-692.e691.

Zimmerman, K.W. (1898). Beiträge zur Kenntniss einiger drüsen und epithelien. Arch Mikr Anat *52*, 552-706.

Zuo, X., Fogelgren, B., and Lipschutz, J.H. (2011). The small GTPase Cdc42 is necessary for primary ciliogenesis in renal tubular epithelial cells. J Biol Chem *286*, 22469-22477.

Zuo, X., Guo, W., and Lipschutz, J.H. (2009). The exocyst protein sec10 is necessary for primary ciliogenesis and cystogenesis in vitro. Mol Biol Cell *20*, 2522-2529.